Institute of Electrical Power Systems
Graz University of Technology

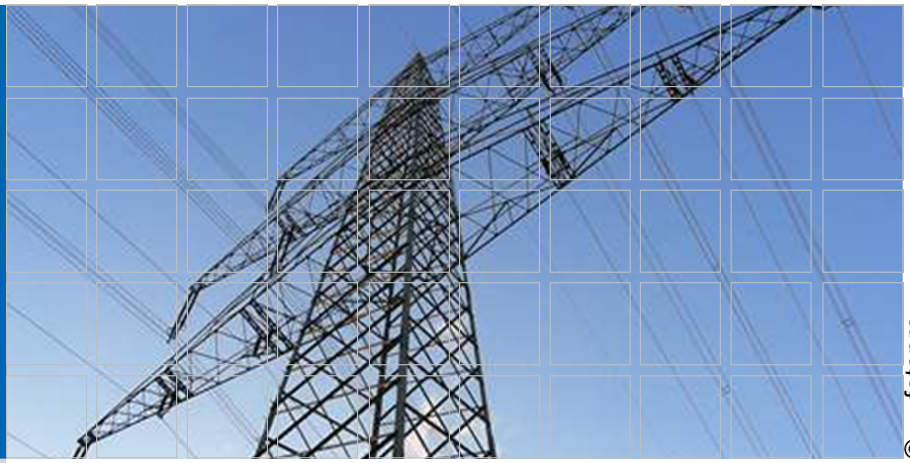



# Analytical optimization and practical verification of reactive power supply for power plants

Wendelin Angermann, BSc

December 2023

ELEKTRISCHE
ANLAGEN & NETZE
TU GRAZ

**TU Graz Institute of Electrical Power Systems**
**Inffeldgasse 18/1**
**8010 Graz Austria**

**Head of Institute**
Robert Schürhuber, Univ.-Prof. DDipl.-Ing. Dr.techn.

**Supervisor**
Robert Schürhuber, Univ.-Prof. DDipl.-Ing. Dr.techn.
Darko Brankovic, Dipl.-Ing. BSc
Philipp Hackl, Dipl.-Ing. BSc

**Author**
Wendelin Angermann, BSc

December 2023

Wendelin Angermann, BSc

# Analytical optimization and practical verification of reactive power supply for power plants

**MASTER'S THESIS**

to achieve the university degree of

Diplom-Ingenieur/Diplom-Ingenieurin

Master's degree programme: Elektrotechnik

submitted to

**Graz University of Technology**

**Supervisor**

Robert Schürhuber, Univ.-Prof. DDipl.-Ing. Dr.techn.
Darko Brankovic, Dipl.-Ing. BSc
Philipp Hackl, Dipl.-Ing. BSc
Institute of Electrical Power Systems

Graz, December 2023

# Abstract

A transformation process of the energy system is necessary and unavoidable in view of the ongoing climate change. The technical development of renewable energy sources through the use of wind power and photovoltaic systems is an important milestone on the path to a climate-neutral future for Austria and Europe. Due to the more decentralized and volatile generation of electricity in the future, special attention must be paid to the stability of the electrical power distribution and transmission grid.

There are technical requirements for the reactive power supply of power-generating facilities at both European and national level. These legal framework conditions form the basis for the secure and stable operation of a power supply system. As part of this master's thesis, a methodology was developed to verify the requirements of the legislator. To do this, it is necessary to carry out load flow analyses, which can be computationally intensive. In order to make this process as efficient as possible, the load flow analyses carried out in this master's thesis are performed using computing time-optimized analytical load flow calculations. For the problems considered here, this type of load flow analysis shows a computing time optimization by a factor of five compared to classical load flow calculation methods. In addition to the calculation time optimization, this method also offers the possibility to investigate the reactive power supply at the point of connection with different control concepts of tap changers.

As an additional part of this master's thesis, an optimized control concept of a tap changer was developed and implemented to maximize the reactive power supply at the point of connection. In addition to the classic calculation of the reactive power supply at the point of connection, it was also possible to calculate the reactive power supply at the generator terminals by applying analytical load flow analysis. This verification method can make the planning process much easier, for new plant implementation and for revisioning of old power plants.

If we look at the Austrian electrical power system, it is primarily characterized by hydropower. The proportion of renewable energy forms is increasing at both European and national level. In most cases, these are connected to the grid via converters. For this reason, a methodology for calculating the reactive power supply at the point of connection of so-called hybrid power-generating facilities was developed in this master's thesis. In the example investigated, the hybrid power-generating facility consists of a converter and a synchronous generator. All calculations were fully implemented in MATLAB.

To ensure that the calculations represents reality as closely as possible, they were verified using an established simulation program (DIgSILENT PowerFactory). In addition, extensive experiments were carried out in active grid operation. The reactive power supply of a power-generating facility in the 110 kV grid was verified using a test concept developed in this master's thesis.

# Kurzzusammenfassung

Eine Transformation des Energiesystems ist angesichts des fortschreitenden Klimawandels notwendig und unausweichlich. Die technische Erschließung erneuerbarer Energiequellen durch den Einsatz von Windkraft- und Photovoltaikanlagen ist ein wichtiger Meilenstein auf dem Weg in eine klimaneutrale Zukunft Österreichs und Europas. Aufgrund der zukünftig dezentraleren und volatileren Stromerzeugung muss besonderes Augenmerk auf die Stabilität des Energieversorgungsnetzes gelegt werden. Auf europäischer als auch auf nationaler Ebene bestehen technische Anforderungen an die Blindleistungsbereitstellung von Stromerzeugungsanlagen.

Diese gesetzlichen Rahmenbedingungen bilden die Grundlage für den sicheren und stabilen Betrieb eines Energieversorgungssystems. Im Rahmen dieser Masterarbeit wurde eine Methodik entwickelt, um die gesetzlichen Anforderungen verifizieren zu können. Hierfür müssen zum Teil rechenintensive Lastflussberechnungen durchgeführt werden. Um diesen Prozess möglichst effizient zu gestalten, werden die in dieser Masterarbeit verwendeten Lastflussberechnungen mit rechenzeitoptimierten analytischen Lastflussberechnungen durchgeführt. Diese Art der Lastflussberechnung weist für die hier betrachteten Problemstellungen eine Rechenzeitoptimierung um den Faktor fünf gegenüber klassischen Lastflussberechnungsmethoden auf. Neben der Rechenzeitoptimierung bietet diese Methode auch die Möglichkeit, die Blindleistungsbereitstellung am Netzanschlusspunkt mit unterschiedlichen Regelkonzepten von Transformatorstufenstellern zu untersuchen.

Im Rahmen dieser Masterarbeit wurde ein optimiertes Regelkonzept eines Transformatorstufenstellers zur Maximierung der Blindleistungsbereitstellung entwickelt und implementiert. Neben der klassischen Berechnung der Blindleistungsbereitstellung am Netzanschlusspunkt konnte durch Anwendung der analytischen Lastflussrechnung auch die Blindleistungsbereitstellung an den Generatorklemmen berechnet werden. Diese Nachweismethodik kann insbesondere für in Planung befindliche Anlagen eine wesentliche Erleichterung darstellen.

Betrachtet man das österreichische Energiesystem, so ist dieses vor allem durch die Wasserkraft geprägt. Sowohl auf europäischer als auch auf nationaler Ebene steigt jedoch der Anteil erneuerbarer Energieformen. Diese werden in den meisten Fällen über Umrichter an das Netz angeschlossen. Deswegen wurde in dieser Masterarbeit eine Methodik zur Berechnung der Blindleistungsbereitstellung von sogenannten Mischanlagen entwickelt. Im untersuchten Beispiel besteht die Mischanlage aus einem Umrichter und einem Synchrongenerator. Alle Berechnungen wurden vollständig in MATLAB implementiert.

Um sicherzustellen, dass die Berechnungen die Realität möglichst gut abbilden, wurden sie mit einem etablierten Simulationsprogramm verifiziert. Zusätzlich wurden umfangreiche Versuche im aktiven Netzbetrieb durchgeführt. Dabei konnte die Blindleistungsbereitstellung einer Stromerzeugungsanlage im 110 kV-Netz mit einem in dieser Masterarbeit entwickelten Versuchskonzept verifiziert werden.

# Symbolslist

| Notation | Description |
|---|---|
| $C'_{\mathrm{line},1}$ | Capacity per unit length of line 1 (positive sequence system) |
| $C'_{\mathrm{line},2}$ | Capacity per unit length of line 2 (positive sequence system) |
| $C_{\mathrm{line},1}$ | Capacity of line 1 (positive sequence system) |
| $C_{\mathrm{line},2}$ | Capacity of line 2 (positive sequence system) |
| $K_1$ | $\mathrm{Re}\left\{\frac{\det\left(\underline{\mathbf{A}}_{\mathrm{g}}\right)}{\underline{a}_{\mathrm{g},(2,2)}} \cdot \underline{u}_{\mathrm{grid,s}}\right\}$ |
| $K_2$ | $\mathrm{Im}\left\{\frac{\det\left(\underline{\mathbf{A}}_{\mathrm{g}}\right)}{\underline{a}_{\mathrm{g},(2,2)}} \cdot \underline{u}_{\mathrm{grid,s}}\right\}$ |
| $K_3$ | $\mathrm{Re}\left\{\frac{\underline{a}_{\mathrm{g},(1,2)}}{\underline{a}_{\mathrm{g},(2,2)}} \cdot (p_{\mathrm{gen,s}} - \mathrm{j} \cdot q_{\mathrm{gen,s}})\right\}$ |
| $K_4$ | $\mathrm{Im}\left\{\frac{\underline{a}_{\mathrm{g},(1,2)}}{\underline{a}_{\mathrm{g},(2,2)}} \cdot (p_{\mathrm{gen,s}} - \mathrm{j} \cdot q_{\mathrm{gen,s}})\right\}$ |
| $L'_{\mathrm{line},1}$ | Inductance per unit length of line 1 (positive sequence system) |
| $L'_{\mathrm{line},2}$ | Inductance per unit length of line 2 (positive sequence system) |
| $L_{\mathrm{line},1}$ | Inductance of line 1 (positive sequence system) |
| $L_{\mathrm{line},2}$ | Inductance of line 2 (positive sequence system) |
| $P_{\mathrm{max}}$ | Maximum capacity of the power-generating facilities |
| $R'_{\mathrm{line},1}$ | Resistance per unit length of line 1 (positive sequence system) |
| $R'_{\mathrm{line},2}$ | Resistance per unit length of line 2 (positive sequence system) |
| $R_{\mathrm{line},1}$ | Ohmic resistance of line 1 (positive sequence system) |
| $R_{\mathrm{line},2}$ | Ohmic resistance of line 2 (positive sequence system) |
| $S_{\mathrm{b}}$ | Base apparent power for per unit values |
| $S_{\mathrm{r,t1}}$ | Rated apparent power transfomer 1 |
| $S_{\mathrm{r,t2}}$ | Rated apparent power transfomer 2 |
| $U_{\mathrm{b,hv}}$ | Base voltage (high voltage side) for per unit values |
| $U_{\mathrm{b,lv,t1}}$ | Base voltage (low voltage side transformer 1) for per unit values |
| $U_{\mathrm{b,lv,t2}}$ | Base voltage (low voltage side transformer 2) for per unit values |

| Notation | Description |
|---|---|
| $U_{\mathrm{c}}$ | Supply voltage at Point of connection (POC) specified in the grid connection contract |
| $U_{\mathrm{r,t1,hv}}$ | Rated voltage at high voltage side of transformer 1 |
| $U_{\mathrm{r,t1,lv}}$ | Rated voltage at low voltage side of transformer 1 |
| $U_{\mathrm{r,t2,hv}}$ | Rated voltage at high voltage side of transformer 2 |
| $U_{\mathrm{r,t2,lv}}$ | Rated voltage at low voltage side of transformer 2 |
| $Z_{\mathrm{b}}$ | Base impedance (high volatge side) per unit values |
| $\Delta u_{\mathrm{r,t1,hv,tap}}$ | Additional voltage per tap on the upper voltage side as a percentage of $U_{\mathrm{r,t1,hv}}$ |
| $\Delta u_{\mathrm{r,t2,hv,tap}}$ | Additional voltage per tap on the upper voltage side as a percentage of $U_{\mathrm{r,t2,hv}}$ |
| $\alpha_{\mathrm{gen,c}}$ | Gradient angle of the simplified stability limit |
| $\delta_{\mathrm{gen,c}}$ | power angle |
| $\gamma_{\mathrm{gen}}$ | Power safety margin for the practical stability limit in percent of the rated apparent power |
| $\kappa_{\mathrm{t1,tap}}$ | Tap changer position of transformer 1 (center position = 0) |
| $\kappa_{\mathrm{t2,tap}}$ | Tap changer position of transformer 2 (center position = 0) |
| $\mathbf{E}_{\mathrm{h,sc}}$ | Identity matrix Matrix in pu |
| e | Euler's number |
| j | Imaginary unit |
| $\omega$ | Grid angular frequency |
| $\underline{\mathbf{A}}_{\mathrm{g}}$ | Complex total grouped chain matrix in pu |
| $\underline{\mathbf{A}}_{\mathrm{line,1,2}}$ | Complex chain matrix of line 1 and line 2 in pu |
| $\underline{\mathbf{A}}_{\mathrm{t1}}$ | Complex chain matrix of transfomer 1 in pu |
| $\underline{\mathbf{I}}_{\mathrm{h,sc}}^{(\xi)}$ | Complex scaled and simplified vector with the node currents in the actual iteration step in pu |
| $\underline{\mathbf{I}}_{\mathrm{h}}^{(\xi)}$ | Complex simplified vector with the node currents in the actual iteration step in pu |
| $\underline{\mathbf{L}}_{\mathrm{h,sc}}$ | Complex strictly lower triangular Matrix in pu |
| $\underline{\mathbf{R}}_{\mathrm{h,sc}}$ | Complex strictly upper triangular Matrix in pu |
| $\underline{\mathbf{U}}_{\mathrm{h}}^{(\xi+1)}$ | Complex simplified vector with the node voltages in the future iteration step in pu |

| Notation | Description |
|---|---|
| $\underline{\mathbf{U}}_{\mathrm{h}}^{(\xi)}$ | Complex simplified vector with the node voltages in the actual iteration step in pu |
| $\underline{\mathbf{Y}}_{\mathrm{c,h}}$ | Complex complete admittance matrix in pu |
| $\underline{\mathbf{Y}}_{\mathrm{h,sc}}$ | Complex scaled and simplified admittance matrix in pu |
| $\underline{\mathbf{Y}}_{\mathrm{h}}$ | Complex simplified admittance matrix in pu |
| $\underline{\mathbf{Y}}_{\mathrm{line,1,2}}$ | Complex admittance matrix of line 1 and line 2 in pu |
| $\underline{\mathbf{Y}}_{\mathrm{line,1}}$ | Complex admittance matrix of line 1 in pu |
| $\underline{\mathbf{Y}}_{\mathrm{line,2}}$ | Complex admittance matrix of line 2 in pu |
| $\underline{\mathbf{Y}}_{\mathrm{t1}}$ | Complex admittance matrix of transfomer 1 in pu |
| $\underline{\mathbf{Y}}_{\mathrm{t2}}$ | Complex admittance matrix of transfomer 2 in pu |
| $\underline{a}_{\mathrm{g,(1,1)}}$ | Complex element row 1 and column 1 of the matrix $\underline{\mathbf{A}}_{\mathrm{g}}$ in pu |
| $\underline{a}_{\mathrm{g,(1,2)}}$ | Complex element row 1 and column 2 of the matrix $\underline{\mathbf{A}}_{\mathrm{g}}$ in pu |
| $\underline{a}_{\mathrm{g,(2,1)}}$ | Complex element row 2 and column 1 of the matrix $\underline{\mathbf{A}}_{\mathrm{g}}$ in pu |
| $\underline{a}_{\mathrm{g,(2,2)}}$ | Complex element row 2 and column 2 of the matrix $\underline{\mathbf{A}}_{\mathrm{g}}$ in pu |
| $\underline{i}_{\mathrm{con,h}}^{(\xi+1)}$ | Complex current at converter terminals in the future iteration step in pu |
| $\underline{i}_{\mathrm{con,h}}^{(\xi)}$ | Complex current at converter terminals in the actual iteration step in pu |
| $\underline{i}_{\mathrm{con,h}}$ | Complex current at converter terminals in pu |
| $\underline{i}_{\mathrm{gen,h}}^{(\xi)}$ | Complex current at generator terminals in the actual iteration step in pu |
| $\underline{i}_{\mathrm{gen,h}}$ | Complex current at generator terminals in pu |
| $\underline{i}_{\mathrm{gen,s}}$ | Complex current at generator terminals in pu |
| $\underline{i}_{\mathrm{grid,h}}$ | Complex current at POC in pu |
| $\underline{i}_{\mathrm{grid,s}}$ | Complex current at POC in pu |
| $\underline{i}_{\mathrm{t1,hv}}$ | Complex high-voltage side terminal current of transformer 1 in pu |
| $\underline{i}_{\mathrm{t1,lv}}$ | Complex low-voltage side terminal current of transformer 1 in pu |
| $\underline{i}_{\mathrm{trans,s}}$ | Complex current at transformer terminals on the high voltage side in pu |

| Notation | Description |
|---|---|
| $\underline{u}_{\mathrm{con,h}}^{(\xi+1)}$ | Complex voltage at converter terminals in the future iteration step in pu |
| $\underline{u}_{\mathrm{con,h}}^{(\xi)}$ | Complex voltage at converter terminals in the actual iteration step in pu |
| $\underline{u}_{\mathrm{con,h}}$ | Complex voltage at converter terminals in pu |
| $\underline{u}_{\mathrm{gen,c}}$ | Complex voltage at generator terminals in pu |
| $\underline{u}_{\mathrm{gen,emf,c}}$ | Complex internal electromotive force in pu |
| $\underline{u}_{\mathrm{gen,h}}^{(\xi+1)}$ | Complex voltage at generator terminals in the future iteration step in pu |
| $\underline{u}_{\mathrm{gen,h}}^{(\xi)}$ | Complex voltage at generator terminals in the actual iteration step in pu |
| $\underline{u}_{\mathrm{gen,h}}$ | Complex voltage at generator terminals in pu |
| $\underline{u}_{\mathrm{gen,s}}$ | Complex voltage at generator terminals in pu |
| $\underline{u}_{\mathrm{grid,h}}$ | Complex voltage at POC in pu |
| $\underline{u}_{\mathrm{grid,s}}$ | Complex voltage at POC in pu |
| $\underline{u}_{\mathrm{t1,hv}}$ | Complex terminal voltage at high voltage side of transformer 1 in pu |
| $\underline{u}_{\mathrm{t1,lv}}$ | Complex terminal voltage at low voltage side of transformer 1 in pu |
| $\underline{u}_{\mathrm{trans,h}}^{(\xi)}$ | Complex voltage at transformer terminals on the high voltage side in the actual iteration step in pu |
| $\underline{u}_{\mathrm{trans,h}}$ | Complex voltage at transformer terminals on the high voltage side in pu |
| $\underline{u}_{\mathrm{trans,s}}$ | Complex voltage at transformer terminals on the high voltage side in pu |
| $\underline{y}_{\mathrm{line,1,(1,1)}}$ | Complex element row 1 and column 1 of the matrix $\underline{\mathbf{Y}}_{\mathrm{line,1}}$ in pu |
| $\underline{y}_{\mathrm{line,1,(1,2)}}$ | Complex element row 1 and column 2 of the matrix $\underline{\mathbf{Y}}_{\mathrm{line,1}}$ in pu |
| $\underline{y}_{\mathrm{line,1,(2,1)}}$ | Complex element row 2 and column 1 of the matrix $\underline{\mathbf{Y}}_{\mathrm{line,1}}$ in pu |
| $\underline{y}_{\mathrm{line,1,(2,2)}}$ | Complex element row 2 and column 2 of the matrix $\underline{\mathbf{Y}}_{\mathrm{line,1}}$ in pu |
| $\underline{y}_{\mathrm{line,1,2,(1,1)}}$ | Complex element row 1 and column 1 of the matrix $\underline{\mathbf{Y}}_{\mathrm{line,1,2}}$ in pu |

| Notation | Description |
|---|---|
| $\underline{y}_{\text{line},1,2,(1,2)}$ | Complex element row 1 and column 2 of the matrix $\underline{\mathbf{Y}}_{\text{line},1,2}$ in pu |
| $\underline{y}_{\text{line},1,2,(2,1)}$ | Complex element row 2 and column 1 of the matrix $\underline{\mathbf{Y}}_{\text{line},1,2}$ in pu |
| $\underline{y}_{\text{line},1,2,(2,2)}$ | Complex element row 2 and column 2 of the matrix $\underline{\mathbf{Y}}_{\text{line},1,2}$ in pu |
| $\underline{y}_{\text{line},2,(1,1)}$ | Complex element row 1 and column 1 of the matrix $\underline{\mathbf{Y}}_{\text{line},2}$ in pu |
| $\underline{y}_{\text{line},2,(1,2)}$ | Complex element row 1 and column 2 of the matrix $\underline{\mathbf{Y}}_{\text{line},2}$ in pu |
| $\underline{y}_{\text{line},2,(2,1)}$ | Complex element row 2 and column 1 of the matrix $\underline{\mathbf{Y}}_{\text{line},2}$ in pu |
| $\underline{y}_{\text{line},2,(2,2)}$ | Complex element row 2 and column 2 of the matrix $\underline{\mathbf{Y}}_{\text{line},2}$ in pu |
| $\underline{y}_{\text{t1}}$ | Complex transformer admittance on the high voltage side in pu |
| $\underline{y}_{\text{t2}}$ | Complex transformer admittance on the high voltage side in pu |
| $\pi$ | The number Pi (Ludolphine number) |
| $\xi$ | Variable for the current integration step |
| $e_{\text{q,min}}$ | Power safety margin for the minimum excitation current limit |
| $f$ | Grid frequency |
| $i_{\text{con,h,max}}$ | Maximum current at converter terminals in pu |
| $l_{\text{line},1}$ | Length of line 1 |
| $l_{\text{line},2}$ | Length of line 2 |
| $p_{\text{con,h}}$ | Active power at converter terminals in pu |
| $p_{\text{gen,c}}$ | Active power at generator terminals in pu |
| $p_{\text{gen,h}}$ | Active power at generator terminals in pu |
| $p_{\text{gen,s}}$ | Active power at generator terminals in pu |
| $p_{\text{grid,h}}$ | Active power at POC in pu |
| $p_{\text{grid,s}}$ | Active power at POC in pu |
| $p_{\text{trans,h}}$ | Active power at transformer terminals on the high voltage side in pu |

| Notation | Description |
|---|---|
| $p_{\mathrm{trans,s}}$ | Active power at transformer terminals on the high voltage side in pu |
| $q_{\mathrm{con,h}}^{(\xi)}$ | Reactive power at converter terminals in the actual iteration step in pu |
| $q_{\mathrm{con,h}}$ | Reactive power at converter terminals in pu |
| $q_{\mathrm{gen,c}}$ | Reactive power at generator terminals in pu |
| $q_{\mathrm{gen,h}}^{(\xi)}$ | Reactive power at generator terminals in the actual iteration step in pu |
| $q_{\mathrm{gen,h}}$ | Reactive power at generator terminals in pu |
| $q_{\mathrm{gen,s}}$ | Reactive power at generator terminals in pu |
| $q_{\mathrm{grid,h}}$ | Reactive power at POC in pu |
| $q_{\mathrm{grid,s}}$ | Reactive power at POC in pu |
| $q_{\mathrm{trans,h}}$ | Reactive power at transformer terminals on the high voltage side in pu |
| $q_{\mathrm{trans,s}}$ | Reactive power at transformer terminals on the high voltage side in pu |
| $t_1$ | transmission ratio of transfomer 1 in pu |
| $t_2$ | transmission ratio of transfomer 2 in pu |
| $u_{\mathrm{con,h,max}}$ | Maximum voltage at converter terminals in pu |
| $u_{\mathrm{k,t1}}$ | Short-circuit voltage transfomer 1 |
| $u_{\mathrm{k,t2}}$ | Short-circuit voltage transfomer 2 |
| $u_{\mathrm{kr,t1}}$ | Ohmic short-circuit voltage transfomer 1 |
| $u_{\mathrm{kr,t2}}$ | Ohmic short-circuit voltage transfomer 2 |
| $x_{\mathrm{d}}$ | direct-axis synchronous reactance |
| $x_{\mathrm{q}}$ | quadrature-axis synchronous reactance |

# Acronyms

| Notation | Description |
|---|---|
| AC | Alternating current |
| DC | Direct current |
| POC | Point of connection |
| RfG | Requirements for Generators |
| TOR | Technische und Organisatorische Regeln für Betreiber und Benutzer von Netzen |

# Contents

# 1 Introduction

## 1.1 Motivation

The currently ongoing climate change is resulting in social, political, economic and infrastructural changes [1]. In the area of energy supply and distribution, the shift towards renewable energy sources and the associated grid expansion should be mentioned in particular. Gross electricity production in Austria has changed significantly in recent years. Figure 1 shows the process of change in gross electricity production in Austria based on data from „Österreichs E-Wirtschaft“ [2]. In 1980, primary electricity generation in Austria was based on energy from hydropower and fossil fuels. Around 40 years later, in 2022, an increase of around 27 TWh in gross power generation can be seen. It is particularly worth mentioning here that the increase was primarily covered by renewable energy sources.

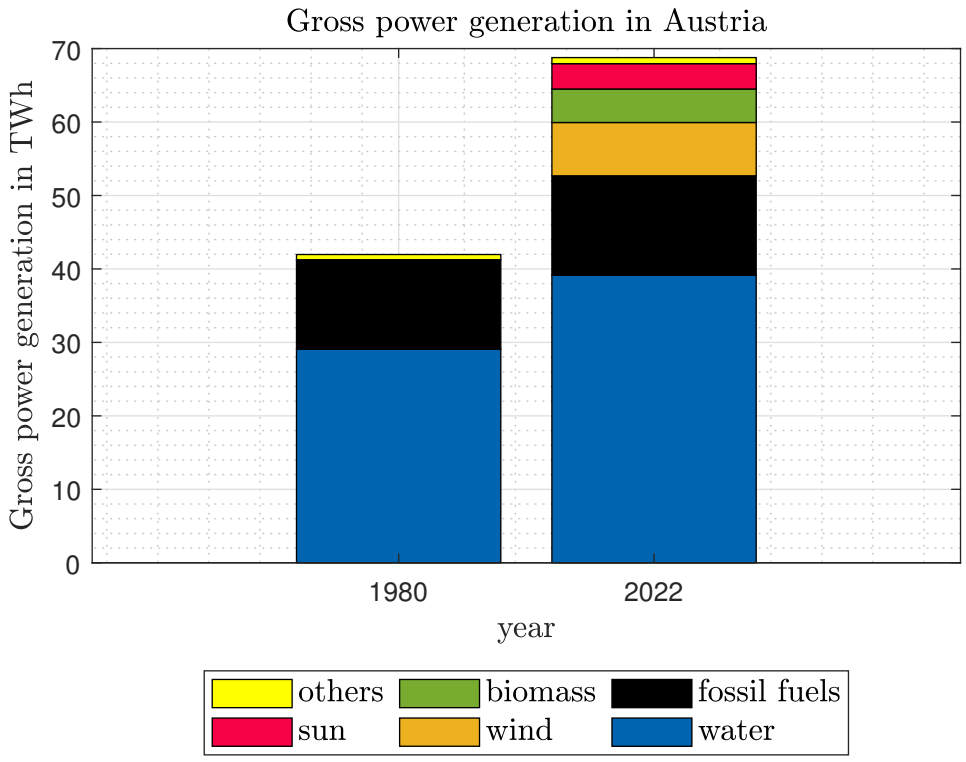


Figure 1: Trend in gross power generation in Austria

Renewable energy sources in particular, which converts energy from the sun or wind, have a crucial technical difference compared to conventional power-generating facilities. In conventional power-generating facilities, energy is converted by means of rotating masses. In modern renewable power-generating facilities, for example photovoltaic plants or wind turbines, energy is fed in via converters (power electronics). In terms of stability, such converters have a much more complex behavior than conventional power-generating facilities. In view of this new

challenge, it is even more important to provide guidelines for the operation of such systems at both national and European level. At European level, there is the so called Requirements for Generators (RfG) [3]. At national level in Austria, the connection of power-generating facilities to the grid infrastructure is regulated by the socalled Technische und Organisatorische Regeln für Betreiber und Benutzer von Netzen (TOR) [4–7]. They contain various general requirements as well as more complex requirements for stationary and transient operating behavior.

In general, it is necessary that the power-generating facilities are able to contribute towards the stability of a power distribution and transmission grid. A distinction is made here between different stability concepts (frequency stability, rotor angle stability and voltage stability) [8, 9]. These stability terms can be further subdivided. In the course of this master's thesis, particular attention is paid to the point of voltage stability in the steady state. Both the RfG and the TOR define requirements with regard to the steady-state voltage stability of power-generating facilities. The master's thesis should help to verify the individual requirements for power-generating facilities on the part of the legislator through optimized mathematical modeling. In addition, the results of this master's thesis offer the possibility of optimizing power-generating facilities with regard to voltage stability in a stationary state by varying important technical parameters. The power-generating facilities are considered in a broad context. As can already be seen in Figure 1, the proportion of renewable energy sources in the energy system is increasing. For this reason, it is also necessary to consider hybrid systems (consisting of a converter and a generator) for the mathematical modeling.

## 1.2 Goals

The aim of this master's thesis is to develop a methodology for calculating the reactive power supply of power-generating facilities and to implement it in MATLAB. The calculations have to be verified by simulations and practical experiments. The following milestones can be defined for this purpose:

- Development of a method for the efficient calculation of the reactive power supply of a synchronous power-generating facility.
- Analysis and calculation of the reactive power supply of a hybrid power-generating facility defined in this master's thesis.
- Verification of the results using a in power industry widely used simulation program (DIgSILENT PowerFactory).
- Development and performing experiments to verify the calculation results in the active grid operation of a power-generating facility (110 kV grid).

# 2 Theory and methods

## 2.1 General relevance and use of the load flow analysis

Load flow analysis is used to calculate the resulting operational states (e.g. the utilized capacity of lines or transformers) of the operating assets in an electric power transmission system based on known or predicted consumption or generation forecasts. The results are the basis for the operation and planning of an energy system [10, 11]. The load flow analysis usually deals with symmetrically operated three-phase electric power systems. For this reason, the calculation is done in the positive sequence system. To further simplify the calculation, the usual practice is to perform the calculations in per unit values. The three-phase apparent power or the line-to-line voltage is often used as the base values [10].

The load flow analysis is the basis for the results of this master's thesis. A symmetrical three-phase system was also assumed. For this reason, all calculations were also done in the positive sequence system with per unit values. In contrast to the classic electrical circuit analysis with known voltage sources or current sources, there are different types of nodes in the load flow analysis, which make the load flow analysis a non-linear problem. In most cases, the node types contain a power constraint (active or reactive power) at a grid node. The non-linearity of the problem arises due to these power constraints. In general, a distinction is usually made between the following nodes (see [10–12]):

- $PQ$ - node:

  The $PQ$ - node indicates a constant active and reactive power input or output at a specific node in the system. In certain cases, the reactive or active power consumption/supply can also be varied using a voltage-dependent function. This node can be used to model a load or a generator.

- $PV$ - node:

  The $PV$ - node specifies the active power consumption/supply and the voltage applied to the node.

- Slack - node:

  The Slack - node defines the voltage apmlitude and angle at the connected node. The slack node is usually a very powerful node in the system. It balances the active and reactive power in the simulation (power balance).

As already mentioned, due to the non-linear power specifications at the grid nodes, a non-linear system of equations must be solved. The methods mostly used today are based on iterative procedures. Until 1930, the necessary technical resources in terms of IT were not available, which is the reason why load flow analyses were carried out manually at that time [13]. Subsequently, different methods were developed for the iterative solution of such problems. Two methods for load flow analysis are excerpted in the list below (see[10, 14]).

- Node method:

  The node method is based on the calculation of the admittance matrix [10]. If the admittance matrix is multiplied by the nodal voltages, this gives the nodal currents. The node currents are not known due to the node types described above (power specifications at the nodes). For this reason, an iterative process is introduced in which the node currents at the different nodes are calculated based on a certain starting distribution of the node voltages. The resulting node voltages can then be recalculated and the process repeated [10]. A more detailed explanation of this process is provided in the following chapters. The nodal method can be further optimized, for example using the Gauss-Seidel method or the relaxation method [10]. The Gauss-Seidel method is a relatively simple and straightforward method. In terms of convergence, more iteration steps are required compared to the Newton method [14].

- Newton method:

  The Newton method is based on the power balance method at the nodes. The solution considers a linearization of the non-linear system. A so-called functional matrix is calculated for this purpose. The method has a faster convergence compared to the Gauss-Seidel method [14]. In addition, it is easier to incorporate a $PV$ - node in this method [10]. The Newton method was not used for this master's thesis, for this reason the calculation with this method is not discussed in detail.

## 2.2 Structure of a classic power-generating facility

The structure of power-generating facilities can differ depending on the region and the structures that have grown historically. In this master's thesis, a structure was chosen that describes as many of the mentioned possibilities for building a power-generating facility (see Figure 2).

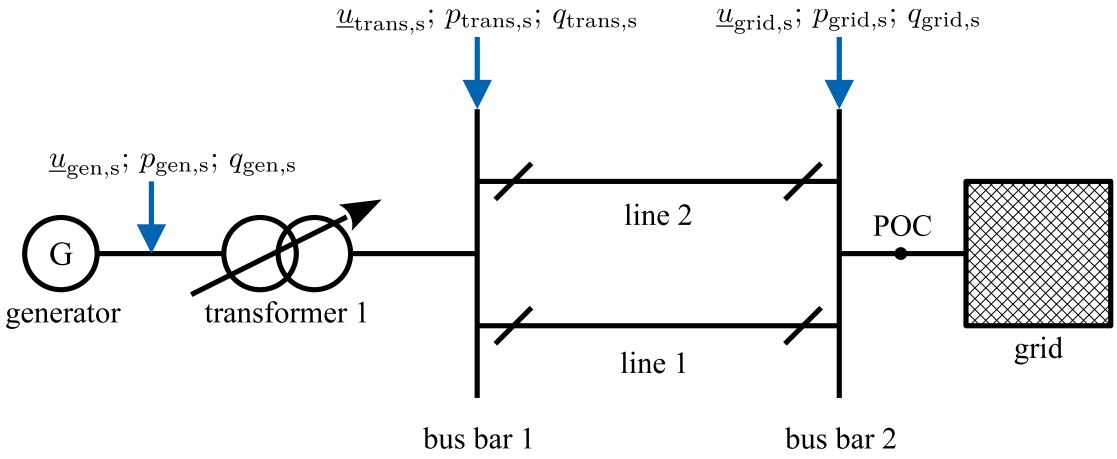


Figure 2: Structure of a classic power-generating facility (single line representation)

This topology can also be used to describe the power-generating facilities that use hydropower, which are very common in Austria. As can be seen in Figure 2, a generator feeds into the grid via a transformer and a double-circuit line. A so-called point of connection POC must be defined for a power-generating facility. This is usually located at the point where the ownership boundaries between the energy supplier and the grid operator lies. The exact position of the point of connection is defined in the grid connection contract [7]. In Figure 2, the POC is located between the line and the grid.

This point was selected on purpose as it requires the most effort for the calculation (reactive power demand of the line and the transformer must be taken into account). If the POC is located between the transformer and the start of the double-circuit line, the calculation is simplified. If there is no line in the grid to be examined, the electrical parameters of the line can be easily adjusted so that they are not included in the calculation. The same is valid for the presence of a simple line instead of a double-circuit line.

## 2.3 Used per unit values for the load flow analysis

As already mentioned in the previous chapters, it is common practice to use per unit values for load flow analysis [10]. In the following chapters, the load flow analysis is carried out for a hybrid power-generating facility and a classic power-generating facility. Both calculations are carried out using per unit values.

Two base voltages are required for the calculation of the classic power-generating facilities due to the transformer. The base voltage $U_{\mathrm{b,lv,t1}}$ is relevant for the variables on the low-voltage side of transformer 1. The base voltage $U_{\mathrm{b,hv}}$ is relevant for variables on the high-voltage side of the transformer. It is also necessary to define a base apparent power $S_{\mathrm{b}}$.

In the case of the hybrid power-generating facility, a base voltage $U_{\mathrm{b,lv,t2}}$ must also be defined for transformer 2 on the low-voltage side of transformer 2. As the two transformers are connected in parallel on the high-voltage side in the hybrid power-generating facility, the base voltage $U_{\mathrm{b,hv}}$ can also be used on the high-voltage side. A base apparent power $S_{\mathrm{b}}$ is also defined for the hybrid power-generating facility.

The reference values described here can be chosen completely freely, but it is recommended to choose meaningful values such as rated voltages or rated apparent power. For this reason, only a general base apparent power $S_{\mathrm{b}}$ or base voltage $U_{\mathrm{b,hv}}$, $U_{\mathrm{b,lv,t1}}$ and $U_{\mathrm{b,lv,t2}}$ is specified in this master's thesis for the derivation of the load flow analysis. For the result plots the base values are seperatly indicated.

The base apparent power and base voltages can then be used to calculate the base impedances. Since all variables were transformed to the upper voltage side of the transformers, only the reference impedance $Z_{\mathrm{b}}$ for the upper voltage side is required for the calculations (see formula (1)).

$$Z_{\mathrm{b}} = \frac{{U_{\mathrm{b,hv}}}^2}{S_{\mathrm{b}}} \tag{1}$$

## 2.4 Modeling of an overhead line or cable

As already mentioned in the introduction, the load flow analysis is carried out for symmetrical three-phase electric power systems. For this reason, all operating assets are modeled in the positive sequence system. Figure 3 and 4 shows the model of an overhead line/cable used in the load flow analysis (see [15, 16]).

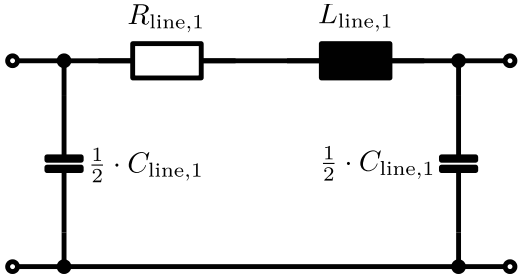


Figure 3: Line 1 model used for the load flow analysis [15]

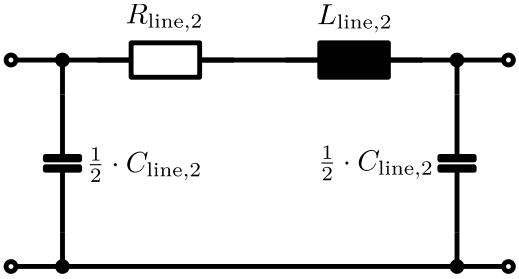


Figure 4: Line 2 model used for the load flow analysis [15]

The resistance $R_{\text{line},1}$ are responsible for the ohmic losses of the line. The inductance $L_{\text{line},1}$ and $L_{\text{line},2}$ models the inductive behavior of the line. In addition to the mentioned components, the quadrature capacitances $C_{\text{line},1}$ and $C_{\text{line},2}$ act in the line model. These capacitances are particularly important for cables due to the capacitive reactive power [15].

Ohmic resistances/admittances are sometimes (for precise loss considerations in the high and extra-high voltage grid) also implemented in quadrature direction. These model corona losses that occur [15]. In the modeling chosen here, these corona losses were neglected. For this purpose, the admittances for the corona losses would only have to be added to the main diagonal of the admittance matrix. It can be assumed that these are not relevant for the load flow analysis in this master's thesis. In most cases, the line parameters (eg. $R'_{\text{line},1}$) are referred to the length. The conversion of these parameters is shown in formula (2) to (7). Line 1 has a length $l_{\text{line},1}$, line 2 has a length $l_{\text{line},2}$.

$$R_{\text{line},1} = R'_{\text{line},1} \cdot l_{\text{line},1} \tag{2}$$

$$L_{\text{line},1} = L'_{\text{line},1} \cdot l_{\text{line},1} \tag{3}$$

$$C_{\text{line},1} = C'_{\text{line},1} \cdot l_{\text{line},1} \tag{4}$$

$$R_{\text{line},2} = R'_{\text{line},2} \cdot l_{\text{line},2} \tag{5}$$

$$L_{\text{line},2} = L'_{\text{line},2} \cdot l_{\text{line},2} \tag{6}$$

$$C_{\text{line},2} = C'_{\text{line},2} \cdot l_{\text{line},2} \tag{7}$$

In order to be able to carry out the load flow analysis, it is necessary to model each asset using an admittance matrix. By representing the line in the form of a pi equivalent circuit diagram, the admittance matrix of the line can be determined directly from the circuit. For this purpose, the main diagonal contains the sum of all admittances at a node. The minor diagonals describe the admittances between 2 nodes. The negative admittances are taken into account in the minor diagonal. The earth potential is selected as the reference node. The admittance matrix of the line thus has the dimension 2x2. Formula (8) to (11) shows the admittance matrix of line 1 and line 2 (with the angular frequency $\omega = 2 \cdot \pi \cdot f$).

$$\underline{\mathbf{Y}}_{\text{line},1} = Z_{\text{b}} \cdot \begin{bmatrix} \frac{1}{R_{\text{line},1}+\text{j}\cdot\omega\cdot L_{\text{line},1}} + \text{j}\cdot\omega\cdot\frac{C_{\text{line},1}}{2} & -\frac{1}{R_{\text{line},1}+\text{j}\cdot\omega\cdot L_{\text{line},1}} \\ -\frac{1}{R_{\text{line},1}+\text{j}\cdot\omega\cdot L_{\text{line},1}} & \frac{1}{R_{\text{line},1}+\text{j}\cdot\omega\cdot L_{\text{line},1}} + \text{j}\cdot\omega\cdot\frac{C_{\text{line},1}}{2} \end{bmatrix} \tag{8}$$

$$\underline{\mathbf{Y}}_{\text{line},1} = \begin{bmatrix} \underline{y}_{\text{line},1,(1,1)} & \underline{y}_{\text{line},1,(1,2)} \\ \underline{y}_{\text{line},1,(2,1)} & \underline{y}_{\text{line},1,(2,2)} \end{bmatrix} \tag{9}$$

$$\underline{\mathbf{Y}}_{\text{line},2} = Z_{\text{b}} \cdot \begin{bmatrix} \frac{1}{R_{\text{line},2}+\text{j}\cdot\omega\cdot L_{\text{line},2}} + \text{j}\cdot\omega\cdot\frac{C_{\text{line},2}}{2} & -\frac{1}{R_{\text{line},2}+\text{j}\cdot\omega\cdot L_{\text{line},2}} \\ -\frac{1}{R_{\text{line},2}+\text{j}\cdot\omega\cdot L_{\text{line},2}} & \frac{1}{R_{\text{line},2}+\text{j}\cdot\omega\cdot L_{\text{line},2}} + \text{j}\cdot\omega\cdot\frac{C_{\text{line},2}}{2} \end{bmatrix} \tag{10}$$

$$\underline{\mathbf{Y}}_{\text{line},2} = \begin{bmatrix} \underline{y}_{\text{line},2,(1,1)} & \underline{y}_{\text{line},2,(1,2)} \\ \underline{y}_{\text{line},2,(2,1)} & \underline{y}_{\text{line},2,(2,2)} \end{bmatrix} \tag{11}$$

## 2.5 Modeling the transformer with tap changer

As can be seen in Figure 2, transformer 1 (step-up transformer) is located after the generator. For the load flow analysis, it is necessary to describe this transformer in terms of an electrical model. The electrical operational behavior of a transformer is generally defined by two tests. The short-circuit test describes the copper losses and the leakage reactance of the transformer [15]. The open-circuit test determines the main reactance or iron losses [15].

When modeling the two step-up transformers in this thesis for load flow analysis, the iron losses and the main reactance were neglected. By taking the main reactance into account, the hysteresis effects and non-linearity would also have to be included in the calculation. This would greatly increase the calculation time. It can be assumed that neglecting the main reactance or iron losses has a minor effect on the results of the load flow analysis. The results of the short-circuit test are usually given as a short-circuit voltage $u_{\text{k,t1}}$ or $u_{\text{k,t2}}$ [15]. Furthermore, the short-circuit test provides an ohmic short-circuit voltage $u_{\text{kr,t1}}$ or $u_{\text{kr,t2}}$ [15]. The ohmic short-circuit voltage describes the ohmic component of the short-circuit impedance,

the short-circuit voltage itself describes the short-circuit impedance. The values are usually given as a percentage of the transformer's base impedance.

An important factor for the load flow analysis is that step-up transformers often have a transformer tap changer. Those makes it possible to change the transmission ratio during operation of the transformer. In most cases, the transformer tap changer is located on the high-voltage side of the transformer. The reason for this is that the current on the high-voltage side is lower than on the low-voltage side and it is therefore technically easier to make the switching contact [17]. By means of complex switching, it is possible to select different taps in the high-voltage winding without interruption using tap changers and thus change the transmission ratio (see blue box in Figure 5) [17].

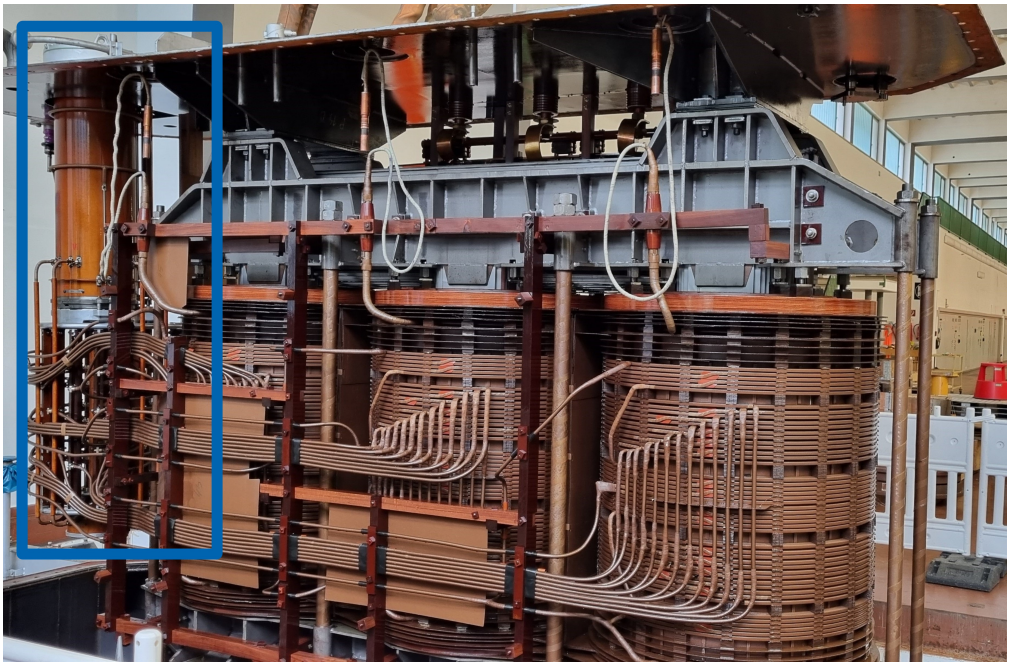

Figure 5: Tap changer with winding taps (blue box) in a step-up transformer in Austria

It should be noted that varying the tap position also slightly changes the short-circuit voltage. In practice an additional voltage ($\Delta u_{\mathrm{r,t1,hv,tap}}$ or $\Delta u_{\mathrm{r,t2,hv,tap}}$) as the percentage of the rated voltage $U_{\mathrm{r,t1,hv}}$ or $U_{\mathrm{r,t2,hv}}$ on the high-voltage side is used for modeling the tap changer. So this additional voltage describes the percentage by which the high-voltage side terminal voltage changes when the tap changer position ($\kappa_{\mathrm{t1,tap}}$ or $\kappa_{\mathrm{t2,tap}}$) is varied by one step. The transformer tap changer is in the middle position when the variables $\kappa_{\mathrm{t1,tap}}$ or $\kappa_{\mathrm{t2,tap}}$ are at the value 0.

Formula (12) and (13) show the admittance transformed to the high-voltage side of the transformer 1 and 2. The tap changer was taken into account in the calculation.

$$\underline{y}_{\mathrm{t1}} = \left(u_{\mathrm{kr,t1}} + \mathrm{j}\sqrt{{u_{\mathrm{k,t1}}}^2 - {u_{\mathrm{kr,t1}}}^2}\right)^{-1} \cdot \frac{S_{\mathrm{r,t1}}}{\left[U_{\mathrm{r,t1,hv}} \cdot (1 + \kappa_{\mathrm{t1,tap}} \cdot \Delta u_{\mathrm{r,t1,hv,tap}})\right]^2} \cdot Z_{\mathrm{b}} \tag{12}$$

$$\underline{y}_{\mathrm{t2}} = \left(u_{\mathrm{kr,t2}} + \mathrm{j}\sqrt{{u_{\mathrm{k,t2}}}^2 - {u_{\mathrm{kr,t2}}}^2}\right)^{-1} \cdot \frac{S_{\mathrm{r,t2}}}{\left[U_{\mathrm{r,t2,hv}} \cdot (1 + \kappa_{\mathrm{t2,tap}} \cdot \Delta u_{\mathrm{r,t2,hv,tap}})\right]^2} \cdot Z_{\mathrm{b}} \tag{13}$$

In formula (14) and (15), the transmission ratio of the two transformers is defined in parts per unit.

$$t_1 = \frac{U_{\mathrm{b,lv,t1}} \cdot U_{\mathrm{r,t1,hv}} \cdot (1 + \kappa_{\mathrm{t1,tap}} \cdot \Delta u_{\mathrm{r,t1,hv,tap}})}{U_{\mathrm{r,t1,lv}} \cdot U_{\mathrm{b,hv}}} \tag{14}$$

$$t_2 = \frac{U_{\mathrm{b,lv,t2}} \cdot U_{\mathrm{r,t2,hv}} \cdot (1 + \kappa_{\mathrm{t2,tap}} \cdot \Delta u_{\mathrm{r,t2,hv,tap}})}{U_{\mathrm{r,t2,lv}} \cdot U_{\mathrm{b,hv}}} \tag{15}$$

In order to be able to carry out the load flow analysis, the transformer model must be available in the form of an admittance matrix. The following calculations describe how to calculate the admittance matrix for transformer 1 [10]. The calculation for transformer 2 is identical to that for transformer 1, which is why only the calculation for the admittance matrix of transformer 1 is carried out.

Figure 6 shows the transformer model taking the transmission ratio into account. Any phase shift between the high and low voltage sides of the transformer is not relevant for the load flow analysis and is therefore not taken into account.

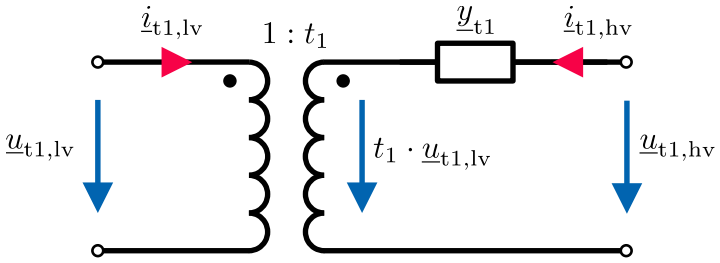


Figure 6: Transformer model of transformer 1

At the beginning of the calculation, the power balance in equation (16) can be set up on the transformer terminals. In equation (16), it can be seen that the transmission ratio is in conjugate form. Since the phase shift between the high-voltage and low-voltage sides of the transformer is not taken into account, the transmission ratio is assumed to be a real value.

$$\underline{u}_{\mathrm{t1,lv}} \cdot \underline{i}_{\mathrm{t1,lv}}{}^{*} + t_1 \cdot \underline{u}_{\mathrm{t1,lv}} \cdot \underline{i}_{\mathrm{t1,hv}}{}^{*} = 0 \text{ VA} \Longrightarrow \underline{i}_{\mathrm{t1,lv}} = -\underbrace{t_1{}^{*}}_{t_1} \cdot \underline{i}_{\mathrm{t1,hv}} \tag{16}$$

Next, it is necessary to express the current on the high-voltage side of the transformer by the high-voltage side and low-voltage side terminal voltage (see equation (17)).

$$\underline{i}_{\mathrm{t1,hv}} = \left(\underline{u}_{\mathrm{t1,hv}} - t_1 \cdot \underline{u}_{\mathrm{t1,lv}}\right) \cdot \underline{y}_{\mathrm{t1}} \tag{17}$$

If equation (17) is inserted into equation (16), the low-voltage-side current is obtained as a function of the high-voltage and low-voltage-side terminal voltage (see equation (18)).

$$\underline{i}_{\mathrm{t1,lv}} = \left(t_1{}^{2} \cdot \underline{u}_{\mathrm{t1,lv}} - t_1 \cdot \underline{u}_{\mathrm{t1,hv}}\right) \cdot \underline{y}_{\mathrm{t1}} \tag{18}$$

Equations (17) and (18) can be used to write the system of equations shown in equation (19). The matrix $\underline{\mathbf{Y}}_{\mathrm{t1}}$ represents the admittance matrix of transformer 1.

$$\begin{bmatrix} \underline{i}_{\mathrm{t1,lv}} \\ \underline{i}_{\mathrm{t1,hv}} \end{bmatrix} = \underbrace{\begin{bmatrix} t_1{}^{2} \cdot \underline{y}_{\mathrm{t1}} & -t_1 \cdot \underline{y}_{\mathrm{t1}} \\ -t_1 \cdot \underline{y}_{\mathrm{t1}} & \underline{y}_{\mathrm{t1}} \end{bmatrix}}_{\underline{\mathbf{Y}}_{\mathrm{t1}}} \cdot \begin{bmatrix} \underline{u}_{\mathrm{t1,lv}} \\ \underline{u}_{\mathrm{t1,hv}} \end{bmatrix} \tag{19}$$

As no phase shift between the high-voltage side and the low-voltage side has been taken into account for the transformer, it is also possible to define a pi equivalent circuit for the two transformers. To do this, it is necessary to rewrite the admittance matrix.

As already mentioned, the main diagonal contains the sum of all admittances at a node. The minor diagonal contains the negative admittances that connect the nodes. Taking this condition into account, the admittance matrices for transformers 1 and 2 are obtained (see formula (20) and (21) ).

$$\underline{\mathbf{Y}}_{\mathrm{t1}} = \begin{bmatrix} {t_1}^2 \cdot \underline{y}_{\mathrm{t1}} & -t_1 \cdot \underline{y}_{\mathrm{t1}} \\ -t_1 \cdot \underline{y}_{\mathrm{t1}} & \underline{y}_{\mathrm{t1}} \end{bmatrix} = \begin{bmatrix} ({t_1}^2 - t_1) \cdot \underline{y}_{\mathrm{t1}} + t_1 \cdot \underline{y}_{\mathrm{t1}} & -t_1 \cdot \underline{y}_{\mathrm{t1}} \\ -t_1 \cdot \underline{y}_{\mathrm{t1}} & (1 - t_1) \cdot \underline{y}_{\mathrm{t1}} + t_1 \cdot \underline{y}_{\mathrm{t1}} \end{bmatrix} \tag{20}$$

$$\underline{\mathbf{Y}}_{\mathrm{t2}} = \begin{bmatrix} {t_2}^2 \cdot \underline{y}_{\mathrm{t2}} & -t_2 \cdot \underline{y}_{\mathrm{t2}} \\ -t_2 \cdot \underline{y}_{\mathrm{t2}} & \underline{y}_{\mathrm{t2}} \end{bmatrix} = \begin{bmatrix} ({t_2}^2 - t_2) \cdot \underline{y}_{\mathrm{t2}} + t_2 \cdot \underline{y}_{\mathrm{t2}} & -t_2 \cdot \underline{y}_{\mathrm{t2}} \\ -t_2 \cdot \underline{y}_{\mathrm{t2}} & (1 - t_2) \cdot \underline{y}_{\mathrm{t2}} + t_2 \cdot \underline{y}_{\mathrm{t2}} \end{bmatrix} \tag{21}$$

Figures 7 and 8 show the pi equivalent circuit diagrams of the two transformers.

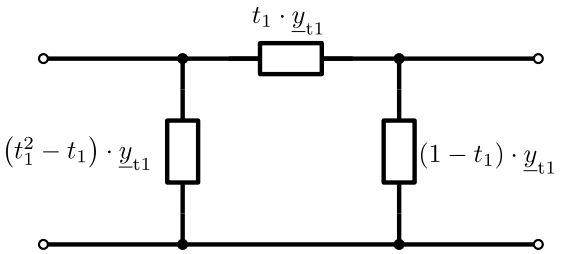


Figure 7: PI-equivalent circuit diagram of transformer 1

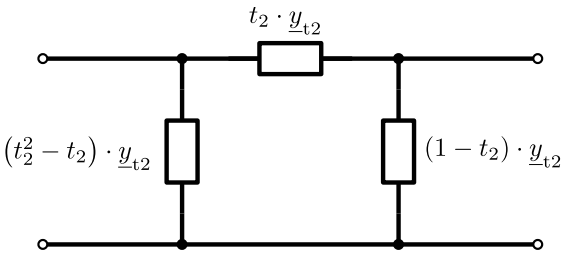


Figure 8: PI-equivalent circuit diagram of transformer 2

## 2.6 Representation of the classic power-generating facilities in the positive sequence system

The previous chapters described how to derive the admittance matrix and the associated PI equivalent circuit for the line and for the transformer. As already mentioned, the calculations were done based on the assumption of a symmetrical three-phase electric power system in the positive sequence system. All variables were converted to the high-voltage side of the transformer and based on the per unit system described above. Figure 9 shows the resulting network. The grid and the generator were generally drawn as AC source/load. Depending on the modeling (see the following chapters), this results in different electrical specifications.

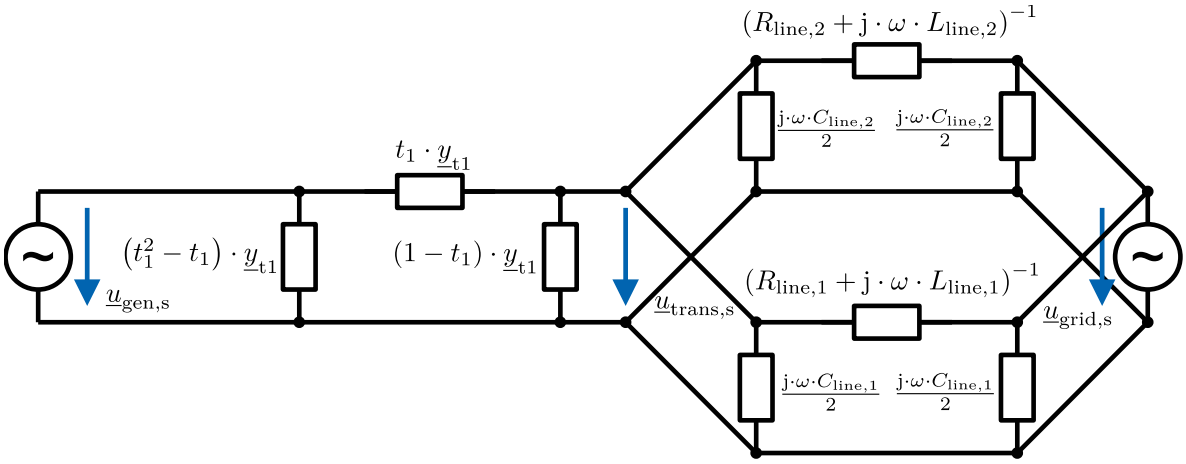


Figure 9: Representation of a classic power-generating facilities with PI-equivalent circuits

### 2.6.1 Simplification of classic power-generating facilities using chain parameters

The following chapters explain how an analytical solution for the load flow analysis can be found for the given network. For this purpose, it is necessary to analyze a circuit that is as simple as possible. To ensure this, the circuit consisting of the transformer and the double-circuit line is combined into an equivalent circuit (also a PI element). Chain parameters are used for this purpose.

Due to the linearity between currents and voltages in a circuit with linear admittances/impedances, this simplification does not lead to any approximation of the resulting outcomes. In the course of the simplification, the node on the high-voltage side of the transformer is removed from the system of equations respectively the circuit. This is not a limitation, as the power or voltage at this node can be determined after the load flow analysis has been carried out.

In the 1st step, the admittance matrices of the two lines are added due to the parallel connection (see equation (22) and (23)). The resulting matrix describes the entire double-circuit line, again in the form of an admittance matrix. Figure 10 shows the resulting network.

$$\underline{\mathbf{Y}}_{\text{line},1,2} = \underline{\mathbf{Y}}_{\text{line},1} + \underline{\mathbf{Y}}_{\text{line},2} = \begin{bmatrix} \underline{y}_{\text{line},1,(1,1)} + \underline{y}_{\text{line},2,(1,1)} & \underline{y}_{\text{line},1,(1,2)} + \underline{y}_{\text{line},2,(1,2)} \\ \underline{y}_{\text{line},1,(2,1)} + \underline{y}_{\text{line},2,(2,1)} & \underline{y}_{\text{line},1,(2,2)} + \underline{y}_{\text{line},2,(2,2)} \end{bmatrix} \tag{22}$$

$$\underline{\mathbf{Y}}_{\text{line},1,2} = \begin{bmatrix} \underline{y}_{\text{line},1,2,(1,1)} & \underline{y}_{\text{line},1,2,(1,2)} \\ \underline{y}_{\text{line},1,2,(2,1)} & \underline{y}_{\text{line},1,2,(2,2)} \end{bmatrix} \tag{23}$$

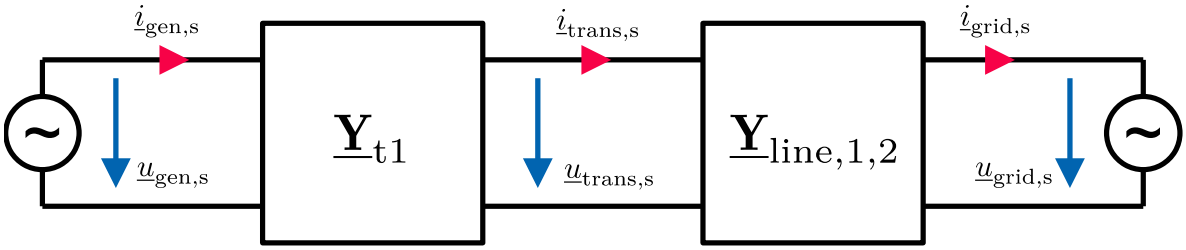


Figure 10: Circuit of a classic power-generating facility with the simplified double-circuit line

Figure 10 shows that the network simplified in the first step consists of an interconnection of 2 admittance matrices. In order to simplify the circuit further, the admittance matrices are converted into chain matrices. The conversion is explained using matrix $\underline{\mathbf{Y}}_{\text{line},1,2}$, the calculation steps are the same for matrix $\underline{\mathbf{Y}}_{\text{t1}}$.

To the beginning it is necessary to set up the system of equations for the two ports of the admittance matrix (see equation (24)). Note that the generator convention was used at the gate at POC and the load convention was used at the gate at the beginning of the double-circuit line. This is advantageous for the resulting chain matrix, but has the consequence that the current $\underline{i}_{\text{grid,s}}$ appears negatively in the equations.

$$\begin{bmatrix} \underline{i}_{\text{trans,s}} \\ -\underline{i}_{\text{grid,s}} \end{bmatrix} = \underbrace{\begin{bmatrix} \underline{y}_{\text{line},1,2,(1,1)} & \underline{y}_{\text{line},1,2,(1,2)} \\ \underline{y}_{\text{line},1,2,(2,1)} & \underline{y}_{\text{line},1,2,(2,2)} \end{bmatrix}}_{\underline{\mathbf{Y}}_{\text{line},1,2}} \cdot \begin{bmatrix} \underline{u}_{\text{trans,s}} \\ \underline{u}_{\text{grid,s}} \end{bmatrix} \tag{24}$$

From the 2nd equation of the system of equations (24), the voltage $\underline{u}_{\mathrm{trans,s}}$ can be represented as in equations (25).

$$\underline{u}_{\mathrm{trans,s}} = -\frac{1}{\underline{y}_{\mathrm{line,1,2,(2,1)}}} \cdot \left(\underline{y}_{\mathrm{line,1,2,(2,2)}} \cdot \underline{u}_{\mathrm{grid,s}} + \underline{i}_{\mathrm{grid,s}}\right) \tag{25}$$

If equation (25) is inserted into the first equation from the system of equations (24), equation (26) and (27) is obtained.

$$\underline{i}_{\mathrm{trans,s}} = -\frac{\underline{y}_{\mathrm{line,1,2,(1,1)}}}{\underline{y}_{\mathrm{line,1,2,(2,1)}}} \cdot \left(\underline{y}_{\mathrm{line,1,2,(2,2)}} \cdot \underline{u}_{\mathrm{grid,s}} + \underline{i}_{\mathrm{grid,s}}\right) + \underline{y}_{\mathrm{line,1,2,(1,2)}} \cdot \underline{u}_{\mathrm{grid,s}} \tag{26}$$

$$\underline{i}_{\mathrm{trans,s}} = -\frac{1}{\underline{y}_{\mathrm{line,1,2,(2,1)}}} \cdot \left(\det\left(\underline{\mathbf{Y}}_{\mathrm{line,1,2}}\right) \cdot \underline{u}_{\mathrm{grid,s}} + \underline{y}_{\mathrm{line,1,2,(1,1)}} \cdot \underline{i}_{\mathrm{grid,s}}\right) \tag{27}$$

The system of equations with the chain parameters can be written from equations (25) and (27) (see equation 15).

$$\begin{bmatrix} \underline{u}_{\mathrm{trans,s}} \\ \underline{i}_{\mathrm{trans,s}} \end{bmatrix} = \underbrace{-\frac{1}{\underline{y}_{\mathrm{line,1,2,(2,1)}}} \cdot \begin{bmatrix} \underline{y}_{\mathrm{line,1,2,(2,2)}} & 1 \\ \det\left(\underline{\mathbf{Y}}_{\mathrm{line,1,2}}\right) & \underline{y}_{\mathrm{line,1,2,(1,1)}} \end{bmatrix}}_{\underline{\mathbf{A}}_{\mathrm{line,1,2}}} \cdot \begin{bmatrix} \underline{u}_{\mathrm{grid,s}} \\ \underline{i}_{\mathrm{grid,s}} \end{bmatrix} \tag{28}$$

Equations (29) and (30) show the chain matrices for transformer 1 and the double-circuit line.

$$\underline{\mathbf{A}}_{\mathrm{line,1,2}} = -\frac{1}{\underline{y}_{\mathrm{line,1,2,(2,1)}}} \cdot \begin{bmatrix} \underline{y}_{\mathrm{line,1,2,(2,2)}} & 1 \\ \det\left(\underline{\mathbf{Y}}_{\mathrm{line,1,2}}\right) & \underline{y}_{\mathrm{line,1,2,(1,1)}} \end{bmatrix} \tag{29}$$

$$\underline{\mathbf{A}}_{\mathrm{t1}} = -\frac{1}{-t_1 \cdot \underline{y}_{\mathrm{t1}}} \cdot \begin{bmatrix} \underline{y}_{\mathrm{t1}} & 1 \\ \det\left(\underline{\mathbf{Y}}_{\mathrm{t1}}\right) & {t_1}^2 \cdot \underline{y}_{\mathrm{t1}} \end{bmatrix} \tag{30}$$

The simplified circuit using the chain matrices is shown in Figure 11.

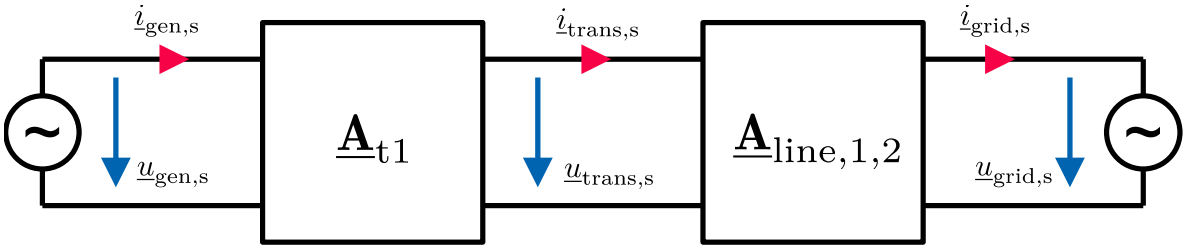


Figure 11: Circuit of a classic power-generating facility with the simplified double-circuit line (chain matrix)

The network shown in Figure 12 can be simplified. Since the port of the chain matrix at the high-voltage side transformer terminals is connected to the port at the beginning of the double-circuit line, the two chain matrices can be combined by multiplication to form a resulting chain matrix. This process is shown in formula (31) and in Figure 12.

$$\underline{\mathbf{A}}_{\mathrm{g}} = \underline{\mathbf{A}}_{\mathrm{t1}} \cdot \underline{\mathbf{A}}_{\mathrm{line,1,2}} = \begin{bmatrix} \underline{a}_{\mathrm{g},(1,1)} & \underline{a}_{\mathrm{g},(1,2)} \\ \underline{a}_{\mathrm{g},(2,1)} & \underline{a}_{\mathrm{g},(2,2)} \end{bmatrix} \tag{31}$$

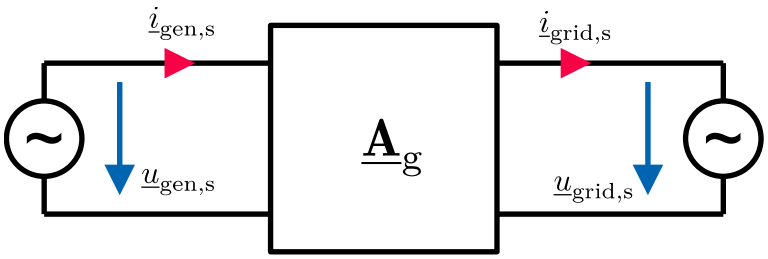


Figure 12: Total grouped circuit of a classic power-generating facility with the simplified double-circuit line (chain matrix)

## 2.7 Aspects of analytical load flow analysis

As already mentioned in the introduction, it is necessary to solve a non-linear system of equations for the load flow analysis based on the power specifications at the nodes. This system of equations is solved in modern load flow calculation programs using iterative procedures. In the course of this master's thesis, a completely different approach was chosen (for the synchronous power-generating facility).

By simplifying the network using chain matrices, it is possible to describe the structure of the classic power-generating facilities using only one remaining chain matrix. As a result, it is now possible to establish a linear relationship between the terminal voltage/current at the generator and the terminal voltage/current at POC using two equations. The power specifications at the generator terminals or at the POC can be implemented in the system of equations using non-linear constraints. This non-linear system of equations can be solved using an analytical approach due to the small number of equations and the quadratic polynomials it contains.

An analytical solution has several advantages compared to an iterative solution. The analytical approach results in all possible solutions for the problem. This point can be interpreted as

both an advantage and a disadvantage. Not every solution represents a stable operating point. For this reason, it is essential that the results are interpreted according to the stability.

In contrast to the iterative solution, the analytical approach is significantly faster in terms of calculation time (approx. factor five for the calculations in this master's thesis). In addition to the calculation time, the convergence of the calculation also plays an important role. There are no problems with convergence for analytical calculations, but convergence problems can occur when performing iterative calculations under unfavorable initial conditions. With iterative methods, it is also necessary to define a termination condition for the calculation. For this reason, every result of an iterative calculation is also subject to a certain degree of uncertainty.

The results of the analytical calculation are only limited in their accuracy by the calculation accuracy of the computer or the physical deviations of the input variables. The advantages and disadvantages of the two calculation methods are listed again in the Figure 13 and 14.

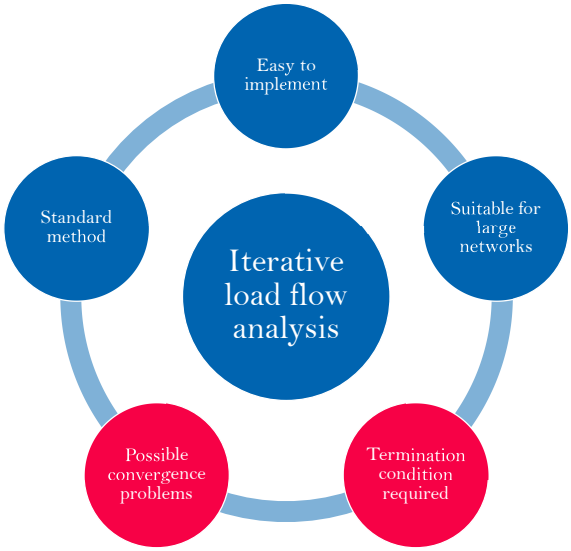


Figure 13: Advantages (blue) and disadvantages (red) of iterative load flow analysis

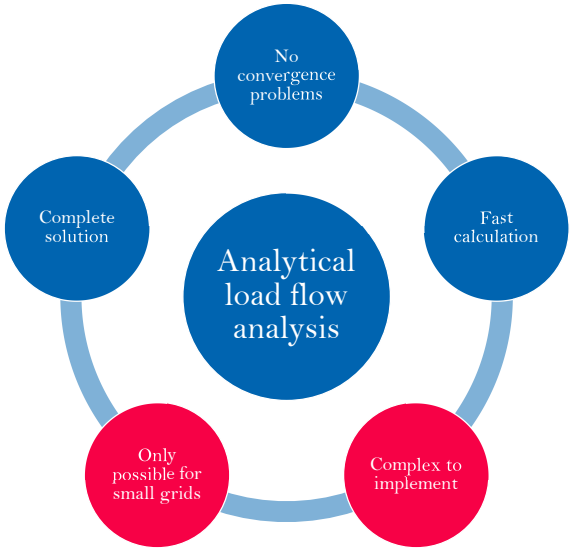


Figure 14: Advantages (blue) and disadvantages (red) of analytical load flow analysis

## 2.8 Analytical load flow analysis using the example of a $PQ$-node (generator) and slack-node (POC)

For the analytical load flow analyses in this master's thesis, the starting point is always the system of equations shown in formula (32). The matrix $\underline{\mathbf{A}}_{\mathrm{g}}$ has already been calculated (see formula (31)).

$$\begin{bmatrix} \underline{u}_{\mathrm{gen,s}} \\ \underline{i}_{\mathrm{gen,s}} \end{bmatrix} = \begin{bmatrix} \underline{a}_{\mathrm{g},(1,1)} & \underline{a}_{\mathrm{g},(1,2)} \\ \underline{a}_{\mathrm{g},(2,1)} & \underline{a}_{\mathrm{g},(2,2)} \end{bmatrix} \cdot \begin{bmatrix} \underline{u}_{\mathrm{grid,s}} \\ \underline{i}_{\mathrm{grid,s}} \end{bmatrix} \tag{32}$$

It is then necessary to define the known variables. Since the grid was modeled as a slack-node, the complex voltage $\underline{u}_{\mathrm{grid,s}}$ is known at this node. The active power $p_{\mathrm{gen,s}}$ and the reactive power $q_{\mathrm{gen,s}}$ are known at the generator terminals. The node at the generator terminals therefore leads to the non-linear constraint (see formula (33)).

$$p_{\mathrm{gen,s}} + \mathrm{j} \cdot q_{\mathrm{gen,s}} = \underline{u}_{\mathrm{gen,s}} \cdot \underline{i}_{\mathrm{gen,s}}{}^{*} \tag{33}$$

The system of equations to be solved can then be written (see formula (34) to (36) ). All elements of the matrix $\underline{\mathbf{A}}_{\mathrm{g}}$, the active power $p_{\mathrm{gen,s}}$, the reactive power $q_{\mathrm{gen,s}}$ and the voltage $\underline{u}_{\mathrm{grid,s}}$ are known. The voltage $\underline{u}_{\mathrm{gen,s}}$ and the currents $\underline{i}_{\mathrm{gen,s}}$ and $\underline{i}_{\mathrm{grid,s}}$ are unknown. To be able to describe the grid completely, it is sufficient to know all the node voltages occurring in the grid. For this reason, the voltage $\underline{u}_{\mathrm{gen,s}}$ is determined from the given system of equations.

$$\underline{u}_{\mathrm{gen,s}} = \underline{a}_{\mathrm{g},(1,1)} \cdot \underline{u}_{\mathrm{grid,s}} + \underline{a}_{\mathrm{g},(1,2)} \cdot \underline{i}_{\mathrm{grid,s}} \tag{34}$$

$$\underline{i}_{\mathrm{gen,s}} = \underline{a}_{\mathrm{g},(2,1)} \cdot \underline{u}_{\mathrm{grid,s}} + \underline{a}_{\mathrm{g},(2,2)} \cdot \underline{i}_{\mathrm{grid,s}} \tag{35}$$

$$p_{\mathrm{gen,s}} + \mathrm{j} \cdot q_{\mathrm{gen,s}} = \underline{u}_{\mathrm{gen,s}} \cdot \underline{i}_{\mathrm{gen,s}}{}^{*} \tag{36}$$

Substituting equation (36) into equation (35) gives equation (37).

$$\frac{p_{\mathrm{gen,s}} - \mathrm{j} \cdot q_{\mathrm{gen,s}}}{\underline{u}_{\mathrm{gen,s}}{}^{*}} = \underline{a}_{\mathrm{g},(2,1)} \cdot \underline{u}_{\mathrm{grid,s}} + \underline{a}_{\mathrm{g},(2,2)} \cdot \underline{i}_{\mathrm{grid,s}} \tag{37}$$

Subsequently, equation (37) is used in equation (34) and further simplified (see equations (38) to (40))

$$\underline{u}_{\mathrm{gen,s}} = \underline{a}_{\mathrm{g},(1,1)} \cdot \underline{u}_{\mathrm{grid,s}} + \frac{\underline{a}_{\mathrm{g},(1,2)}}{\underline{a}_{\mathrm{g},(2,2)}} \cdot \left( \frac{p_{\mathrm{gen,s}} - \mathrm{j} \cdot q_{\mathrm{gen,s}}}{\underline{u}_{\mathrm{gen,s}}^{*}} - \underline{a}_{\mathrm{g},(2,1)} \cdot \underline{u}_{\mathrm{grid,s}} \right) \tag{38}$$

$$\begin{aligned} \underline{u}_{\mathrm{gen,s}} \cdot \underline{u}_{\mathrm{gen,s}}^{*} = \frac{1}{\underline{a}_{\mathrm{g},(2,2)}} \Big[ & \left( \underline{a}_{\mathrm{g},(1,1)} \cdot \underline{a}_{\mathrm{g},(2,2)} - \underline{a}_{\mathrm{g},(2,1)} \cdot \underline{a}_{\mathrm{g},(1,2)} \right) \cdot \underline{u}_{\mathrm{grid,s}} \cdot \underline{u}_{\mathrm{gen,s}}^{*} \\ & + \underline{a}_{\mathrm{g},(1,2)} \cdot (p_{\mathrm{gen,s}} - \mathrm{j} \cdot q_{\mathrm{gen,s}}) \Big] \end{aligned} \tag{39}$$

$$\underline{u}_{\mathrm{gen,s}} \cdot \underline{u}_{\mathrm{gen,s}}^{*} = \frac{\det\left(\underline{\mathbf{A}}_{\mathrm{g}}\right)}{\underline{a}_{\mathrm{g},(2,2)}} \cdot \underline{u}_{\mathrm{grid,s}} \cdot \underline{u}_{\mathrm{gen,s}}^{*} + \frac{\underline{a}_{\mathrm{g},(1,2)}}{\underline{a}_{\mathrm{g},(2,2)}} \cdot (p_{\mathrm{gen,s}} - \mathrm{j} \cdot q_{\mathrm{gen,s}}) \tag{40}$$

In equation (40), the only unknown variable is the voltage $\underline{u}_{\mathrm{gen,s}}$. However, this voltage also appears in the conjugate form in the equation. For this reason, it is necessary to divide the equation into a real part and an imaginary part (see equation (41)). To make the equation simpler, the known variables are substituted ($K_1$, $K_2$, $K_3$, $K_4$).

$$\underbrace{\frac{\underbrace{\underline{u}_{\mathrm{gen,s}} \cdot \underline{u}_{\mathrm{gen,s}}^{*}}}{\mathrm{Re}\left\{\underline{u}_{\mathrm{gen,s}}\right\}^2 + \mathrm{Im}\left\{\underline{u}_{\mathrm{gen,s}}\right\}^2}}_{} = \underbrace{\frac{\det\left(\underline{\mathbf{A}}_{\mathrm{g}}\right)}{\underline{a}_{\mathrm{g},(2,2)}} \cdot \underline{u}_{\mathrm{grid,s}}}_{K_1 + \mathrm{j} \cdot K_2} \cdot \underbrace{\frac{\underbrace{\underline{u}_{\mathrm{gen,s}}^{*}}}{\mathrm{Re}\left\{\underline{u}_{\mathrm{gen,s}}\right\} - \mathrm{j} \cdot \mathrm{Im}\left\{\underline{u}_{\mathrm{gen,s}}\right\}}}_{} + \underbrace{\frac{\underline{a}_{\mathrm{g},(1,2)}}{\underline{a}_{\mathrm{g},(2,2)}} \cdot (p_{\mathrm{gen,s}} - \mathrm{j} \cdot q_{\mathrm{gen,s}})}_{K_3 + \mathrm{j} \cdot K_4} \tag{41}$$

If equation (41) is separated into an equation for the real part and one for the imaginary part, equations (42) and (43) are obtained.

$$\mathrm{Re}\left\{\underline{u}_{\mathrm{gen,s}}\right\}^2 + \mathrm{Im}\left\{\underline{u}_{\mathrm{gen,s}}\right\}^2 = K_1 \cdot \mathrm{Re}\left\{\underline{u}_{\mathrm{gen,s}}\right\} + K_2 \cdot \mathrm{Im}\left\{\underline{u}_{\mathrm{gen,s}}\right\} + K_3 \tag{42}$$

$$0 = K_2 \cdot \mathrm{Re}\left\{\underline{u}_{\mathrm{gen,s}}\right\} - K_1 \cdot \mathrm{Im}\left\{\underline{u}_{\mathrm{gen,s}}\right\} + K_4 \tag{43}$$

Equation (43) can be used to determine the imaginary part of the voltage $\mathrm{Im}\left\{\underline{u}_{\mathrm{gen,s}}\right\}$ as a function of the real part of the voltage $\mathrm{Re}\left\{\underline{u}_{\mathrm{gen,s}}\right\}$ (see Equation (44)).

$$\mathrm{Im}\left\{\underline{u}_{\mathrm{gen,s}}\right\} = \frac{K_2}{K_1} \cdot \mathrm{Re}\left\{\underline{u}_{\mathrm{gen,s}}\right\} + \frac{K_4}{K_1} \tag{44}$$

Inserting equation (44) into equation (42) results in a quadratic equation (see equation (45)).

$$\begin{aligned} \mathrm{Re}\left\{\underline{u}_{\mathrm{gen,s}}\right\}^2 + \frac{2 \cdot K_2 \cdot K_4 - {K_1}^3 - K_1 \cdot {K_2}^2}{{K_1}^2 + {K_2}^2} \cdot \mathrm{Re}\left\{\underline{u}_{\mathrm{gen,s}}\right\} \\ + \frac{{K_4}^2 - K_1 \cdot K_2 \cdot K_4 - {K_1}^2 \cdot K_3}{{K_1}^2 + {K_2}^2} = 0 \end{aligned} \tag{45}$$

The solution for $\mathrm{Re}\left\{\underline{u}_{\mathrm{gen,s}}\right\}$ can be written as shown in equation (46).

$$\mathrm{Re}\left\{\underline{u}_{\mathrm{gen,s}}\right\} = -\frac{2\cdot K_2\cdot K_4 - {K_1}^3 - K_1\cdot {K_2}^2}{({K_1}^2+{K_2}^2)\cdot 2} \pm \left[\left(\frac{2\cdot K_2\cdot K_4 - {K_1}^3 - K_1\cdot {K_2}^2}{({K_1}^2+{K_2}^2)\cdot 2}\right)^2 - \frac{{K_4}^2 - K_1\cdot K_2\cdot K_4 - {K_1}^2\cdot K_3}{{K_1}^2+{K_2}^2}\right]^{-\frac{1}{2}} \tag{46}$$

To find the imaginary part of the voltage $\mathrm{Im}\left\{\underline{u}_{\mathrm{gen,s}}\right\}$, it is only necessary to insert the solution from equation (46) into equation (44). Equation (46) shows that it is a quadratic equation for the real part of the voltage, for this reason there are also 2 solutions. The interpretation of the two solutions is discussed in the following chapters. By setting up mesh and node equations and use of equation (36), it is possible to calculate the voltage at the high-voltage side transformer terminals (see equation (47)-(48)).

$$\underline{u}_{\mathrm{trans,s}} = \underline{u}_{\mathrm{gen,s}} - \left(\underline{i}_{\mathrm{gen,s}} - \underline{u}_{\mathrm{gen,s}}\cdot\left({t_1}^2 - t_1\right)\cdot \underline{y}_{\mathrm{t1}}\right)\cdot\frac{1}{t_1\cdot\underline{y}_{\mathrm{t1}}} \tag{47}$$

$$\underline{u}_{\mathrm{trans,s}} = \underline{u}_{\mathrm{gen,s}}\cdot t_1 - \frac{p_{\mathrm{gen,s}} - \mathrm{j}\cdot q_{\mathrm{gen,s}}}{{\underline{u}_{\mathrm{gen,s}}}^*\cdot t_1\cdot\underline{y}_{\mathrm{t1}}} \tag{48}$$

The current $\underline{i}_{\mathrm{grid,s}}$ can be calculated based on equation (34) as shown in equation (49).

$$\underline{i}_{\mathrm{grid,s}} = \frac{\underline{u}_{\mathrm{gen,s}}}{\underline{a}_{\mathrm{g},(1,2)}} - \frac{\underline{a}_{\mathrm{g},(1,1)}\cdot\underline{u}_{\mathrm{grid,s}}}{\underline{a}_{\mathrm{g},(1,2)}} \tag{49}$$

Finally the power at POC can be calculated using formula (50).

$$p_{\mathrm{grid,s}} + \mathrm{j}\cdot q_{\mathrm{grid,s}} = \underline{u}_{\mathrm{grid,s}}\cdot {\underline{i}_{\mathrm{grid,s}}}^* \tag{50}$$

## 2.9 Analytical load flow analysis with different constraints

Looking at the analytical load flow analysis procedure, it is clear that the constraints can be chosen freely. In addition to the usual constraints at the nodes, more unusual constraints can also be selected. This is particularly necessary in view of the computational speed and efficient problem solving in the course of this master's thesis.

For the following examples, only the approach for solving the systems of equations is given. The analytical solution of these systems of equations is mathematically quite time-consuming. For the development of the MATLAB code, all systems of equations listed here were calculated analytically by the author. An exact execution of these calculations is not useful for the written part of the master's thesis due to the relatively high calculation effort.

### 2.9.1 Analytical load flow calculation of a $p_{\mathrm{gen,s}}$, $\left|\underline{u}_{\mathrm{gen,s}}\right|$ node (generator) and slack-node (POC)

For this load flow analysis, the absolute value of the voltage $\left|\underline{u}_{\mathrm{gen,s}}\right|$ and the active power $p_{\mathrm{gen,s}}$ are known at the generator terminals. Furthermore, the complex voltage $\underline{u}_{\mathrm{grid,s}}$ at the POC is known. Equations (34) and (35) are required for the calculations. In addition, equation (53) must be added as a constraint. In this case, it makes sense to determine the real- and the imaginary part of the complex exponential function $\mathrm{e}^{\mathrm{j}\cdot\arg\left\{\underline{u}_{\mathrm{gen,s}}\right\}}$. This leads to the situation that a further constraint is required (see equation (54)).

$$\left|\underline{u}_{\mathrm{gen,s}}\right| \cdot \mathrm{e}^{\mathrm{j}\cdot\arg\left\{\underline{u}_{\mathrm{gen,s}}\right\}} = \underline{a}_{\mathrm{g},(1,1)} \cdot \underline{u}_{\mathrm{grid,s}} + \underline{a}_{\mathrm{g},(1,2)} \cdot \underline{i}_{\mathrm{grid,s}} \tag{51}$$

$$\underline{i}_{\mathrm{gen,s}} = \underline{a}_{\mathrm{g},(2,1)} \cdot \underline{u}_{\mathrm{grid,s}} + \underline{a}_{\mathrm{g},(2,2)} \cdot \underline{i}_{\mathrm{grid,s}} \tag{52}$$

$$p_{\mathrm{gen,s}} + \mathrm{j} \cdot q_{\mathrm{gen,s}} = \left|\underline{u}_{\mathrm{gen,s}}\right| \cdot \mathrm{e}^{\mathrm{j}\cdot\arg\left\{\underline{u}_{\mathrm{gen,s}}\right\}} \cdot \underline{i}_{\mathrm{gen,s}}{}^{*} \tag{53}$$

$$1 = \mathrm{Re}\left\{\mathrm{e}^{\mathrm{j}\cdot\arg\left\{\underline{u}_{\mathrm{gen,s}}\right\}}\right\}^2 + \mathrm{Im}\left\{\mathrm{e}^{\mathrm{j}\cdot\arg\left\{\underline{u}_{\mathrm{gen,s}}\right\}}\right\}^2 \tag{54}$$

Looking at the system of equations (see equation (51)-(54)), it can be seen that the currents $\underline{i}_{\mathrm{gen,s}}$ and $\underline{i}_{\mathrm{grid,s}}$, the reactive power $q_{\mathrm{gen,s}}$ and the angle $\arg\left\{\underline{u}_{\mathrm{gen,s}}\right\}$ are unknown. The unknown variables can be determined using the four given equations. To do this, it is most efficient to start by determining the real and imaginary parts of the complex exponential function $\mathrm{e}^{\mathrm{j}\cdot\arg\left\{\underline{u}_{\mathrm{gen,s}}\right\}}$. Therefore it is necessary to separate the equations into real and imaginary parts. Subsequently, the reactive power at the generator terminals can be determined. Finally, the remaining unknown variables in the circuit can be calculated using formulas (48), (49) and (50).

### 2.9.2 Analytical load flow calculation of a $q_{\mathrm{gen,s}}$ node (generator) and $p_{\mathrm{grid,s}}$, $\underline{u}_{\mathrm{grid,s}}$ node (POC)

For this load flow analysis, the reactive power $q_{\mathrm{gen,s}}$ is known at the generator terminals. Furthermore, the complex voltage $\underline{u}_{\mathrm{grid,s}}$ and the active power $p_{\mathrm{grid,s}}$ at the POC are known. Equations (34) and (35) are required for the calculations. In addition, equations (57) and (58) must be added as a constraint.

$$\underline{u}_{\mathrm{gen,s}} = \underline{a}_{\mathrm{g},(1,1)} \cdot \underline{u}_{\mathrm{grid,s}} + \underline{a}_{\mathrm{g},(1,2)} \cdot \underline{i}_{\mathrm{grid,s}} \tag{55}$$

$$\underline{i}_{\mathrm{gen,s}} = \underline{a}_{\mathrm{g},(2,1)} \cdot \underline{u}_{\mathrm{grid,s}} + \underline{a}_{\mathrm{g},(2,2)} \cdot \underline{i}_{\mathrm{grid,s}} \tag{56}$$

$$p_{\mathrm{gen,s}} + \mathrm{j} \cdot q_{\mathrm{gen,s}} = \underline{u}_{\mathrm{gen,s}} \cdot \underline{i}_{\mathrm{gen,s}}^{\,*} \tag{57}$$

$$p_{\mathrm{grid,s}} + \mathrm{j} \cdot q_{\mathrm{grid,s}} = \underline{u}_{\mathrm{grid,s}} \cdot \underline{i}_{\mathrm{grid,s}}^{\,*} \tag{58}$$

Looking at the system of equations (see equation (55) to (58)), it can be seen that the currents $\underline{i}_{\mathrm{gen,s}}$ and $\underline{i}_{\mathrm{grid,s}}$, the active power $p_{\mathrm{gen,s}}$, the reactive power $q_{\mathrm{grid,s}}$ and the voltage $\underline{u}_{\mathrm{gen,s}}$ are unknown. This means that 3 complex and 2 real variables are unknown. The given system of equations consists of 4 complex-valued equations, which can be divided into real and imaginary parts. This gives eight real-valued equations. With them, it is possible to determine the real and imaginary part of the voltage $\underline{u}_{\mathrm{gen,s}}$. Subsequently, it is necessary to determine the active power $p_{\mathrm{gen,s}}$ at the generator terminals from the given equations. The remaining unknown variables in the circuit can be calculated using formulas (48), (49) and (50).

### 2.9.3 Analytical load flow calculation of a $\left|\underline{u}_{\mathrm{gen,s}}\right|$ node (generator) and $p_{\mathrm{grid,s}}$, $\underline{u}_{\mathrm{grid,s}}$ node (POC)

For this load flow analysis, the absolute value of the voltage $\left|\underline{u}_{\mathrm{gen,s}}\right|$ is known at the generator terminals. Furthermore, the complex voltage $\underline{u}_{\mathrm{grid,s}}$ and the active power $p_{\mathrm{grid,s}}$ at the POC are known. Equations (34) and (35) are required for the calculations. In addition, equations (61), (62) and (63) must be added as a constraint.

$$\left|\underline{u}_{\mathrm{gen,s}}\right| \cdot \mathrm{e}^{\mathrm{j} \cdot \arg\left\{\underline{u}_{\mathrm{gen,s}}\right\}} = \underline{a}_{\mathrm{g},(1,1)} \cdot \underline{u}_{\mathrm{grid,s}} + \underline{a}_{\mathrm{g},(1,2)} \cdot \underline{i}_{\mathrm{grid,s}} \tag{59}$$

$$\underline{i}_{\mathrm{gen,s}} = \underline{a}_{\mathrm{g},(2,1)} \cdot \underline{u}_{\mathrm{grid,s}} + \underline{a}_{\mathrm{g},(2,2)} \cdot \underline{i}_{\mathrm{grid,s}} \tag{60}$$

$$p_{\mathrm{gen,s}} + \mathrm{j} \cdot q_{\mathrm{gen,s}} = \left|\underline{u}_{\mathrm{gen,s}}\right| \cdot \mathrm{e}^{\mathrm{j} \cdot \arg\left\{\underline{u}_{\mathrm{gen,s}}\right\}} \cdot \underline{i}_{\mathrm{gen,s}}^{\,*} \tag{61}$$

$$p_{\mathrm{grid,s}} + \mathrm{j} \cdot q_{\mathrm{grid,s}} = \underline{u}_{\mathrm{grid,s}} \cdot \underline{i}_{\mathrm{grid,s}}^{\,*} \tag{62}$$

$$1 = \mathrm{Re}\left\{\mathrm{e}^{\mathrm{j} \cdot \arg\left\{\underline{u}_{\mathrm{gen,s}}\right\}}\right\}^2 + \mathrm{Im}\left\{\mathrm{e}^{\mathrm{j} \cdot \arg\left\{\underline{u}_{\mathrm{gen,s}}\right\}}\right\}^2 \tag{63}$$

Looking at the system of equations (see equation (59) to (63)), it can be seen that the currents $\underline{i}_{\mathrm{gen,s}}$ and $\underline{i}_{\mathrm{grid,s}}$, the reactive power $q_{\mathrm{gen,s}}$ and $q_{\mathrm{grid,s}}$, the active power $p_{\mathrm{gen,s}}$ and the angle $\arg\left\{\underline{u}_{\mathrm{gen,s}}\right\}$ are unknown. Again, the approach for solving the equation is similar. It is necessary to determine the real and imaginary parts of the complex exponential function $\mathrm{e}^{\mathrm{j}\cdot\arg\left\{\underline{u}_{\mathrm{gen,s}}\right\}}$. To do this, the complex-valued equations must again be separated into real and imaginary parts. In contrast to the previous calculations, in this system of equations it is necessary to determine both the active power $p_{\mathrm{gen,s}}$ and the reactive power $q_{\mathrm{gen,s}}$ at the generator terminals from the equation. The remaining variables can then be calculated using the using formulas (48), (49) and (50).

### 2.9.4 Analytical load flow calculation of a $\underline{u}_{\mathrm{grid,s}}$, $p_{\mathrm{grid,s}}$, $q_{\mathrm{grid,s}}$ node (POC)

This load flow analysis is a special case, the complex voltage $\underline{u}_{\mathrm{grid,s}}$, the active power $p_{\mathrm{grid,s}}$ and the reactive power $q_{\mathrm{grid,s}}$ are known at POC. Equations (34) and (35) are required for the calculations. In addition, equations (66) must be added as a constraint.

$$\underline{u}_{\mathrm{gen,s}} = \underline{a}_{\mathrm{g},(1,1)} \cdot \underline{u}_{\mathrm{grid,s}} + \underline{a}_{\mathrm{g},(1,2)} \cdot \underline{i}_{\mathrm{grid,s}} \tag{64}$$

$$\underline{i}_{\mathrm{gen,s}} = \underline{a}_{\mathrm{g},(2,1)} \cdot \underline{u}_{\mathrm{grid,s}} + \underline{a}_{\mathrm{g},(2,2)} \cdot \underline{i}_{\mathrm{grid,s}} \tag{65}$$

$$p_{\mathrm{grid,s}} + \mathrm{j} \cdot q_{\mathrm{grid,s}} = \underline{u}_{\mathrm{grid,s}} \cdot \underline{i}_{\mathrm{grid,s}}^{\,*} \tag{66}$$

Solving the system of equations (equations (64) to (66)) is quite simple. To do this, equation (66) is reformulated to the current $\underline{i}_{\mathrm{grid,s}}$. The resulting equation can then be inserted into equations (64)and (65). This gives the voltage $\underline{u}_{\mathrm{gen,s}}$ and the current $\underline{i}_{\mathrm{gen,s}}$. By applying equation (36), the active and reactive power at the generator terminals is obtained. The remaining variables can then be calculated using the using formulas (48), (49) and (50).

## 2.10 Interpretation of the two solutions of the analytical load flow analysis regarding stability

It is already clear from the previous chapters that the results of the analytical load flow analysis of a classic power-generating facility (see Figure 2) are based on the solution of quadratic polynomials. This means that the solutions must be analyzed with regard to their stability. In the following, the investigation with regard to stability is discussed in more detail. In Figure 15, the absolut value of the voltage $\underline{u}_{\mathrm{grid,s}}$ is plotted over the reactive power $q_{\mathrm{grid,s}}$.The calculations were performed using an analytical load flow calculation of a $\left|\underline{u}_{\mathrm{gen,s}}\right|$, $p_{\mathrm{gen,s}}$ node (generator) and slack-node (POC) (see chapter 2.9.1). The generator active power $p_{\mathrm{gen,s}}$ and generator terminal voltage $\underline{u}_{\mathrm{gen,s}}$ were kept constant at a value of 1 pu. Subsequently, the grid voltage $\underline{u}_{\mathrm{grid,s}}$ could be varied within the limits shown. The resulting reactive power is shown in the plot below.

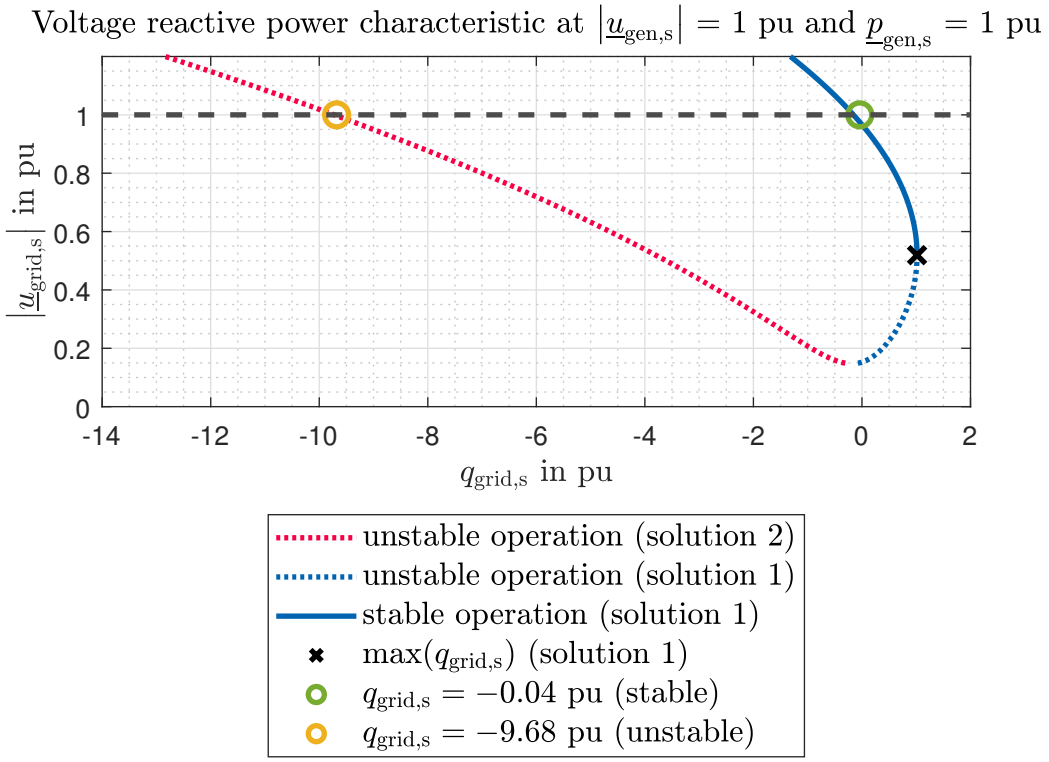


Figure 15: Representation of the two solutions of the analytical load flow analysis (load convention)

The solution of the quadratic polynomial provides 2 results (red and blue curve) for the reactive power $q_{\mathrm{grid,s}}$. In order to ensure static stability (for a standard load), it is known that only those points that lie above the maximum of the blue curve are stable (see [18]). With regard to the stability in respect to the transmission angle, another plot must be made.

Figure 16 shows both the generator active power $p_{\mathrm{gen,s}}$ and the reactive power $q_{\mathrm{grid,s}}$ at POC. It should be noted that, in contrast to Figure 15, the generator convention was used here. The choice of the convention was made on purpose, as both representations in the literature [18] usually take this form.

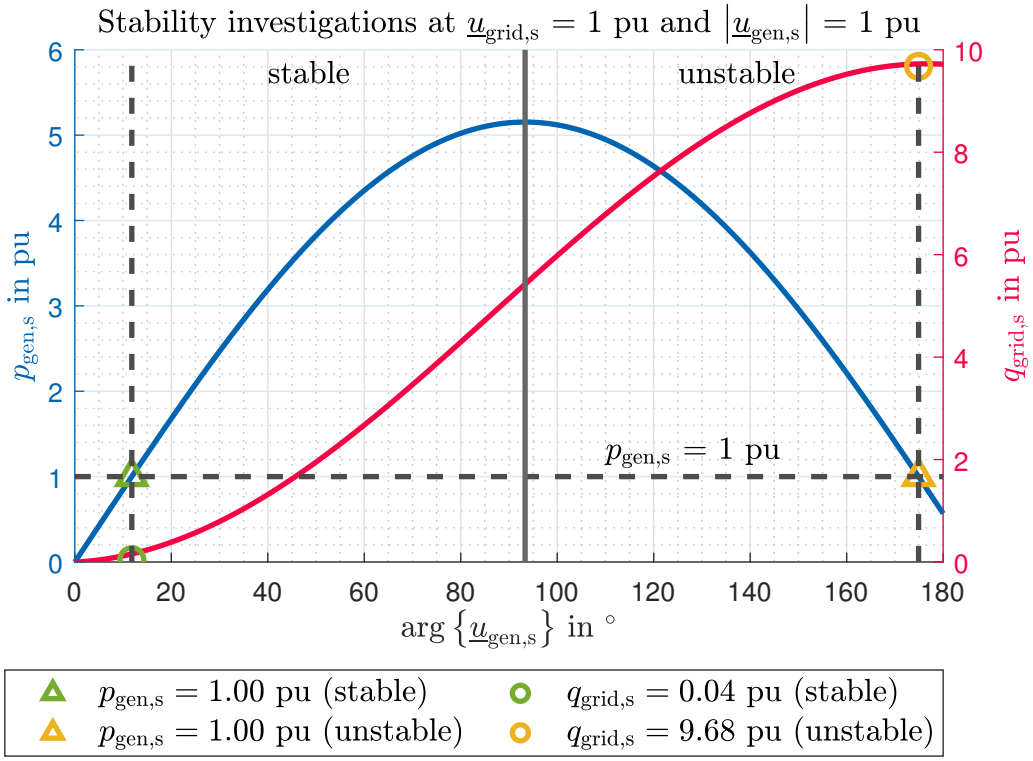


Figure 16: Investigation of stability with regard to the transmission angle (generator convention)

Looking at Figure 16, the solid black line represents the maximum of the active power curve. Angles arg $\{\underline{u}_{\mathrm{gen,s}}\}$ below this so-called critical angle are stable operating points. This can be interpreted as follows [15, 18]. An increase in the mechanical power at the turbine leads to an increase in the angle arg $\{\underline{u}_{\mathrm{gen,s}}\}$. For stable operating points (left part of the curve), this also means an increase in the electrically delivered power $p_{\mathrm{gen,s}}$. On the left-hand side of the curve, an increase in the angle arg $\{\underline{u}_{\mathrm{gen,s}}\}$ would mean a reduction in the active power output $p_{\mathrm{gen,s}}$ and thus lead to an unstable operating point (see [18]). In general, it should also be noted that it is not the absolute value of the angle arg $\{\underline{u}_{\mathrm{gen,s}}\}$ that is relevant, but the angle difference between the angles arg $\{\underline{u}_{\mathrm{grid,s}}\}$ and arg $\{\underline{u}_{\mathrm{gen,s}}\}$. Since the angle arg $\{\underline{u}_{\mathrm{grid,s}}\}$ is 0° in the selected example, the chosen interpretation is valid. The curves shown in Figure 16 were plotted at a grid voltage $\underline{u}_{\mathrm{grid,s}}$ of 1 pu. Furthermore, the value of the generator terminal voltage $\underline{u}_{\mathrm{gen,s}}$ was fixed at 1 pu.

For both Figure 15 and 16, the tap changer position was set to the middle position and a standard 110 kV overhead line was used for the calculation. Figure 16 shows the reactive power values for an active power $p_{\mathrm{gen,s}}$ of 1 pu at a given grid voltage $\underline{u}_{\mathrm{grid,s}}$ of 1 pu (see orange and green circle). If you compare this with Figure 15, you can see that the intersection of the horizontal line matches the results from Figure 16 ( please notice the sign due to the different conventions). It can thus be seen that the red dashed line represents unstable operating points due to the transmission angle.

## 2.11 Structures of a hybrid power-generating facility

In the introduction to this master's thesis, it was already mentioned that due to the increasing share of renewable energy sources for the purpose of electricity generation, the consideration of hybrid power-generating facilities is becoming increasingly important. A hybrid power-generating facility is usually defined as a combination of several power-generating facilities behind a point of connection (see [19]). This definition is also associated with a large number of possible variants for such hybrid power-generating facilities. The aim of this master's thesis is to develop a methodology for calculating the reactive power supply of a hybrid power-generating facility. For this reason, the structure of a hybrid power-generating facility shown in Figure 17 was chosen.

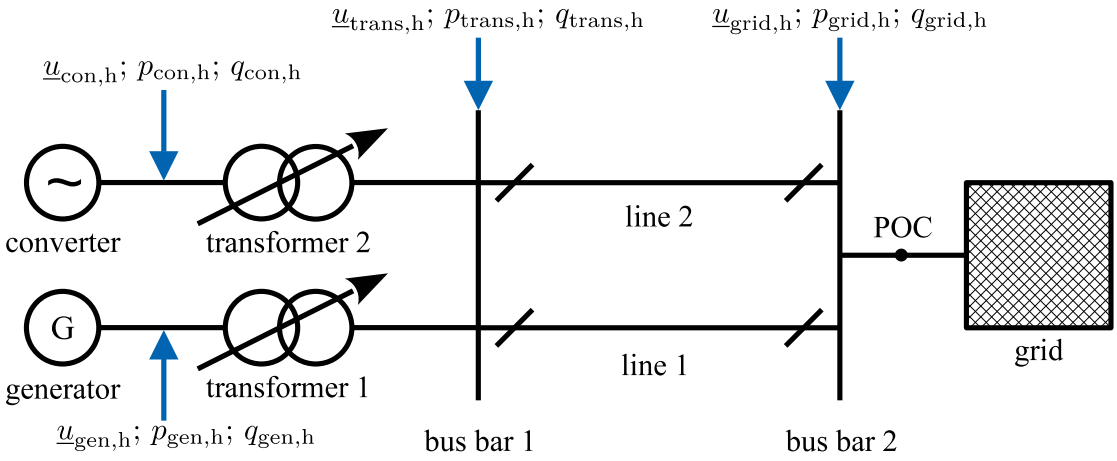


Figure 17: Structure of a hybrid power-generating facility (single line representation)

This structure can also be simulated in the planned test procedure. The hybrid power-generating facility discussed in this master's thesis has a synchronous generator on the one hand and a converter on the other.

The generator and the converter each have a step up transformer (transformer 1 and transformer 2) connected in parallel on the high-voltage side. The energy is transported via a double-circuit line (line 1 and line 2). At the end of the double-circuit line is the point of connection, which connects the line to the grid. The tap changer of the two step up transformers is also taken into account for the modeling.

## 2.12 Electrical modeling of the hybrid power-generating facility using addmittance matrices

Figure 18 shows a hybrid power-generating facility in the form of a PI equivalent circuit diagram.

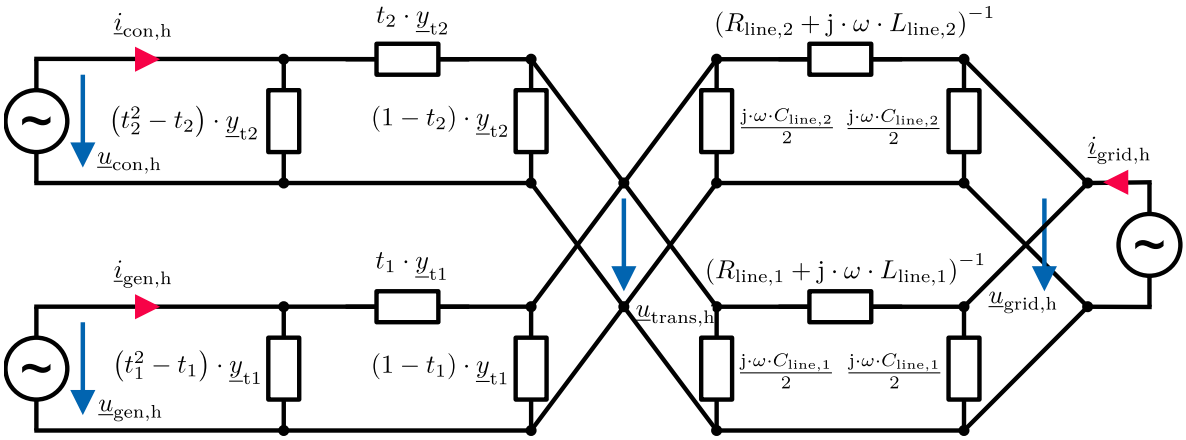


Figure 18: Representation of a hybrid power-generating facility with PI equivalent circuits

In principle, it is also possible to carry out an analytical load flow analysis for the hybrid power-generating facility. For this purpose, a system of equations is set up by applying the Helmholtz superposition principle, taking into account the non-linear constraints. This system of equations consists of 4 coupled equations. The equations again contain second degree polynomials. The solution of such systems of equations requires an iterative mathematical approach.

The analytical approach described here has the advantage that, similar to the example already described, the entirety of all possible solutions is obtained. As this is not necessary for the load flow analysis presented here and no calculation time is saved from the analytical load flow analysis due to the mathematical iterative solution, the load flow calculations for calculating the hybrid power-generating facility were carried out using an iterative load flow calculation method (Gauss-Seidel method).

In most cases, the starting point for an iterative load flow analysis is the admittance matrix of the circuit. The electrical derivation of the PI equivalent circuit diagrams was done in chapters 2.4 and 2.5. The generator, converter and grid were again generally modeled AC sources due to the different constraints. In contrast to analytical load flow analysis (using chain matrices), the source at POC is drawn in the generator convention.

## 2.13 Performing the iterative load flow analysis for the hybrid power-generating facility

At the beginning of the calculations, it is necessary to set up the admittance matrix of the circuit to be examined (see equation (67)) [10]. To keep the matrix as simple as possible, the results of equation (23) were chosen to describe the elements of the double-circuit line.

$$\underbrace{\begin{bmatrix} {t_1}^2 \cdot \underline{y}_{\mathrm{t1}} & 0 & -t_1 \cdot \underline{y}_{\mathrm{t1}} & 0 \\ 0 & {t_2}^2 \cdot \underline{y}_{\mathrm{t2}} & -t_2 \cdot \underline{y}_{\mathrm{t2}} & 0 \\ -t_1 \cdot \underline{y}_{\mathrm{t1}} & -t_2 \cdot \underline{y}_{\mathrm{t2}} & \underline{y}_{\mathrm{t1}} + \underline{y}_{\mathrm{t2}} + \underline{y}_{\mathrm{line,1,2,(1,1)}} & \underline{y}_{\mathrm{line,1,2,(1,2)}} \\ 0 & 0 & \underline{y}_{\mathrm{line,1,2,(1,2)}} & \underline{y}_{\mathrm{line,1,2,(2,2)}} \end{bmatrix}}_{\underline{\mathbf{Y}}_{\mathrm{c,h}}} \cdot \begin{bmatrix} \underline{u}_{\mathrm{gen,h}} \\ \underline{u}_{\mathrm{con,h}} \\ \underline{u}_{\mathrm{trans,h}} \\ \underline{u}_{\mathrm{grid,h}} \end{bmatrix} = \begin{bmatrix} \underline{i}_{\mathrm{gen,h}} \\ \underline{i}_{\mathrm{con,h}} \\ 0 \\ \underline{i}_{\mathrm{grid,h}} \end{bmatrix} \tag{67}$$

For all calculations to be performed, the complex voltage at POC is known (slack-node). For this reason, the last row and column of the system of equations (see equation (67)) can be eliminated. The iteration variable $\xi$ was introduced as part of this. It specifies the current iteration step. For example, if the inverse of the admittance matrix is multiplied by the node current vector, one iteration has passed.

$$\begin{bmatrix} {t_1}^2 \cdot \underline{y}_{\mathrm{t1}} & 0 & -t_1 \cdot \underline{y}_{\mathrm{t1}} \\ 0 & {t_2}^2 \cdot \underline{y}_{\mathrm{t2}} & -t_2 \cdot \underline{y}_{\mathrm{t2}} \\ -t_1 \cdot \underline{y}_{\mathrm{t1}} & -t_2 \cdot \underline{y}_{\mathrm{t2}} & \underline{y}_{\mathrm{t1}} + \underline{y}_{\mathrm{t2}} + \underline{y}_{\mathrm{line,1,2,(1,1)}} \end{bmatrix} \cdot \begin{bmatrix} \underline{u}^{(\xi)}_{\mathrm{gen,h}} \\ \underline{u}^{(\xi)}_{\mathrm{con,h}} \\ \underline{u}^{(\xi)}_{\mathrm{trans,h}} \end{bmatrix} = \begin{bmatrix} \underline{i}^{(\xi)}_{\mathrm{gen,h}} \\ \underline{i}^{(\xi)}_{\mathrm{con,h}} \\ 0 \end{bmatrix} - \begin{bmatrix} 0 \\ 0 \\ \underline{y}_{\mathrm{line,1,2,(1,2)}} \end{bmatrix} \cdot \underline{u}_{\mathrm{grid,h}} \tag{68}$$

For a better structure, equation (68) is substituted with the following variables (see equation (69)).

$$\underline{\mathbf{Y}}_{\mathrm{h}} \cdot \underline{\mathbf{U}}^{(\xi)}_{\mathrm{h}} = \underline{\mathbf{I}}^{(\xi)}_{\mathrm{h}} \tag{69}$$

Subsequently, the Gauss-Seidel method is implemented based on [10]. For this purpose, equation (69) is multiplied by a diagonal matrix from the left, with the result that the main diagonal elements of $\underline{\mathbf{Y}}_{\mathrm{h,sc}}$ become 1 (see equation (70) to (74))

$$\underline{\mathbf{Y}}_{\mathrm{h,sc}} = \begin{bmatrix} {t_1}^2 \cdot \underline{y}_{\mathrm{t1}} & 0 & 0 \\ 0 & {t_2}^2 \cdot \underline{y}_{\mathrm{t2}} & 0 \\ 0 & 0 & \underline{y}_{\mathrm{t1}} + \underline{y}_{\mathrm{t2}} + \underline{y}_{\mathrm{line,1,2,(1,1)}} \end{bmatrix}^{-1} \cdot \begin{bmatrix} {t_1}^2 \cdot \underline{y}_{\mathrm{t1}} & 0 & -t_1 \cdot \underline{y}_{\mathrm{t1}} \\ 0 & {t_2}^2 \cdot \underline{y}_{\mathrm{t2}} & -t_2 \cdot \underline{y}_{\mathrm{t2}} \\ -t_1 \cdot \underline{y}_{\mathrm{t1}} & -t_2 \cdot \underline{y}_{\mathrm{t2}} & \underline{y}_{\mathrm{t1}} + \underline{y}_{\mathrm{t2}} + \underline{y}_{\mathrm{line,1,2,(1,1)}} \end{bmatrix} \tag{70}$$

$$\underline{\mathbf{Y}}_{\mathrm{h,sc}} = \begin{bmatrix} 1 & 0 & {-t_1}^{-1} \\ 0 & 1 & {-t_2}^{-1} \\ \frac{-t_1 \cdot \underline{y}_{\mathrm{t1}}}{\underline{y}_{\mathrm{t1}} + \underline{y}_{\mathrm{t2}} + \underline{y}_{\mathrm{line,1,2,(1,1)}}} & \frac{-t_2 \cdot \underline{y}_{\mathrm{t2}}}{\underline{y}_{\mathrm{t1}} + \underline{y}_{\mathrm{t2}} + \underline{y}_{\mathrm{line,1,2,(1,1)}}} & 1 \end{bmatrix} \tag{71}$$

$$\underline{\mathbf{I}}_{\mathrm{h,sc}}^{(\xi)} = \begin{bmatrix} {t_1}^2 \cdot \underline{y}_{\mathrm{t1}} & 0 & 0 \\ 0 & {t_2}^2 \cdot \underline{y}_{\mathrm{t2}} & 0 \\ 0 & 0 & \underline{y}_{\mathrm{t1}} + \underline{y}_{\mathrm{t2}} + \underline{y}_{\mathrm{line,1,2,(1,1)}} \end{bmatrix}^{-1} \cdot \left( \begin{bmatrix} \underline{i}_{\mathrm{gen,h}}^{(\xi)} \\ \underline{i}_{\mathrm{con,h}}^{(\xi)} \\ 0 \end{bmatrix} - \begin{bmatrix} 0 \\ 0 \\ \underline{y}_{\mathrm{line,1,2,(1,2)}} \end{bmatrix} \cdot \underline{u}_{\mathrm{grid,h}} \right) \tag{72}$$

$$\underline{\mathbf{I}}_{\mathrm{h,sc}}^{(\xi)} = \begin{bmatrix} \frac{\underline{i}_{\mathrm{gen,h}}^{(\xi)}}{{t_1}^2 \cdot \underline{y}_{\mathrm{t1}}} \\ \frac{\underline{i}_{\mathrm{con,h}}^{(\xi)}}{{t_2}^2 \cdot \underline{y}_{\mathrm{t2}}} \\ \frac{-\underline{y}_{\mathrm{line,1,2,(1,2)}}}{\underline{y}_{\mathrm{t1}} + \underline{y}_{\mathrm{t2}} + \underline{y}_{\mathrm{line,1,2,(1,1)}}} \cdot \underline{u}_{\mathrm{grid,h}} \end{bmatrix} \tag{73}$$

$$\underline{\mathbf{Y}}_{\mathrm{h,sc}} \cdot \underline{\mathbf{U}}_{\mathrm{h}}^{(\xi)} = \underline{\mathbf{I}}_{\mathrm{h,sc}}^{(\xi)} \tag{74}$$

The matrix $\underline{\mathbf{Y}}_{\mathrm{h,sc}}$ is decomposed into a strictly upper triangular matrix $\underline{\mathbf{R}}_{\mathrm{h,sc}}$, a strictly lower triangular matrix $\underline{\mathbf{L}}_{\mathrm{h,sc}}$ and the identity matrix $\mathbf{E}_{\mathrm{h,sc}}$ (see equation (75) to (78)). This decomposition is necessary because the calculation takes into account that the already known values of the current iteration step must also be considered when calculating the new values. This leads to a faster convergence of the iterative load flow analysis.

$$\underline{\mathbf{Y}}_{\mathrm{h,sc}} = \underline{\mathbf{L}}_{\mathrm{h,sc}} + \mathbf{E}_{\mathrm{h,sc}} + \underline{\mathbf{R}}_{\mathrm{h,sc}} \tag{75}$$

$$\underline{\mathbf{L}}_{\mathrm{h,sc}} = \begin{bmatrix} 0 & 0 & 0 \\ 0 & 0 & 0 \\ \frac{-t_1 \cdot \underline{y}_{\mathrm{t1}}}{\underline{y}_{\mathrm{t1}} + \underline{y}_{\mathrm{t2}} + \underline{y}_{\mathrm{line,1,2,(1,1)}}} & \frac{-t_2 \cdot \underline{y}_{\mathrm{t2}}}{\underline{y}_{\mathrm{t1}} + \underline{y}_{\mathrm{t2}} + \underline{y}_{\mathrm{line,1,2,(1,1)}}} & 0 \end{bmatrix} \tag{76}$$

$$\mathbf{E}_{\mathrm{h,sc}} = \begin{bmatrix} 1 & 0 & 0 \\ 0 & 1 & 0 \\ 0 & 0 & 1 \end{bmatrix} \tag{77}$$

$$\underline{\mathbf{R}}_{\mathrm{h,sc}} = \begin{bmatrix} 0 & 0 & -{t_1}^{-1} \\ 0 & 0 & -{t_2}^{-1} \\ 0 & 0 & 0 \end{bmatrix} \tag{78}$$

Since the strictly lower triangular matrix now appears in the equation, it is possible to use actual values for the calculation of the nodal voltages in the $\xi + 1$ iteration step. For this reason, the matrix $\underline{\mathbf{L}}_{\mathrm{h,sc}}$ is multiplied by the vector $\underline{\mathbf{U}}_{\mathrm{h}}^{(\xi+1)}$. The calculation rule is as follows (see equation (79) to (80)) [10].

$$\left(\underline{\mathbf{L}}_{\mathrm{h,sc}} + \mathbf{E}_{\mathrm{h,sc}}\right) \cdot \underline{\mathbf{U}}_{\mathrm{h}}^{(\xi+1)} + \underline{\mathbf{R}}_{\mathrm{h,sc}} \cdot \underline{\mathbf{U}}_{\mathrm{h}}^{(\xi)} = \underline{\mathbf{I}}_{\mathrm{h,sc}}^{(\xi)} \tag{79}$$

$$\underline{\mathbf{U}}_{\mathrm{h}}^{(\xi+1)} = -\left(\underline{\mathbf{L}}_{\mathrm{h,sc}} + \mathbf{E}_{\mathrm{h,sc}}\right)^{-1} \cdot \underline{\mathbf{R}}_{\mathrm{h,sc}} \cdot \underline{\mathbf{U}}_{\mathrm{h}}^{(\xi)} + \left(\underline{\mathbf{L}}_{\mathrm{h,sc}} + \mathbf{E}_{\mathrm{h,sc}}\right)^{-1} \cdot \underline{\mathbf{I}}_{\mathrm{h,sc}}^{(\xi)} \tag{80}$$

### 2.13.1 Iterativ load flow calculation of a $p_{\mathbf{gen,h}}$, $\left|\underline{u}_{\mathbf{gen,h}}\right|$ node (generator) and $p_{\mathbf{con,h}}$, $\left|\underline{u}_{\mathbf{con,h}}\right|$ node (converter) with a slack node at POC

For this calculation, the active power $p_{\mathrm{gen,h}}$ and the magnitude of the terminal voltage $\underline{u}_{\mathrm{gen,h}}$ are known at the generator terminals. Furthermore, the active power $p_{\mathrm{con,h}}$ and the magnitude of the terminal voltage $\underline{u}_{\mathrm{con,h}}$ are also known at the converter terminals. The load flow analysis will be performed with these constraints.

A start voltage distribution is defined at the beginning of the iterative load flow analysis. The complex voltage is already known at the point of connection. At the generator terminals and at the converter terminals, the magnitude of the voltage is known, the angle is at beginning assumed to be 0°. In the course of the iteration, it is necessary to calculate the reactive power for the actual node voltages in the iteration. This is done using formula (81) and (82) , which can be determined with the help of equation (67) (the convention must be observed).

$$q_{\mathrm{gen,h}}^{(\xi)} = \mathrm{Im}\left\{\left({t_1}^2 \cdot \underline{y}_{\mathrm{t1}} \cdot \underline{u}_{\mathrm{gen,h}}^{(\xi)} - t_1 \cdot \underline{y}_{\mathrm{t1}} \cdot \underline{u}_{\mathrm{trans,h}}^{(\xi)}\right)^* \cdot \underline{u}_{\mathrm{gen,h}}^{(\xi)}\right\} \tag{81}$$

$$q_{\mathrm{con,h}}^{(\xi)} = \mathrm{Im}\left\{\left({t_2}^2 \cdot \underline{y}_{\mathrm{t2}} \cdot \underline{u}_{\mathrm{con,h}}^{(\xi)} - t_2 \cdot \underline{y}_{\mathrm{t2}} \cdot \underline{u}_{\mathrm{trans,h}}^{(\xi)}\right)^* \cdot \underline{u}_{\mathrm{con,h}}^{(\xi)}\right\} \tag{82}$$

Subsequently, the vector $\underline{\mathbf{I}}_{\mathrm{h,sc}}^{(\xi)}$ can be calculated using formula (83) and (84).

$$\underline{i}_{\mathrm{gen,h}}^{(\xi)} = \left(\frac{p_{\mathrm{gen,h}} + \mathrm{j} \cdot q_{\mathrm{gen,h}}^{(\xi)}}{\underline{u}_{\mathrm{gen,h}}^{(\xi)}}\right)^* \tag{83}$$

$$\underline{i}_{\mathrm{con,h}}^{(\xi)} = \left(\frac{p_{\mathrm{con,h}} + \mathrm{j} \cdot q_{\mathrm{con,h}}^{(\xi)}}{\underline{u}_{\mathrm{con,h}}^{(\xi)}}\right)^* \tag{84}$$

Now all values required for the load flow analysis are known and the load flow calculation can be done with formula (80). After the load flow analysis, the iteration variable $\xi$ is increased by 1. The voltages at the generator terminals and the converter terminals resulting from the load flow analysis do not correspond to the specifications in terms of magnitude. For this reason, it is necessary to correct the magnitude of the voltages (the angle remains).

As already mentioned, it is required to define a termination condition for the iterative load flow analysis. In this master's thesis, a termination condition was defined in terms of the change in active or reactive power at the nodes between 2 iteration steps. Depending on the system to be examined, this value is in the tenths to hundredths of a percent range of the maximum capacity. Figure 19 shows the flow chart for the load flow analysis described.

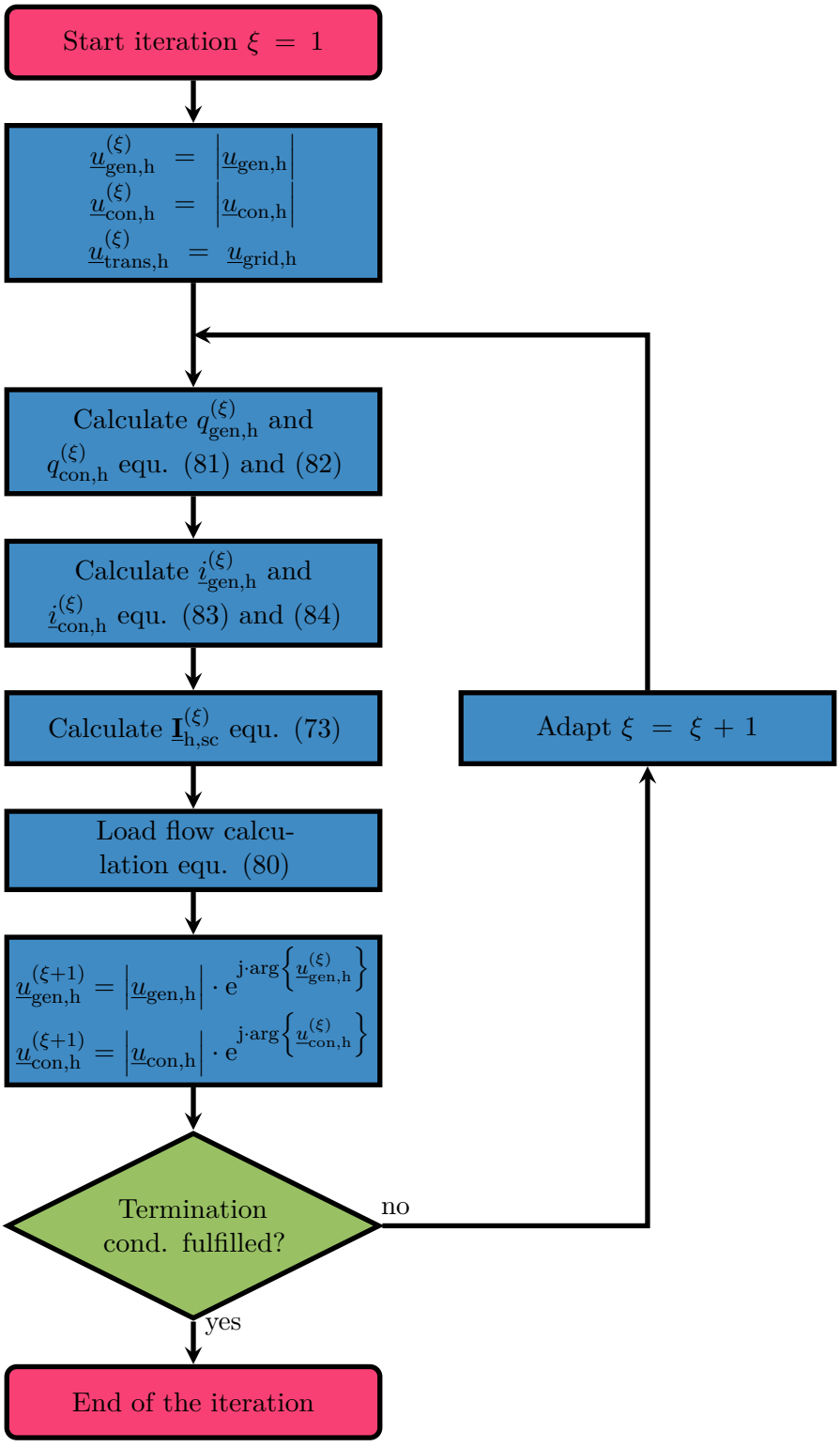


Figure 19: Flow chart of the iterativ calculation of a $p_{\mathrm{gen,h}}$, $\left|\underline{u}_{\mathrm{gen,h}}\right|$ node (generator) and $p_{\mathrm{con,h}}$, $\left|\underline{u}_{\mathrm{con,h}}\right|$ node (converter) with a slack node at POC

### 2.13.2 Iterativ load flow calculation of a $p_{\mathrm{gen,h}}$, $\left|\underline{u}_{\mathrm{gen,h}}\right|$ node (generator) and $p_{\mathrm{con,h}}$, $\left|\underline{i}_{\mathrm{con,h}}\right|$ node (converter) with a slack node at POC

With this type of load flow analysis, the active power $p_{\mathrm{gen,h}}$ and the magnitude of the voltage $\underline{u}_{\mathrm{gen,h}}$ are known at the generator terminals. The magnitude of the current $\underline{i}_{\mathrm{con,h}}$ and the output active power $p_{\mathrm{con,h}}$ of the converter are known at the converter terminals. This type of load flow analysis is quite unusual.

Due to the active power specification at the converter terminals and the generator terminals, this is still a non-linear problem. For this reason, an iterative load flow analysis is also needed. It must be noted that if the magnitude of the current $\underline{i}_{\mathrm{con,h}}$ is specified, there are 2 stable solutions. One of the two stable solutions represents a voltage-increasing (overexcited) solution and the other a voltage-reducing (underexcited) solution. Both solutions are relevant for modeling the converter. The iterative load flow analysis only converges to one of the two solutions. For this reason, the convergence of the load flow analysis must be triggered depending on the desired solution (voltage-increasing or voltage-reducing). In this master's thesis this is done using the initial condition. The two solutions differ due to their angle of the current $\underline{i}_{\mathrm{con,h}}$. By correctly selecting the initial condition for the current $\underline{i}_{\mathrm{con,h}}$, the convergence can be triggered in the desired direction (see Figure 20).

The calculations for the constraints at the generator terminals remain the same as in the example described above. It is again necessary to correct the magnitude of the voltage $\underline{u}_{\mathrm{gen,h}}$ in the iteration. Similar to the adjustment of the magnitude of the voltage $\underline{u}_{\mathrm{gen,h}}$, the magnitude of the current $\underline{i}_{\mathrm{con,h}}$ must also be adjusted. For this purpose, the reactive power output $q_{\mathrm{con,h}}^{(\xi)}$ of the converter is calculated in the iteration step (see formula (82)). Subsequently, the current $\underline{i}_{\mathrm{con,h}}^{(\xi)}$ resulting from the actual values of the iteration can be calculated using formula (84). In the last step, it is again necessary to correct the magnitude of the converter current for the following iteration step. The angle from the converter current of the corresponding iteration step is not changed (see equation (85))

$$\underline{i}_{\mathrm{con,h}}^{(\xi+1)} = \left|\underline{i}_{\mathrm{con,h}}\right| \cdot \mathrm{e}^{\mathrm{j}\cdot\arg\left\{\underline{i}_{\mathrm{con,h}}^{(\xi)}\right\}} \tag{85}$$

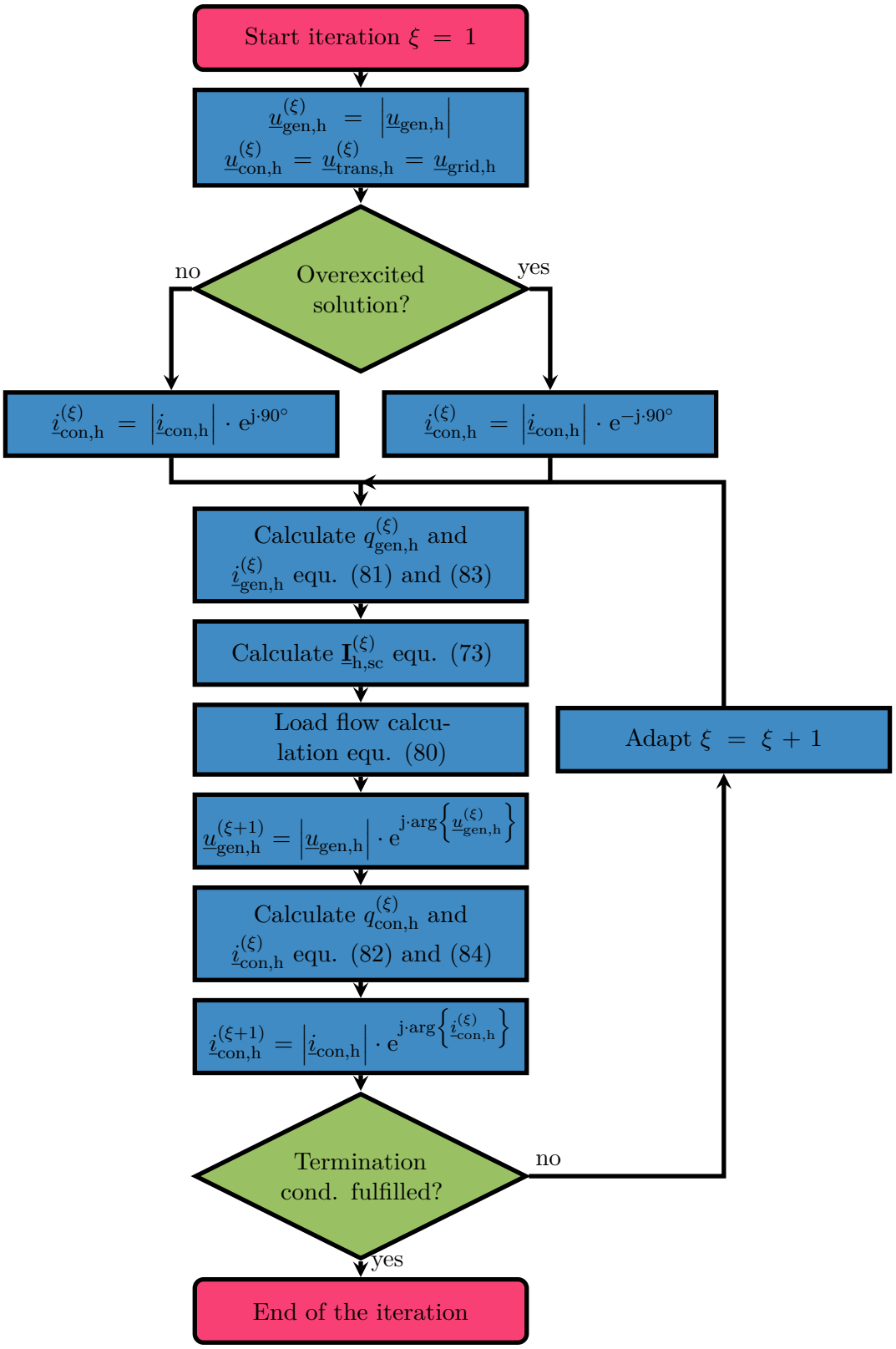


Figure 20: Flow chart of the iterativ calculation of a $p_{\mathrm{gen,h}}$, $\left|\underline{u}_{\mathrm{gen,h}}\right|$ node (generator) and $p_{\mathrm{con,h}}$, $\left|\underline{i}_{\mathrm{con,h}}\right|$ node (converter) with a slack node at POC

The iterative load flow analysis with a current specification can be quite challenging due to the convergence triggering. In the following, I would like to briefly discuss other important aspects that are required for the desired convergence. It must be ensured that the initial conditions for the node voltages, which are not described by a voltage specification, are selected as homogeneously as possible (flat start). For this reason, the voltage at the converter terminals and the voltage at POC were assumed to be the same as initial condition. This is necessary because deviations in the voltage amplitude have a major influence on the reactive power flow in the grid.

Nevertheless, there is a possibility that with certain configurations in the grid, although the initial conditions are chosen correctly, the calculation may still converge to the undesired solution. Such cases are relatively easy to recognize, because the reactive power $q_{\mathrm{con,h}}^{(\xi)}$ already takes the undesired sign (plus or minus depending on the choice of the overexcited or underexcited solution) in the 1st iteration step. The solution therefore converges in the undesired direction. To prevent this, the sign of the reactive power simply needs to be adjusted in the first two to four iteration steps. As this is only necessary in special cases, this adjustment is not shown in the flow chart in Figure 20.

It is also necessary to define a termination condition for this calculation, the termination condition is the same as in the example described above.

### 2.13.3 Iterativ load flow calculation of a $p_{\mathrm{gen,h}}$, $q_{\mathrm{gen,h}}$ node (generator) and $p_{\mathrm{con,h}}$, $\left|\underline{i}_{\mathrm{con,h}}\right|$ node (converter) with a slack node at POC

In this load flow analysis, the active power $p_{\mathrm{gen,h}}$ and the reactive power $q_{\mathrm{gen,h}}$ at the generator terminals are known. The magnitude of the current $\underline{i}_{\mathrm{con,h}}$ and the active power output $p_{\mathrm{con,h}}$ at the converter terminals are also known. The calculation with regard to the converter current constraint is the same as in the example described above. In this example, both the active and reactive power are specified at the generator terminals. This simplifies the calculation. In the iteration steps, it is only necessary to determine the generator terminal current using formula (86). In contrast to the previous examples, it is not necessary to calculate the reactive power, as this is already given. A so-called flat start was used as the initial voltage distribution [10]. In this case, all node voltages in the initial condition are equal. The termination condition in this example is also the same as in the two previous examples. Figure 21 shows the corresponding flow chart.

$$\underline{i}_{\mathrm{gen,h}}^{(\xi)} = \left( \frac{p_{\mathrm{gen,h}} + \mathrm{j} \cdot q_{\mathrm{gen,h}}}{\underline{u}_{\mathrm{gen,h}}^{(\xi)}} \right)^{*} \tag{86}$$

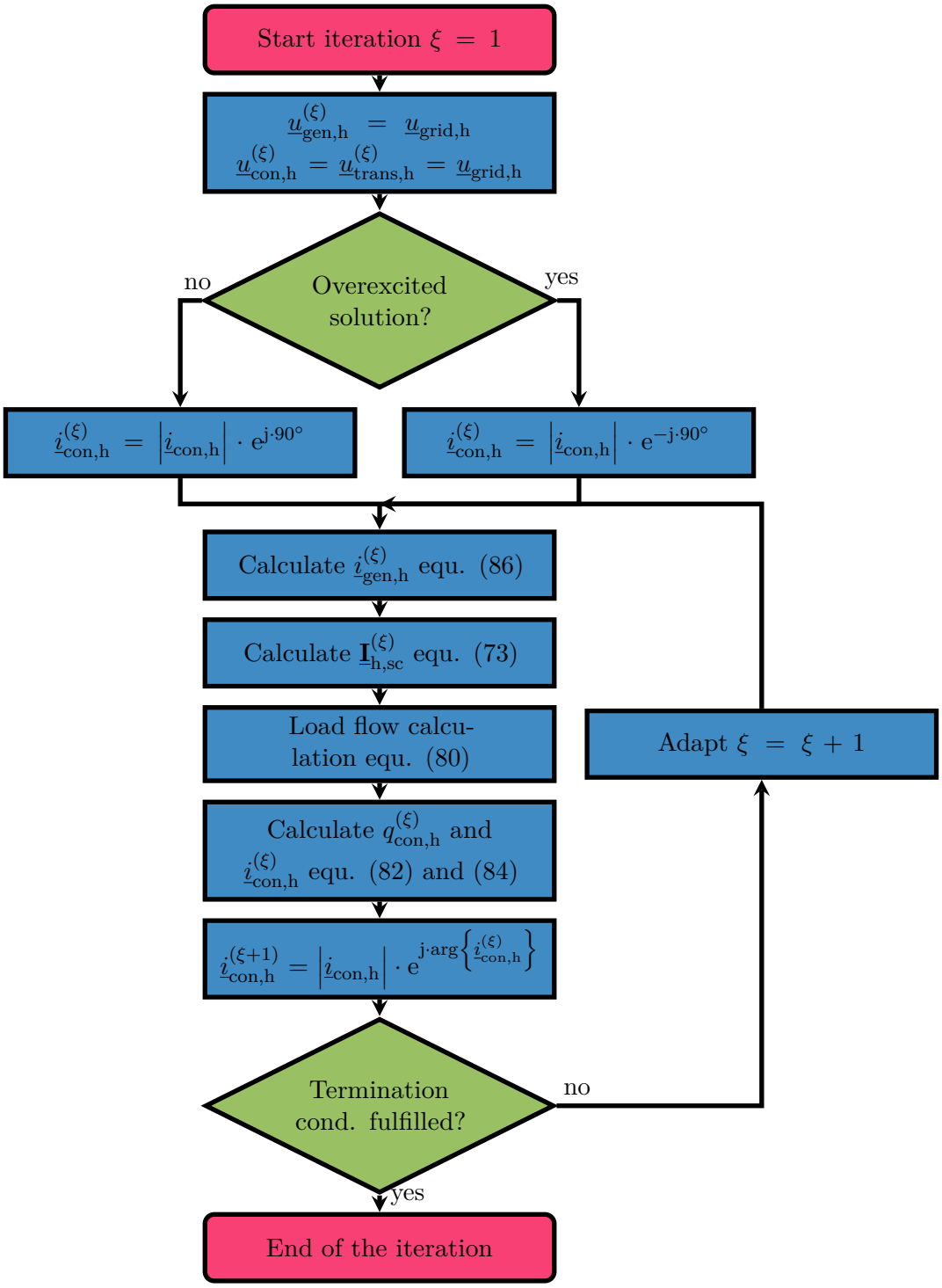


Figure 21: Flow chart of the iterativ calculation of a $p_{\mathrm{gen,h}}$, $q_{\mathrm{gen,h}}$ node (generator) and $p_{\mathrm{con,h}}$, $\left|\underline{i}_{\mathrm{con,h}}\right|$ node (converter) with a slack node at POC

### 2.13.4 Iterativ load flow calculation of a $p_{\mathrm{gen,h}}$, $q_{\mathrm{gen,h}}$ node (generator) and $p_{\mathrm{con,h}}$, $q_{\mathrm{con,h}}$ node (converter) with a slack node at POC

In this load flow analysis, the active power $p_{\mathrm{gen,h}}$ and the reactive power $q_{\mathrm{gen,h}}$ at the generator terminals are known. The active power $p_{\mathrm{con,h}}$ and the reactive power $q_{\mathrm{con,h}}$ at the converter terminals are also known. This load flow analysis is relatively simple compared to the other load flow analyses already performed. Since the active and reactive power is known at both the generator terminals and the converter terminals, the current in the corresponding iteration can be easily determined using formulas (86) and (87) . A so-called flat start was used as the initial voltage distribution [10]. The termination condition in this example is also the same as in the previous examples. Figure 22 shows the corresponding flow chart.

$$\underline{i}_{\mathrm{con,h}}^{(\xi)} = \left( \frac{p_{\mathrm{con,h}} + \mathrm{j} \cdot q_{\mathrm{con,h}}}{\underline{u}_{\mathrm{gen,h}}^{(\xi)}} \right)^{*} \tag{87}$$

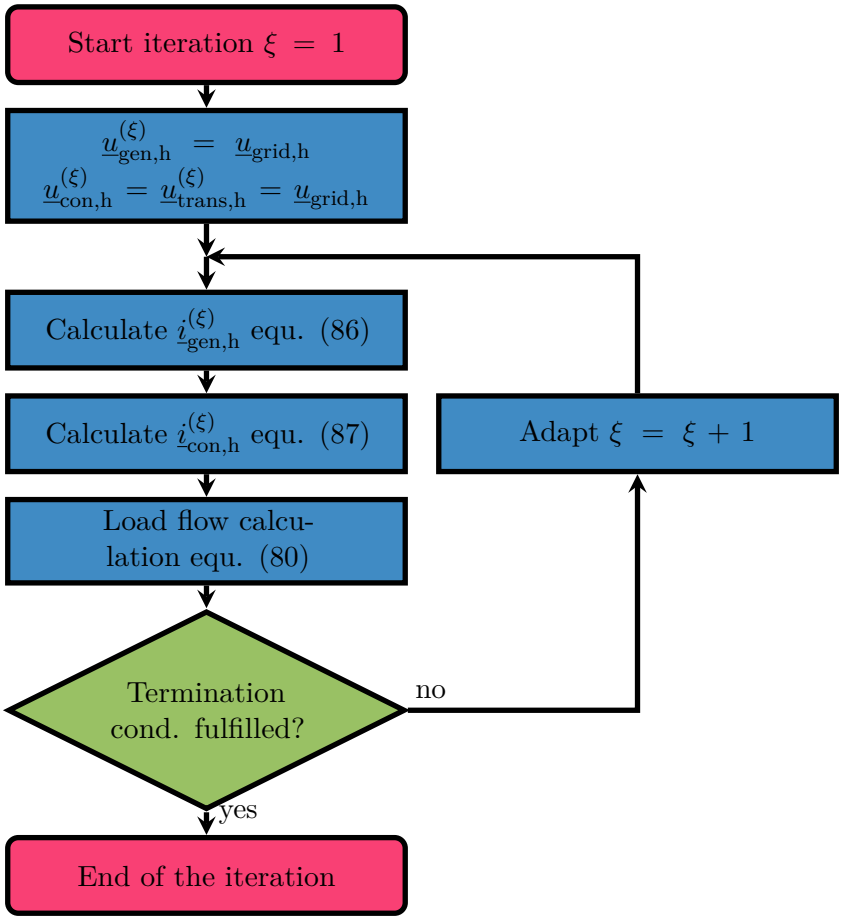


Figure 22: Flow chart of the iterativ calculation of a $p_{\mathrm{gen,h}}$, $q_{\mathrm{gen,h}}$ node (generator) and $p_{\mathrm{con,h}}$, $q_{\mathrm{con,h}}$ node (converter) with a slack node at POC

## 2.14 Verification of the load flow analysis using DIgSILENT PowerFactory

To ensure that the calculations from the load flow analyses described above were correct, they were checked with a frequently used load flow analysis program (DIgSILENT PowerFactory 2022). The models shown in Figure 23 and 24 were created for this purpose. It is then necessary to transfer the electrical parameters to the simulation. The parameters are entered for the simulation in a similar way to the MATLAB script created in the course of this master's thesis. The tap changer position can also be taken into account in the simulation. In order to be able to check the load flow analyses, the power or voltages at the generator terminals resulting from the calculations can simply be entered to the simulation. The resulting node voltages can then be compared with those from the calculations. If the calculated node voltages and the node voltages of the simulated network are the same, then the simulation match the calculation.

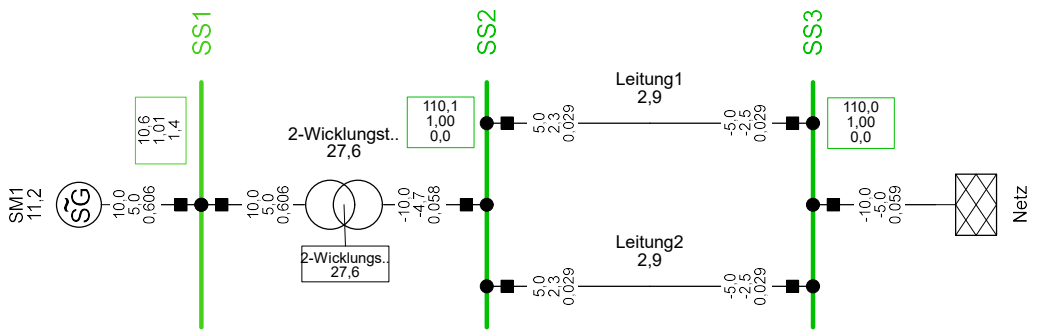


Figure 23: Verification of the classic power-generating facilities using DIgSILENT PowerFactory

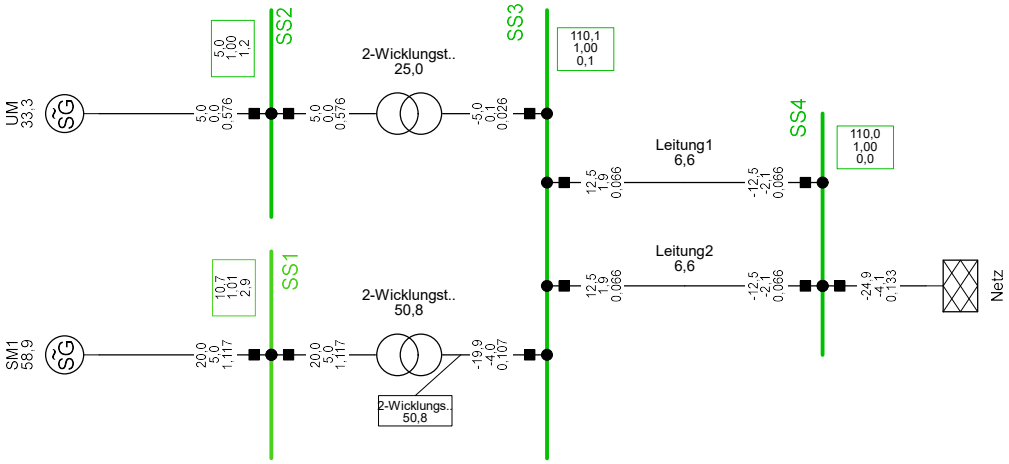


Figure 24: Verification of the hybrid power-generating facility using DIgSILENT PowerFactory

## 2.15 Stationary operating behaviour of the synchronous machine

The previous chapters focused in particular on load flow analysis. It was evident that a wide range of power settings can be made at the nodes in the form of auxiliary conditions. In the examples discussed here, that power is provided by a converter or a synchronous machine. The stationary operating behavior of the synchronous machine is examined in more detail below.

### 2.15.1 Limits in the capability diagram of a synchronous machine

The stationary operating behavior of a synchronous machine is described in terms of power supply by a so-called capability diagram [20, 21]. In the capability diagram, the active power $p_{\mathrm{gen,c}}$ is plotted against the reactive power $q_{\mathrm{gen,c}}$ at the generator terminals. In a capability diagram, it is assumed that the terminal voltage at the generator is constant (operation on a powerful grid). Feeding in reactive power therefore does not result in a change in the terminal voltage. For this reason, the variable names (power and voltages) also differ from those of the hybrid power-generating facilities or the classic power-generating facility. Such a capability diagram has a voltage dependency. This means that different power can be delivered depending on the terminal voltage [20]. Operators of power-generating facilities usually receive a capability diagram from the manufacturer of the synchronous generator. This can be used to determine the power delivery of the generator for a handful (usually three) generator terminal voltages. In order to calculate the reactive power supply at the point of connection, it is necessary to be able to determine the reactive power supply of the generator for a wide range of generator terminal voltages. For this reason, it is necessary in most cases to model the existing graphical capability diagram using a mathematical model.

Current excited synchronous machines can be roughly divided into salient pole synchronous machines and round rotor machines [15]. The major difference between the two machines lies in the design of the rotor. The round rotor machine has no distinct poles. The salient pole synchronous machines have distinct pole bodies with a pole gap in between [15, 20]. For this reason, it is necessary to distinguish between direct-axis synchronous reactance $x_{\mathrm{d}}$ and quadrature-axis synchronous reactance $x_{\mathrm{q}}$. The quadrature-axis synchronous reactance is lower than the direct-axis synchronous reactance. The reason for this is the longer air gap length due to the pole gap [15].

Figure 25 shows the rotor of a salient-pole synchronous machine.

Figure 25: Rotor of a vertical salient-pole synchronous machine

The differences in the operating behavior of the two machines can also be seen in the capability diagram. Especially at the stability limit, the behavior of the salient-pole machine differs from that of the round rotor machine [20]. In contrast to the round rotor machine, the salient pole machine has a so-called reluctance torque due to the magnetic asymmetry (see [20]). As a result, the critical angle of the salient-pole synchronous machine is less than 90° (approx. 70°) [15, 20]. This also has an impact on the design of the stability limit (see the following explanations). The calculations performed in this master's thesis all refer to salient-pole synchronous machines.

The modeling of salient pole synchronous machines is generally slightly more complex than that of round rotor machines. In principle, the behavior of round rotor synchronous machines can also be modeled with the equations described here by equalizing the direct-axis synchronous reactance $x_\mathrm{d}$ and the quadrature-axis synchronous reactance $x_\mathrm{q}$ [15]. Another reason for modeling the salient-pole synchronous machines in this master's thesis is that, as already described in the previous chapters, hydropower plays a crucial role for energy supply in Austria. Due to the design of the rotor, salient-pole synchronous generators are used in hydropower plants with relatively slowly rotating turbines [15]. Round rotor machines, on the other hand, are often used in thermal plants with high speeds [15].

Figure 26 shows the simplified construction of such a capability diagram [15, 20].

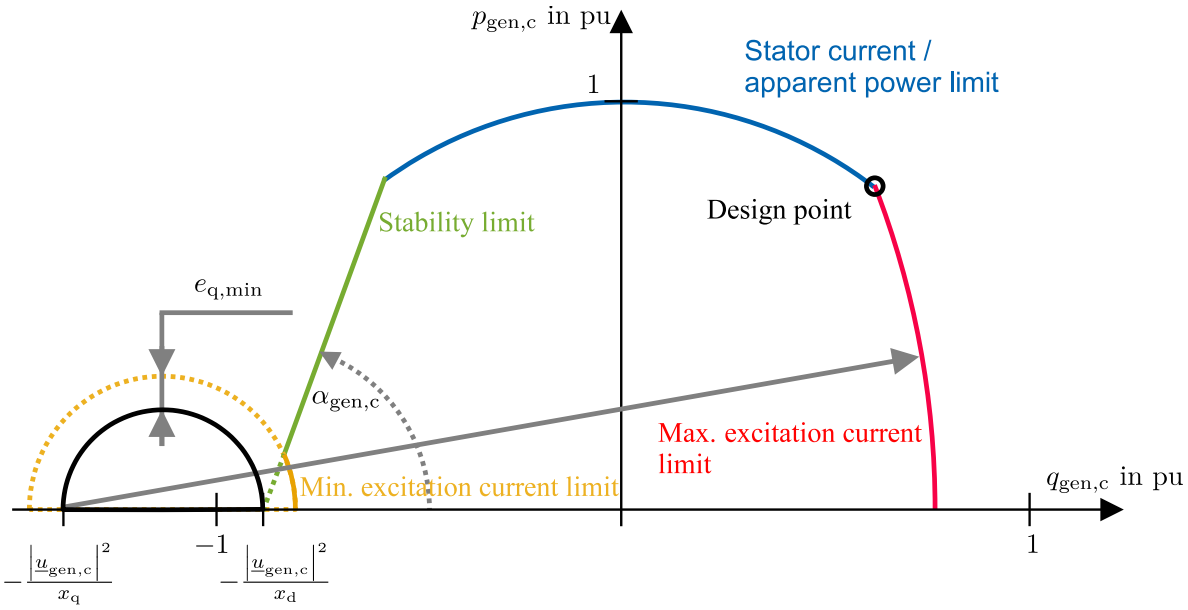


Figure 26: Construction of a simplified capability diagram at $|\underline{u}_{\mathrm{gen,c}}| = 1$ pu

It can be seen that a wide variety of limits are applied in the capability diagram. The capability diagrams presented here are based on the generator convention. The maximum excitation current limit (red curve) is located in the overexcited or voltage-increasing range. This limit is determined by the operating behavior of the excitation system. The excitation system is designed so that the rated excitation current flows at the design point of the machine when the rated voltage is applied to the generator terminals [20]. If the active power output is reduced at this point while the excitation current is kept constant, this results in the maximum excitation current limit. It is relatively complex to determine a mathematical model for this limit (see [22]). Due to the high currents, the saturation of the iron cannot generally be neglected for the maximum excitation current limit [20]. It is therefore necessary to implement the iron saturation or the magnetization characteristic of the machine in the calculations. The calculation of the reactive power supply is already relatively computationally complex, and modeling the maximum excitation current limit while taking the magnetization characteristic into account would lead to a significant increase in the computation time (see [22]). For this reason, an alternative method for modeling the maximum excitation current limit was used.

Assuming that the saturated direct-axis synchronous reactance corresponds approximately to the quadrature-axis synchronous reactance, the maximum excitation current limit can be constructed approximately as shown in Figure 26 [20]. The construction is based on a semicircle with the center at $-\left|\underline{u}_{\mathrm{gen,c}}\right|^2 / x_{\mathrm{q}}$. The semicircle passes through the design point of the machine.

The modeling is based in parts on the explanations from [20]. In the course of the bachelor thesis (see [22]) it was experimentally determined that the simplified modeling of the maximum excitation current limit described here is a sufficiently accurate approximation. For this reason, no further refinements were made to the modeling of the maximum excitation current limit.

The maximum excitation current limit intersects the stator current limit at the design point. This limit describes the maximum apparent power that can be supplied or the maximum flowing terminal current of the generator. In the modeling, this limit has the shape of an semicircle. In the course of this master's thesis, two models were developed for a capability diagram. In one, the apparent power of the generator is kept constant and in the other, the terminal current of the generator is kept constant (see explanations below).

The stability limit intersects the stator current or apparent power limit in the underexcited range (voltage-reducing range). It results directly from the balance of angular momentum (see [20]). If the stability limit is exceeded, unstable operation of the machine occurs. This can lead to the destruction of the machine. Figure 26 shows the stability limit in simplified form as a straight line. In generator protection devices, the stability limit is often modeled by a straight line. In the simplified model, the stability limit has a base point at the value $-\left|\underline{u}_{\mathrm{gen,c}}\right|^2 / x_{\mathrm{d}}$. The gradient of the stability limit is usually indicated by an angle $\alpha_{\mathrm{gen,c}}$. The minimum excitation current limit is also located in the underexcited range. The minimum excitation current limit results from a stability consideration [20]. Within this black semicircle (see Figure 26), stable operation of the machine is only possible with a negative excitation current (see [20]). In order to maintain a safety margin for this semicircle, the value $e_{\mathrm{q,min}}$ is added to the radius of the semicircle. This gives the minimum excitation current limit (see [20]).

### 2.15.2 Modeling the stability limit by means of limacons of Pascal

In the previous explanations, it has already been mentioned that the stability limit can be approximated by a linear function. A theoretical stability limit can also be defined from the power equations (see equations (88) and (89)) of a salient-pole synchronous machines [20, 21]. The voltage $\underline{u}_{\mathrm{gen,emf,c}}$ describes the internal electromotive force induced in the winding. The angle $\delta_{\mathrm{gen,c}}$ corresponds to the power angle.

$$p_{\mathrm{gen,c}} = \frac{\left|\underline{u}_{\mathrm{gen,emf,c}}\right| \cdot \left|\underline{u}_{\mathrm{gen,c}}\right|}{x_{\mathrm{d}}} \cdot \sin\left(\delta_{\mathrm{gen,c}}\right) + \frac{\left|\underline{u}_{\mathrm{gen,c}}\right|^2}{2} \cdot \frac{x_{\mathrm{d}} - x_{\mathrm{q}}}{x_{\mathrm{d}} \cdot x_{\mathrm{q}}} \cdot \sin\left(2 \cdot \delta_{\mathrm{gen,c}}\right) \tag{88}$$

$$q_{\mathrm{gen,c}} = \frac{\left|\underline{u}_{\mathrm{gen,emf,c}}\right| \cdot \left|\underline{u}_{\mathrm{gen,c}}\right|}{x_{\mathrm{d}}} \cdot \cos\left(\delta_{\mathrm{gen,c}}\right) + \frac{\left|\underline{u}_{\mathrm{gen,c}}\right|^2}{x_{\mathrm{d}}} \cdot \left(1 + \frac{x_{\mathrm{d}} - x_{\mathrm{q}}}{x_{\mathrm{q}}} \cdot \sin^2\left(2 \cdot \delta_{\mathrm{gen,c}}\right)\right) \tag{89}$$

If the mechanical power of the turbine is increased, the power angle $\delta_{\mathrm{gen,c}}$ increases due to the transient angular acceleration. As a result, the electrical active power must also increase. For this reason, the requirement arises that only those points are stable at which an increase in the power angle also results in an increase in active power [18]. In other words, this corresponds to the requirement that the derivative of the active power $p_{\mathrm{gen,c}}$ with respect to the power angle $\delta_{\mathrm{gen,c}}$ must be positive. If we now consider the power equations in equations (88) and (89) and plot the active power $p_{\mathrm{gen,c}}$ over the reactive power $q_{\mathrm{gen,c}}$, so-called limacons of Pascal are formed [20].

These describe the stationary operating behavior of the salient pole synchronous generator at constant generator terminal voltage and internal electromotive force. The internal electromotive force is a function of the flowing excitation current. Each limacon of Pascal can therefore be clearly assigned to a internal electromotive force. For the construction of the limacon of Pascal, the power angle is varied from 0° to 180°. In order to be able to meet the stability condition described above, the points at which a marginally stable behavior occurs are looked for. This is exactly the case at the maxima of the limacon of Pascal.

The blue curve in Figure 27 connects the maxima of the limacon of Pascal and corresponds to the theoretical stability limit [20]. In practice it is necessary to take a certain safety margin into account. For this reason, the active power of the theoretical stability limit is reduced by a defined value at constant internal electromotive force (see [20, 21]). The resulting curve (red curve) corresponds to the practical stability limit. In this master's thesis, the safety factor $\gamma_{\mathrm{gen}}$ is given as a percentage of the rated apparent power.

Figure 27 shows the construction of the practical and theoretical stability limit.

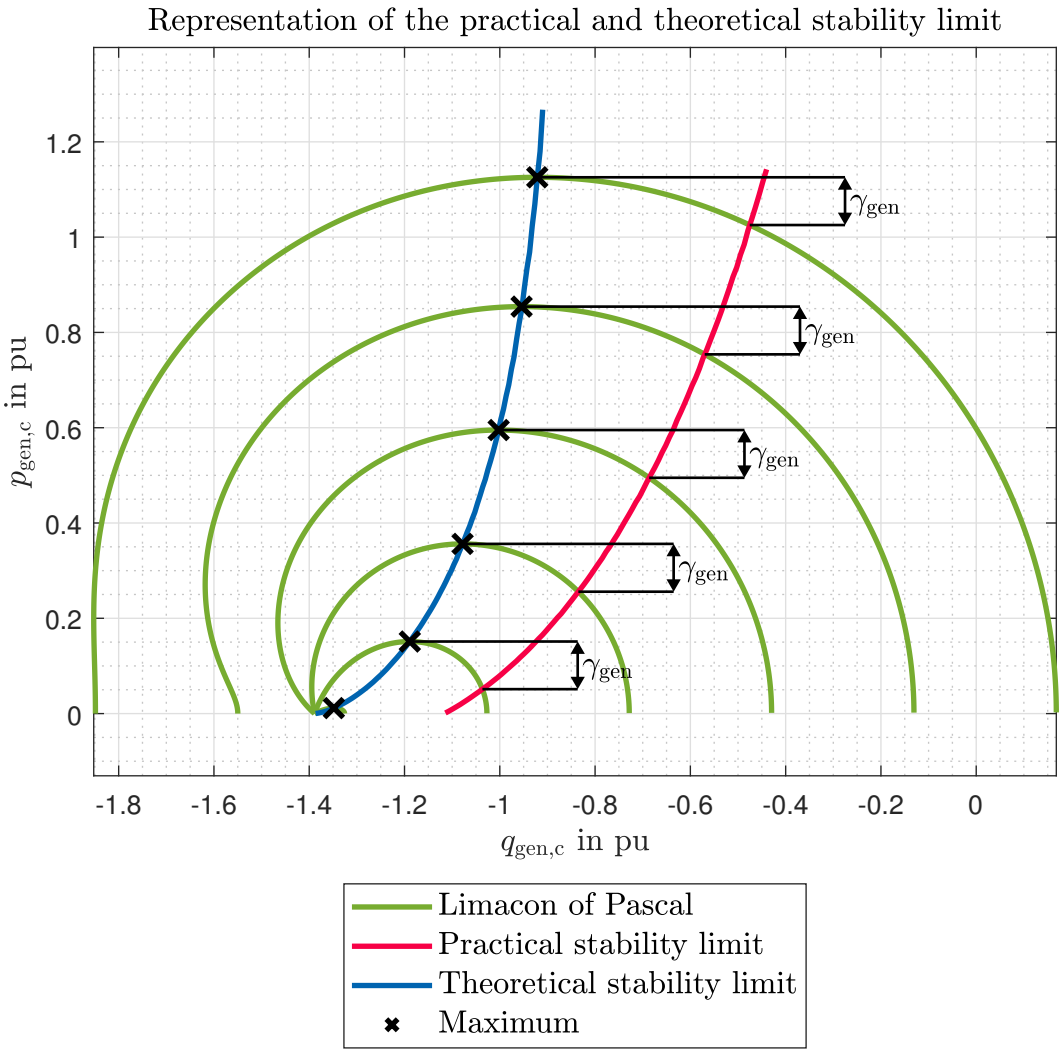


Figure 27: Construction of the theoretical and practical stability limit using limacons of Pascal at $\left|\underline{u}_{\mathrm{gen,c}}\right| = 1$ pu

The theoretical stability limit is relatively easy to determine analytically by deriving equation (88) and setting it to zero. The practical stability limit is much more difficult to determine analytically. For this reason, a numerical approach was chosen for the calculation. It should be noted that the maxima of the limacons of Pascal are relatively flat. For this reason, a suitable resolution must be ensured in the numerical calculation.

### 2.15.3 Calculation results of the mathematical modeling of the capability diagrams

Figures 28 and 29 each show capability diagrams with constant apparent power modeling.

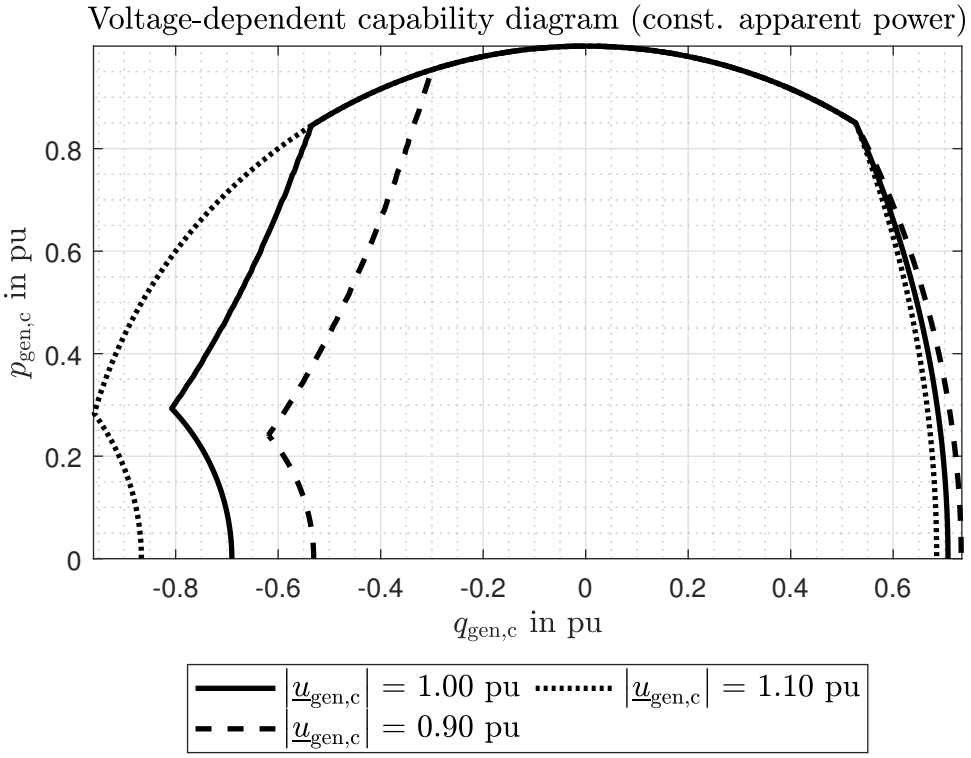


Figure 28: Capability diagram of a salient-pole synchronous generator with constant apparent power modeling

It can be seen that the limit of the constant apparent power lies on a semicircle. The semicircle is bounded by the stability limit in the underexcited range and by the maximum excitation current limit in the overexcited range. When the generator terminal voltage is varied, the apparent power output of the generator remains the same at the constant apparent power limit. This is linked to the fact that the generator current exceeds the rated current at voltages below the rated voltage.

According to [20], this exceeding of the terminal current also corresponds to a permitted operating state in the steady state. The generator windings are also designed for this operating state (the voltage range may only change within the permitted range). The capability diagrams shown here with constant apparent power modeling are technically very common.

In Figure 29, the stability limit is modeled by a straight line and in Figure 28, the stability limit is modeled using the limacon of Pascal (practical stability limit).

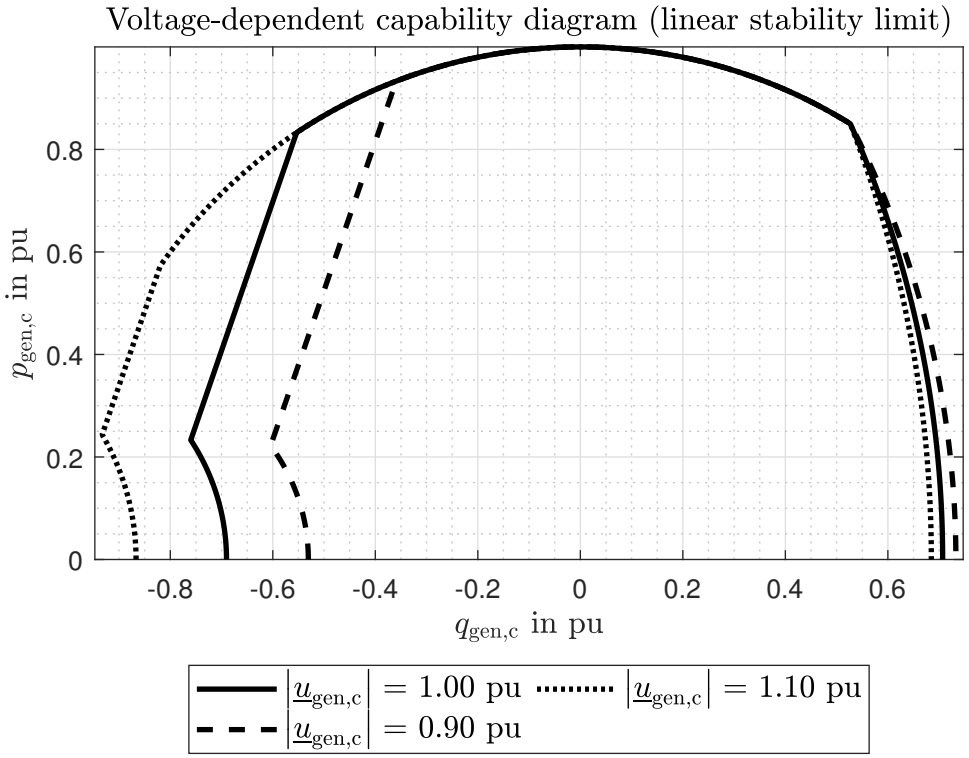


Figure 29: Capability diagram of a salient-pole synchronous generator with constant apparent power and linear stability limit modeling

In addition to modeling with constant apparent power, a model with a constant generator current was also developed in this master's thesis. Here, the apparent power output of the generator varies with the applied terminal voltage so that the rated current is not exceeded.

It is already known from the introduction that the maximum excitation current limit intersects the stator current limit at the design point. This type of modeling results in a shift of the stator current limit when the generator terminal voltage is varied. The modeling was selected so that the maximum excitation current limit always intersects the stator current limit at the point at which the rated power factor occurs [20].

The yellow line (see Figure 30) indicates the points at which the power factor corresponds to the rated power factor. In order to be able to use this modeling, it must be ensured that the excitation system can provide the required excitation current, especially for higher voltages (the excitation winding must also be designed for this operation).

This modeling of the capability diagram in Figure 30 is rather unusual. Furthermore, it must be ensured that the turbine can also provide the active power.

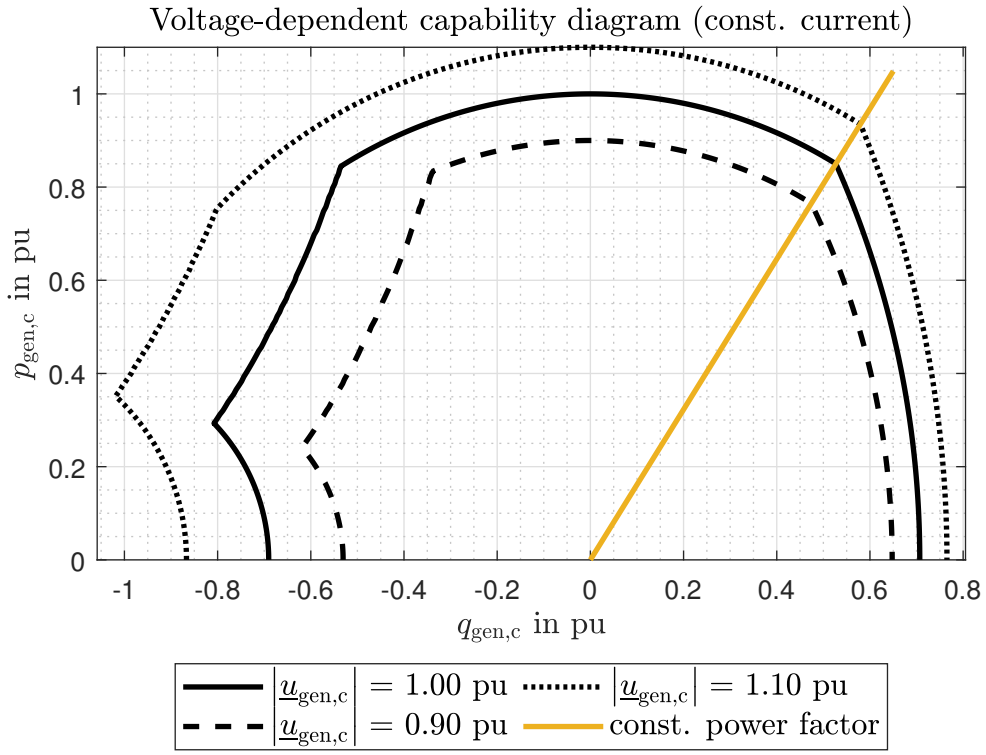


Figure 30: Capability diagram of a salient-pole synchronous generator with constant current modeling

In summary, Figure 31 shows the possible modeling variants of the capability diagrams in this master's thesis.

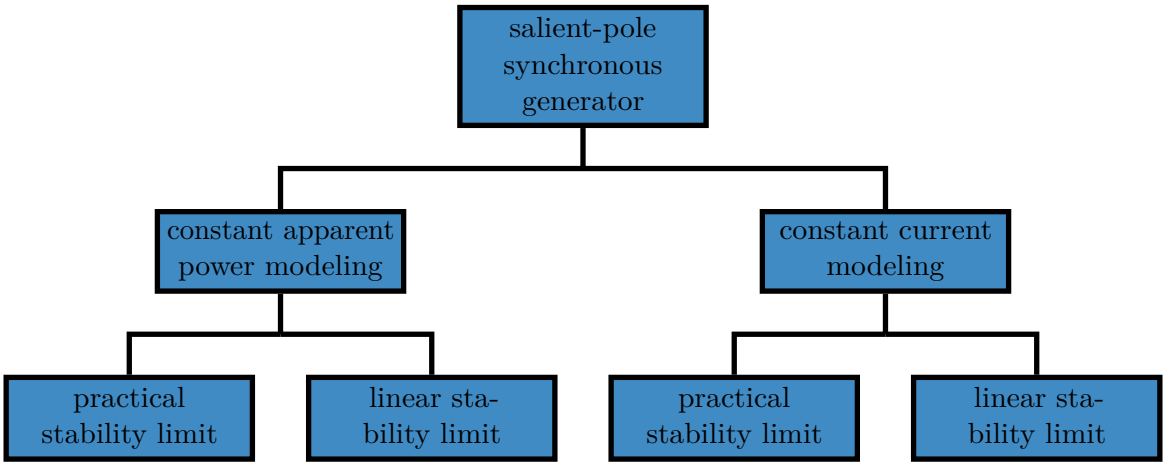


Figure 31: Possible modeling variants of the capability diagrams in this Master's thesis

## 2.16 Stationary operating behaviour of the converter

In order to be able to describe the reactive power supply of the hybrid power-generating facilities, it is necessary to mathematically model the stationary behavior of the converter. In the course of this master's thesis, it is sufficient to model the operating behavior of the converter as simply as possible. No distinction is made between the different types of converters. According to [23] and [24], the operating behavior of the converter is limited by the following three variables.

- The maximum voltage applied to the converter terminals $u_{\mathrm{con,h,max}}$.
- The maximum current occurring at the converter terminals $i_{\mathrm{con,h,max}}$.
- Active power limited by the DC circuit.

Only the first two points are used for the considerations made in this master's thesis. Active power is only limited in the form of the converter's rated power and the resulting rated current (or the current $i_{\mathrm{con,h,max}}$). The last point with the limited active power output would be relevant, if the converter is supplied by a DC cable with a limited active power transport.

Looking at the two variables listed, it can be seen that, as with the synchronous generator, the terminal current is limiting. This leads to a semi-circular capability diagram in generator operation. In the overexcited (voltage-increasing) range, the reactive power output must be limited due to the maximum terminal voltage occurring at the converter terminals.

It is already clear from these explanations that the short-circuit power (grid impedance) and thus also the actual grid voltage or the feed-in of the generator in the hybrid power-generating facility will be relevant for the calculation of the capability diagram. The capability diagram calculated here therefore always applies to a specific grid status. This means that the reactive power output of the converter also changes when the mentioned parameters in the grid change.

In the topology examined in this master's thesis (see 17), the grid voltage is the most significant influencing variable on the converter's capability diagram. It should not be forgotten that the transformers have tap changers, which is why the position of the tap changer is also relevant for creating the capability diagram.

Figure 32 shows a flow chart for creating the converter capability diagram under the assumptions described above. At the beginning, it is necessary to define the grid voltage $\underline{u}_{\mathrm{grid,h}}$ for the calculation of the capability diagram. The other parameters, the tap changer positions and the active power or reactive power output of the generator can then be defined.

For the calculation, it is assumed in the first step that the converter has an active power output of 0 pu. In the next step, it is necessary to check whether one of the limiting parameters ( $u_{\mathrm{con,h,max}}$ or $i_{\mathrm{con,h,max}}$) is violated with the selected active power output of the converter. If this is not the case, the overexcited (voltage-increasing) reactive power output at the maximum converter terminal current $i_{\mathrm{con,h,max}}$ can be determined in the next step using the load flow analysis described in chapter 2.13.3 (the active power output remains at the set value).

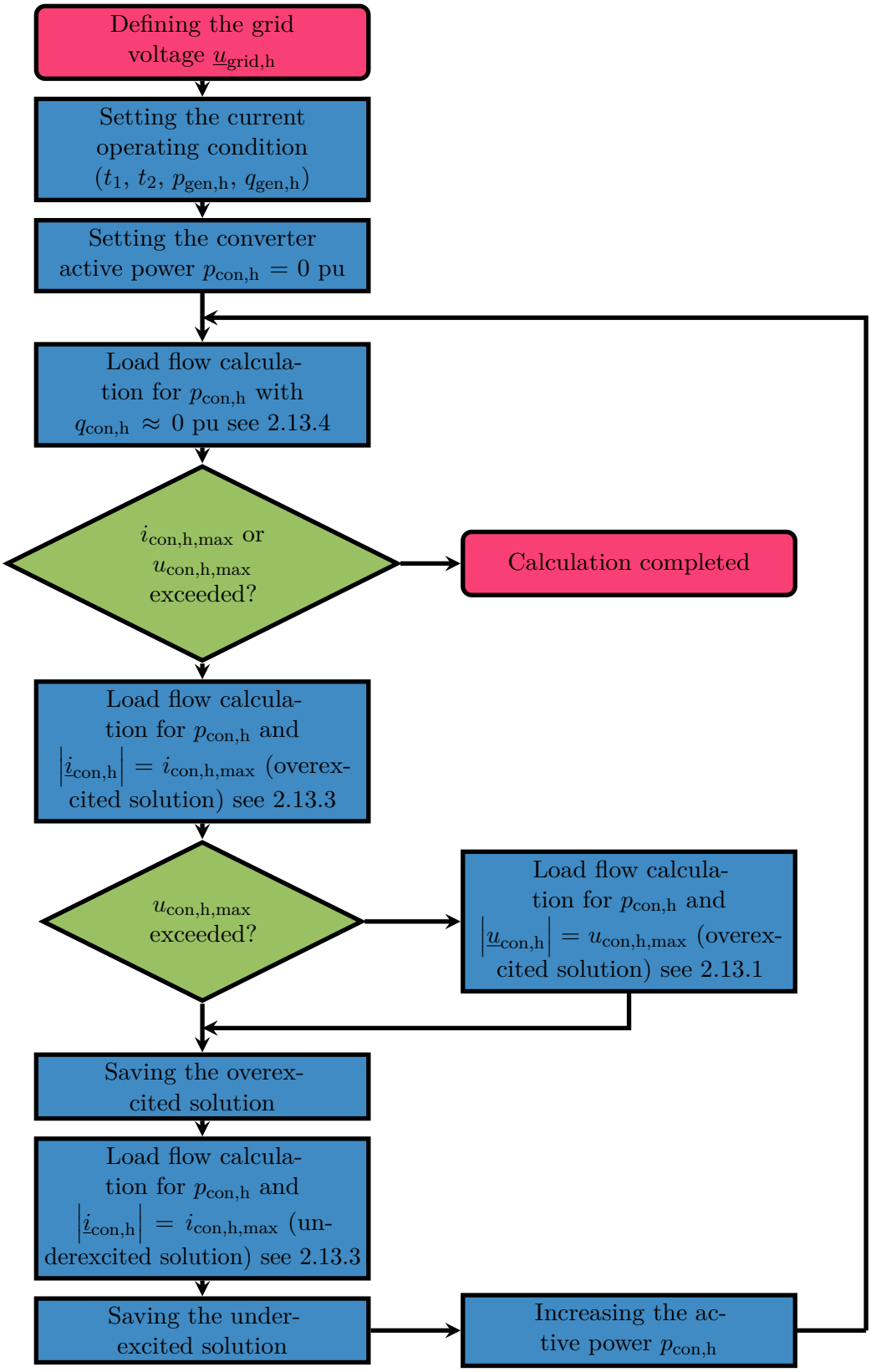


Figure 32: Flow chart of the calculation of the capability diagram of a converter (operation in a hybrid power-generating facility see Figure 17)

The result of this load flow analysis is evaluated regarding the converter terminals voltage. If the converter terminals voltage exceeds the limit, a load flow analysis is then carried out as described in chapter 2.13.1. The load flow analysis is performed at the selected active power output of the converter and the maximum converter terminal voltage $u_{\mathrm{con,h,max}}$.

If the voltage limits are not exceeded, the previously calculated value of the load flow analysis is saved. Otherwise, the result of the load flow analysis from chapter 2.13.1 is saved. In the next step, it is necessary to carry out the load flow analysis in the underexcited (voltage-reducing) range. The load flow analysis from chapter 2.13.3 is carried out for the underexcited case and the maximum converter terminal current $i_{\mathrm{con,h,max}}$. The result is also saved.

In the underexcited case, it is not necessary to check the maximum converter terminal voltage. Subsequently, the actual active power of the converter is increased and the process starts again. If operation of the converter is no longer possible at the selected active power, the calculation is terminated.

For the purpose of completeness, one further point should be mentioned. In the calculation step in which it is checked whether operation of the converter is possible with the currently selected active power output, the set reactive power output of the converter is set to around 0 pu in the flow chart. This formulation was chosen on purpose. Figure 33 shows that the maximum active power output does not occur exactly at a reactive power output of 0 pu. Therefore, it is also necessary to set the reactive power accordingly (it is usually close to 0 pu) in order to check compliance with the limiting parameters ( $u_{\mathrm{con,h,max}}$ or $i_{\mathrm{con,h,max}}$). This is done numerically in the MATLAB code.

Figure 33 illustrates the capability diagram of a converter during operation in the hybrid power-generating facility shown in Figure 17.

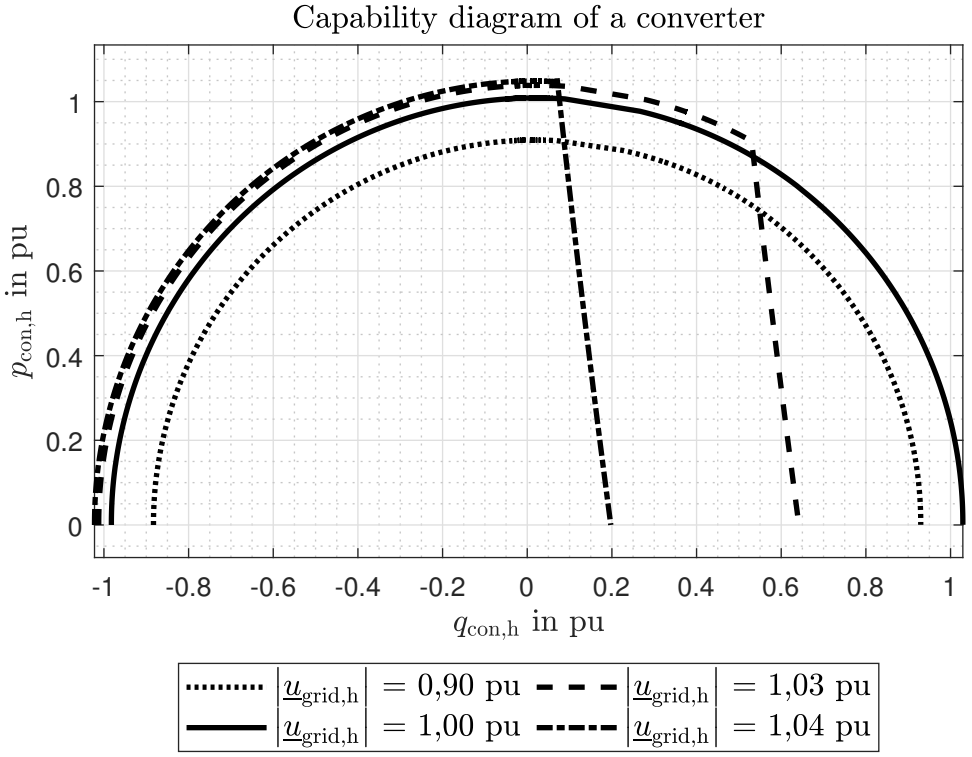


Figure 33: Capability diagram of the converter at different grid voltages and constant apparent power supply of the generator

It can be seen that the reactive or active power output of the converter changes with different grid voltages. In the overexcited area, the maximum converter terminal voltage is limiting. The converter must reduce the overexcited (voltage-increasing) reactive power supply in order not to exceed the maximum terminal voltage. For these calculations the tap changer positions are in the center position.

## 2.17 Requirements on the part of TOR

It has already been mentioned in the introduction that there are specifications at both European and national level regarding the reactive power supply of power-generating facilities. At European level, guidelines for the stationary and transient operation of power-generating facilities are defined in the RfG [3]. For stationary operation, there are guidelines in the RfG for the reactive power supply of power-generating facilities. In Austria, the TOR define guidelines for the operation of power-generating facilities. The TOR is divided into four types.

- Type A: Power-generating facilities with a maximum capacity of less than 250 kW and a nominal voltage at POC of less than 110 kV [4].

- Type B: Power-generating facilities with a maximum capacity greater than or equal to 250 kW and less than 35 MW and a nominal voltage at POC less than 110 kV [5].

- Type C: Power-generating facilities with a maximum capacity greater than or equal to 35 MW and less than 50 MW and a nominal voltage at POC less than 110 kV [6].

- Type D: Power-generating facilities with a maximum capacity greater than or equal to 50 MW or a nominal voltage at POC greater than or equal to 110 kV [7].

Only type D is considered in this master's thesis. In type D, plants with a maximum capacity of more than 50 MW or a nominal voltage at POC of more than 110 kV are considered. In general, the maximum capacity corresponds to the rated active power of the power-generating facilities [7]. The maximum capacity is defined in the grid connection contract. In the case of power-generating facilities that contain several power-generating modules, the maximum capacity corresponds to the maximum rated active power of the entire system [7].

The reactive power capacity at the point of connection POC is defined in TOR. Figure 34 shows the reactive power capacity at the point of connection at maximum capacity.

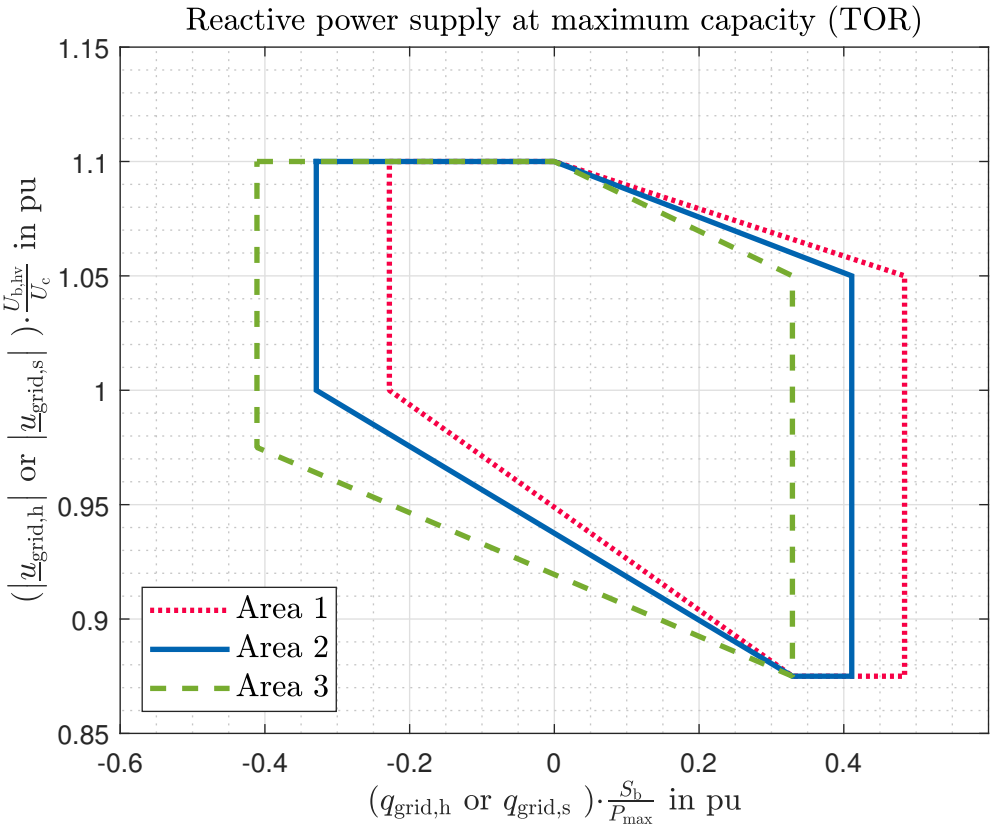


Figure 34: Reactive power supply according TOR at maximum capacity

Here, the grid voltage is plotted against the reactive power at the POC (in the plots, the voltage and the reactive power for the hybrid power-generating facility and the classic power generation were referred to the maximum capacity).

The plot refers to the generator convention. It can be seen that a distinction is made between three areas. Area 2 is generally used. In special cases, the responsible grid operator can also request area 1 or are 3 in the grid connection contract [7].

In addition to the reactive power supply at maximum capacity, there is also a requirement for the reactive power supply below maximum capacity (see Figure 35).

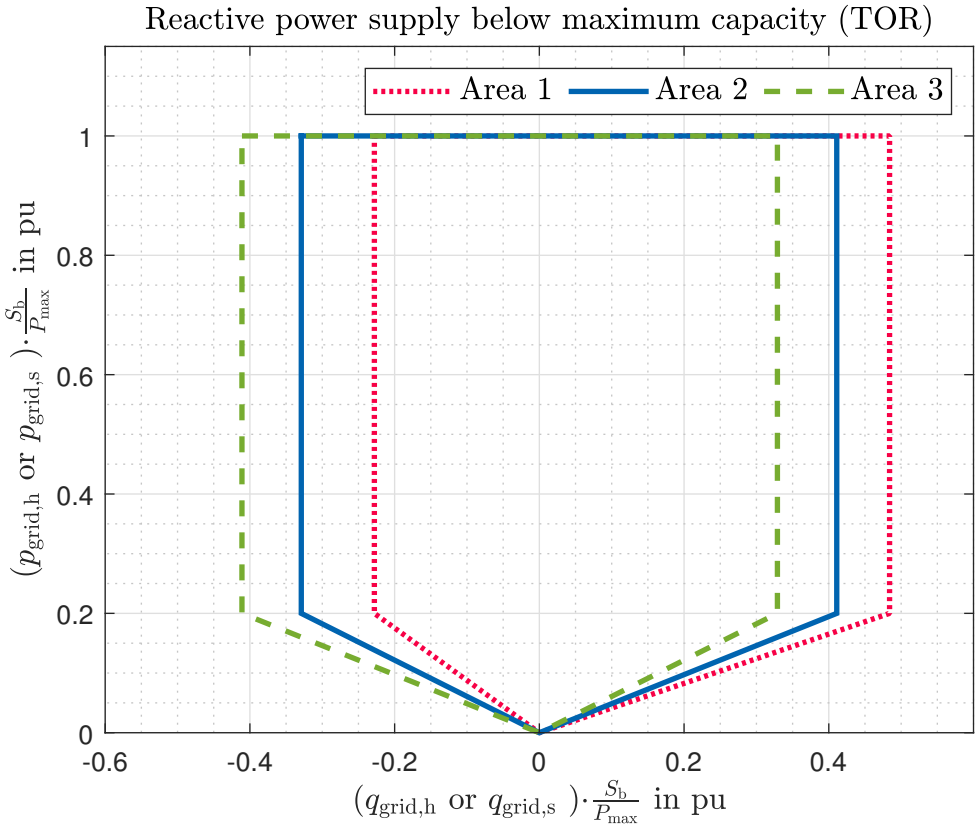


Figure 35: Reactive power supply according TOR below maximum capacity

This generally applies to non-synchronous power-generating facilities. However, the TOR describe that synchronous power-generating facilities should also comply with the reactive power supply shown in Figure 35 in their basic design. In Figure 35, the active power at the POC is plotted over the reactive power at the POC (generator convention). A distinction is again made between the 3 areas described. The data in Figures 34 and 35 are taken from [7].

In this master's thesis, the reactive power supply at maximum capacity is considered. The reactive power supply below the maximum capacity is usually achieved if the reactive power supply at maximum capacity is complied with [22].

## 2.18 Calculation approaches for the calculation of the reactive power supply at POC (classic power-generating facilities)

The previous chapter described the requirements of TOR with regard to the reactive power supply at the point of connection. The load flow analysis methods described in the previous chapters are used to perform this calculation. In the course of this master's thesis, different calculation methods for the reactive power supply at the point of connection were developed.

An important difference between the calculation methods is the modeling of the tap changer. In one method, the tap changer is controlled in such a way that the maximum reactive power supply is achieved at the point of connection (optimal controlled tap changer). In practice, controlled tap changers are often used. Here, the tap changer attempts to keep the generator terminal voltage constant by means of an upper or lower threshold (hysteresis). If the generator terminal voltage reaches the upper or lower switching threshold, the tap changer changes the tap position. This control behavior generally deviates from the optimum control behavior. For this reason, control by means of an upper and lower switching threshold (classically controlled tap changer) was also integrated into the calculations.

In addition to the differentiation with regard to the control strategy of the transformer tap changer, attention is also paid to the active power output. In the TOR, the reactive power supply at the POC is specified at maximum capacity. As a result, the active power losses of the transformer and line must also be taken into account. For this reason, there is the option of keeping the active power at the generator terminals or the active power at the point of connection constant for both the controlled and the optimized tap changer. Both variants were implemented in this master's thesis.

The reason for this is the calculation time. As discussed in the following chapters, the calculation effort increases significantly with constant active power at the point of connection. In addition, the active power losses of the transformer or the line are relatively low in classic power-generating facilities. For this reason, the active power losses could also be approximately compensated by a slightly increased active power output of the generator. Strictly speaking, this would only be an approximation, as the active power losses change slightly due to the reactive power output. Due to the extremely low active power losses, this approximation is accurate enough. In addition, the active power at the POC is almost uncorrelated with the reactive power at the POC for these small deviations. Figure 36 shows the described modeling variants.

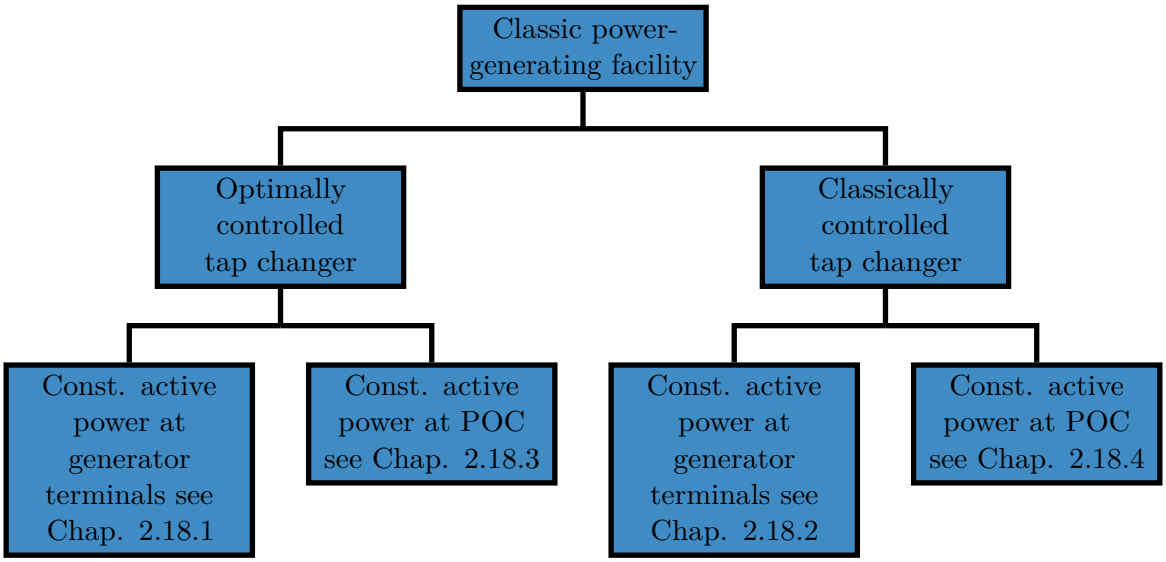


Figure 36: Calculation approaches for the reactive power supply at the POC of a classic power-generating facility

### 2.18.1 Calculation of the reactive power supply with optimally controlled tap changer and constant active power at the generator terminals

With this calculation method, the tap changer is optimally controlled. This means that the tap changer position is set in such a way that the maximum reactive power supply at the point of connection is guaranteed. With a constant grid voltage, there is therefore a different tap changer position for both the overexcited and underexcited case.

In addition to controlling the transformer tap changer, this calculation method keeps the active power at the generator terminals constant. The calculation is based on the following considerations. With a given grid voltage at POC and a defined active power output (maximum capacity) at the generator terminals, a corresponding reactive power output $q_{\mathrm{gen,s}}$ at the generator terminals can be determined for each value of the magnitude of the generator terminal voltage $\underline{u}_{\mathrm{gen,s}}$ using the calculation in chapter 2.9.1. The characteristic resulting from this calculation is referred to as the grid characteristic in this master's thesis (see Figure 37).

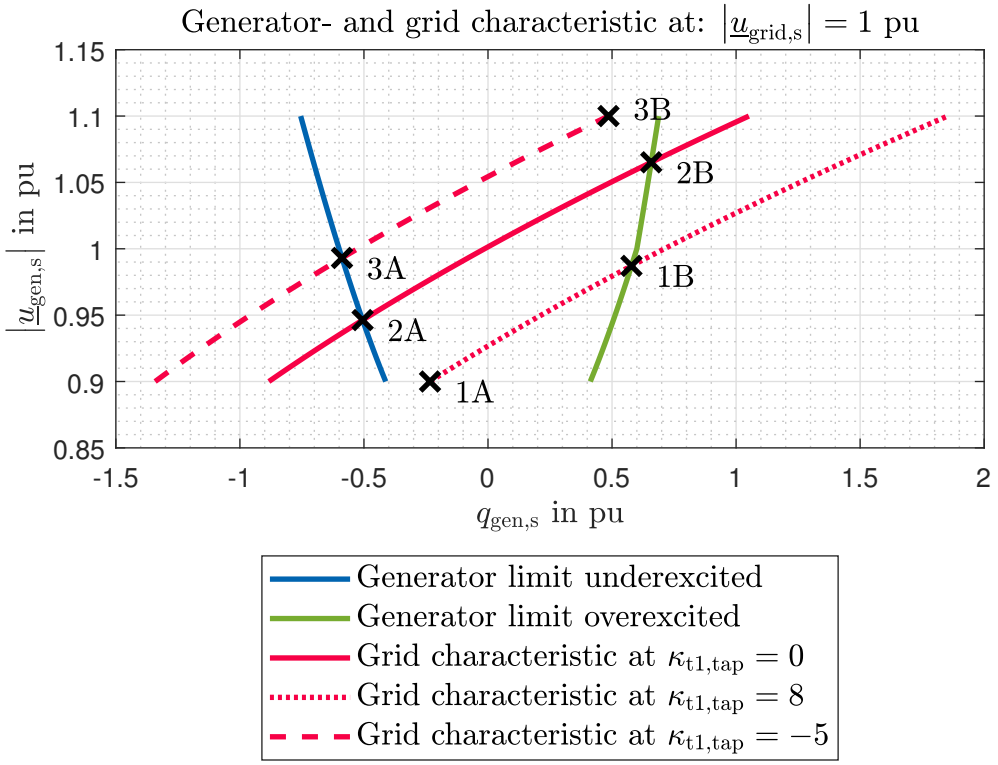


Figure 37: Reactive power supply at the generator terminals with optimum tap changer control

The maximum value of the reactive power supply at the point of connection is not only characterized by the grid characteristic but also by the limiting characteristics with regard to the generator's capability diagram. Since the active power at the generator terminals is known, the overexcited or underexcited reactive power of the generator can be determined for each generator terminal voltage $\underline{u}_{\mathrm{gen,s}}$ using the methods described in chapter 2.15. This results in the blue and green curves. The active power output of the generator is always constant for the modeling described here, regardless of the actual grid voltage or other parameters. The grid characteristics, on the other hand, change when the tap changer position is varied. For this reason, it is necessary to calculate a grid characteristic for each tap changer position. Figure 37 shows an example of three grid characteristics for different tap changer positions $\kappa_{\mathrm{t1,tap}}$.

In Figure 37, the magnitude of the generator terminal voltage $\underline{u}_{\mathrm{gen,s}}$ is plotted against the reactive power $q_{\mathrm{gen,s}}$ at the generator terminals. The operation of the generator is not only limited by the capability diagram, in most cases there is also a minimum or maximum generator terminal voltage. For this reason, the curves shown in Figure 37 are plotted within the maximum or minimum generator terminal voltage. By looking at the grid characteristics at the tap changer position $\kappa_{\mathrm{t1,tap}} = 0$ (red solid line), it can be seen that there are two intersections with the generator characteristics (points 2A and 2B). These two points represent

the maximum reactive power that can be supplied at the generator terminals with the tap changer position $\kappa_{\mathrm{t1,tap}} = 0$ and a grid voltage of $\underline{u}_{\mathrm{grid,s}} = 1$ pu. The intersection points 2A and 2B can each be assigned a limiting variable (stability limit, minimum excitation current limit, etc.) in the generator capability diagram. By looking at the grid characteristic curve with a tap changer position of $\kappa_{\mathrm{t1,tap}} = 8$ (red dotted line), the intersection 1B with the overexcited generator characteristic curve can be observed. There is no intersection with the underexcited generator characteristic curve. Since the minimum generator terminal voltage is effective first. This means that the underexcited reactive power output of the generator is limited by the minimum excitation current limit in 1A. Looking at the grid characteristics for the tap changer position $\kappa_{\mathrm{t1,tap}} = -5$ (red dashed line), it can be seen that the point 3A is limited by the underexcited generator characteristics. In the overexcited range, the maximum generator terminal voltage is limiting (see point 3B). The entire Figure 37 is valid for a grid voltage of $\underline{u}_{\mathrm{grid,s}} = 1$ pu. If the grid voltage changes, the corresponding grid characteristics change. The generator characteristics remain the same in this modeling.

The process for calculating the reactive power supply at the point of connection for the modeling described in this section is shown approximately in the flow chart in Figure 38. This is only a schematic representation of the calculation. In the original code, several different cases or termination conditions must be taken into account for the most efficient calculation possible. The flowchart shown here is therefore only a schematic representation of the code.

In the first step, the two generator characteristics (overexcited and underexcited) can be calculated. In the next step, the grid voltage is set to the minimum grid voltage (see TOR). The tap changer position $\kappa_{\mathrm{t1,tap}}$ is also placed at the minimum level. It is then necessary to calculate the grid characteristics for the actual set grid voltage. A corresponding grid characteristic must also be calculated for each tap changer position $\kappa_{\mathrm{t1,tap}}$. Note that Figure 37 shows the grid characteristic for only three tap changer positions. The intersection points with the generator characteristics and the minimum and maximum generator terminal voltage are then determined. The intersection points thus provide the reactive power that can be delivered by the generator for the different tap changer positions and the actual set grid voltage. Since the active power output of the generator is constant in this modeling, the reactive power supply at POC can be determined for each tap changer position by applying the calculation described in chapter 2.8. In the last step, it is only necessary to calculate and filter the minimum and maximum reactive power at POC resulting from the calculations with the corresponding tap changer position. The grid voltage is then increased and the calculation is performed again. This process is repeated until the maximum grid voltage is reached.

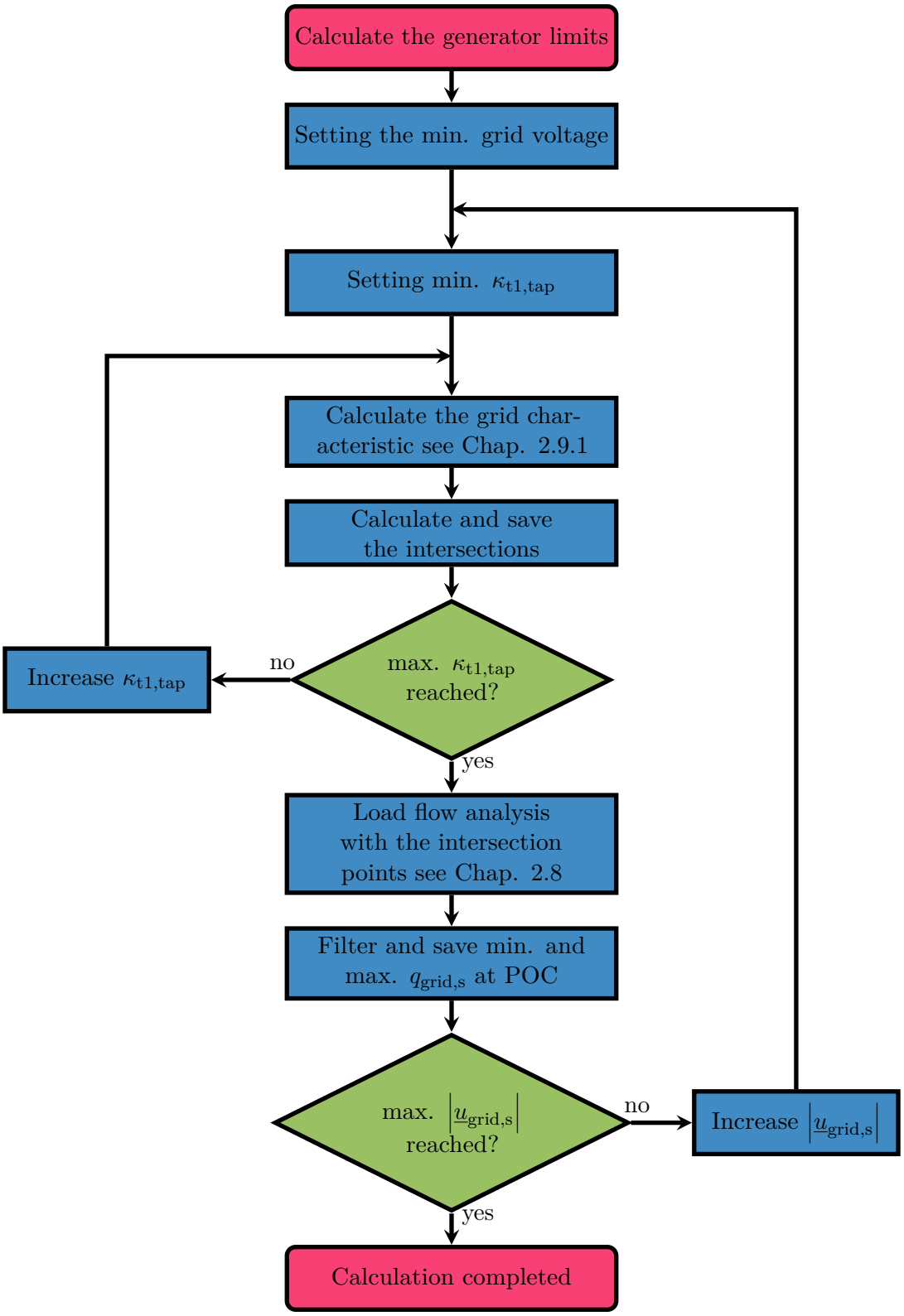


Figure 38: Flow chart of the reactive power supply with optimally controlled tap changer and constant active power at the generator terminals

### 2.18.2 Calculation of the reactive power supply with a classically controlled tap changer and constant active power at the generator terminals

In contrast to the calculation described above, a controlled tap changer is used for this method of calculation. The transformer tap-changer control is set that the generator terminal voltage is kept as constant as possible. This is achieved by implementing a minimum and maximum switching threshold. If the generator terminal voltage exceeds or falls below this switching point (see black dashed lines in Figure 39), the tap changer position is adjusted. Figure 39 again shows the grid characteristics for the different tap changer positions and the generator characteristics.

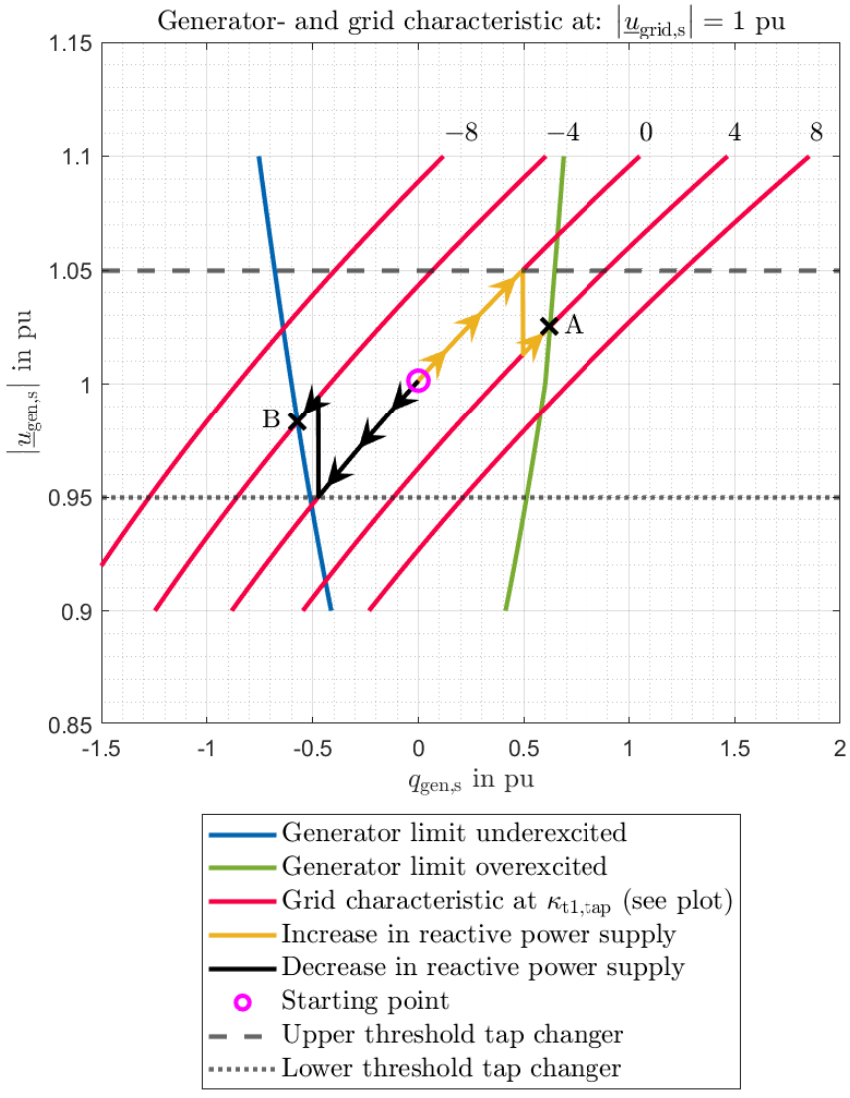


Figure 39: Reactive power supply at the generator terminals with standard tap changer control

The characteristic curves were calculated in the same way as in the model described above. The graph shown applies to a constant grid voltage $\underline{u}_{\mathrm{grid,s}} = 1$ pu. In order to calculate the reactive power supply at the point of connection, this model requires a starting point to be known. This point is characterized by a tap changer position and by the reactive power delivered at the generator terminals. Starting from this point, the generator feeds overexcited reactive power into the grid (yellow curve). If the generator terminal voltage reaches the upper switching threshold, the tap changer position increases the tap.

For better visualization, a step increment of four steps was selected in this illustration. In practice the intermediate stages are not usually skipped. In our example the tap changer jumps from position 0 to position 4. By changing the tap changer position, the associated grid characteristic also changes. The generator continues to increase the reactive power as long as either the switching threshold is reached again (than the tap changes again) or it intersects the generator characteristics and thus one of the limiting variables of the generator becomes effective. These considerations lead to the resulting tap changer position and the maximum overexcited reactive power at the generator terminals that can be supplied for this modeling (see point A).

In the next step, the reactive power output of the generator is reduced again starting from the starting point (black curve). When the generator terminal voltage reaches the lower switching threshold, the tap changer reduces the tap and a new grid characteristic is set. The generator reduces the reactive power until either the minimum switching threshold (than the tap changes again) or the underexcited generator characteristic curve is reached. Again, this leads to the used tap changer position and the minimum underexcited reactive power at the generatortermianls that can be fed in for this modeling (see point B).

Figure 40 shows a flow chart for the described modeling. Again, this is only a schematic representation of the calculation. The generator characteristics are calculated at the beginning. The grid voltage is then set to the minimum value. In general, a starting point can be defined separately for each grid voltage (tap changer position and generator terminal reactive power). A function was also developed in MATLAB that calculates a realistic starting value for the given grid voltage. For higher grid voltages, the tap changer position is usually not at the center position. The implementation of this function is also based on analytical load flow analysis (see documentation in the MATLAB code).

It is then possible to determine the tap changer position. In the MATLAB code, it is not necessary to calculate the entire grid characteristic. To find the used tap changer position, the grid characteristic is calculated at this point where the intersection with the upper or lower switching threshold is for the first time outside the generator characteristics (with repect to an increasing or decreasing order of the tap changer position). In Figure 39, this corresponds to the grid characteristic for tap changer position 4 or $-4$. This method significantly reduces the calculation time.

Once the resulting tap changer position has been determined, the intersection points with the generator characteristics or with the maximum or minimum generator terminal voltage can also be calculated.The intersection points are then converted to the point of connection as described in chapter 2.8. The grid voltage is subsequently increased and the process is repeated. This continues until the maximum grid voltage has been reached.

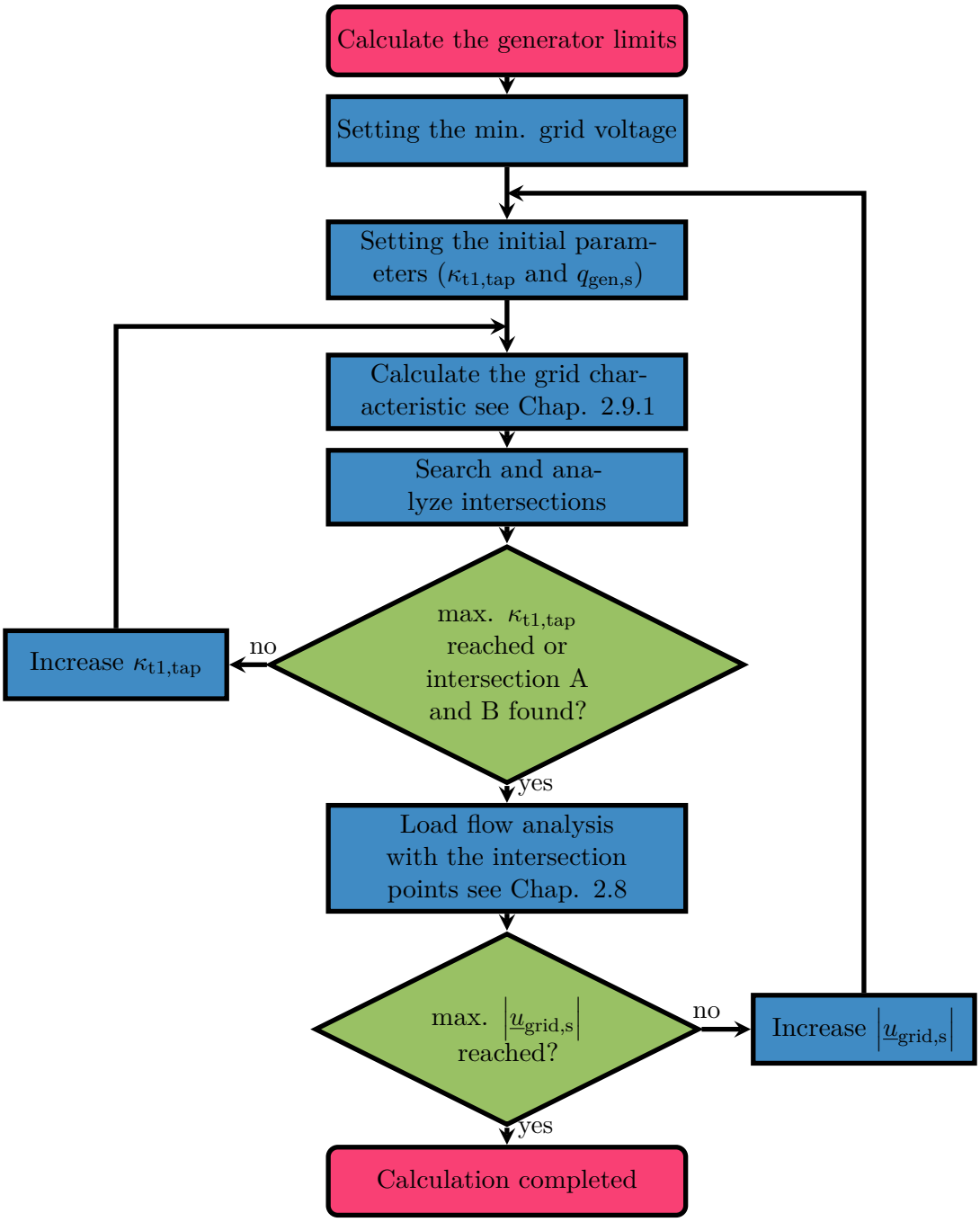


Figure 40: Flow chart of the reactive power supply with a classically controlled tap changer and constant active power at the generator terminals

### 2.18.3 Calculation of the reactive power supply with optimally controlled tap changer and constant active power at POC

The calculation method presented here is similar to those in chapter 2.18.1. In this example, the transformer tap changer is also controlled in such a way that the reactive power supply at the point of connection is maximized or minimized. The difference between the two calculation methods is that the active power at the POC is now constant. As a result, the generator provides a different active power depending on the operating point. The generator therefore covers the active power losses at the transformer and at the line. In Figure 41, the voltage at the generator terminals is plotted against the reactive power at the generator terminals in the upper diagram.

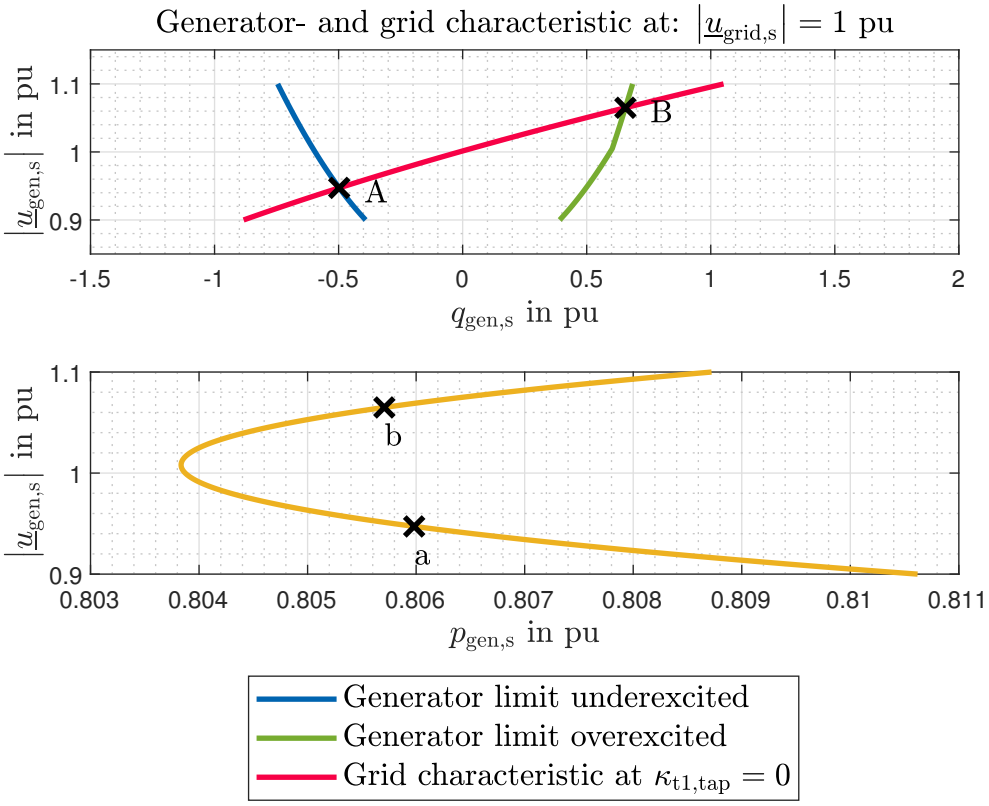


Figure 41: Reactive power supply at the generator terminals with optimum tap changer control and constant active power at POC

The generator characteristics and the grid characteristics were calculated. In this example, the intersection points A and B again correspond to the minimum and maximum reactive power that can be supplied at the generator terminals. In contrast to the calculation method from chapter 2.18.1, the active power output at intersection points A and B is not equal to the maximum capacity. The lower diagram shows the generator terminal voltage over the active power at the generator terminals, so that the active power at the point of connection is

constant. If the generator terminal voltage is taken from the upper diagram at both intersection points A and B and inserted into the lower diagram, the corresponding points a and b are obtained. The analytical load flow analysis described in chapter 2.9.3 was used to calculate the grid characteristic and the yellow characteristic from the lower plot. In this example, it should be noted that the active power output of a generator terminal is a function of the generator terminal voltage. For this reason, the generator characteristic curves (blue and green characteristic curve) also change. This means that there are different generator characteristics for each tap changer position.

Figure 42 shows the flow chart for the calculation method presented here. The calculation is similar to that shown in Figure 38. It is necessary to calculate generator characteristics separately for each tap changer position. The grid characteristic and the active power output of the generator is calculated using the load flow analysis from chapter 2.9.3. The remaining calculation does not differ from those in Figure 38. The calculation of the generator characteristics for each tap changer position has the result that the calculation time of the method presented here is significantly higher than that from chapter 2.18.1.

### 2.18.4 Calculation of the reactive power supply with classically controlled tap changer and constant active power at POC

The calculation presented here is similar to that in chapter 2.18.2. In this calculation the active power at the point of connection is constant to the maximum capacity. This means that the generator covers the active power losses of the transformer and the line. Depending on the generator terminal voltage applied, the active power output of the generator also changes. The grid characteristics required for this and the active power output of the generator are determined by applying the load flow analysis in chapter 2.9.3. The generator characteristics differ from those in chapter 2.18.2 due to the dependence of the active power output on the generator terminal voltage. This also means that the generator characteristics are calculated separately for each tap changer position. Figure 43 shows the corresponding flow chart.

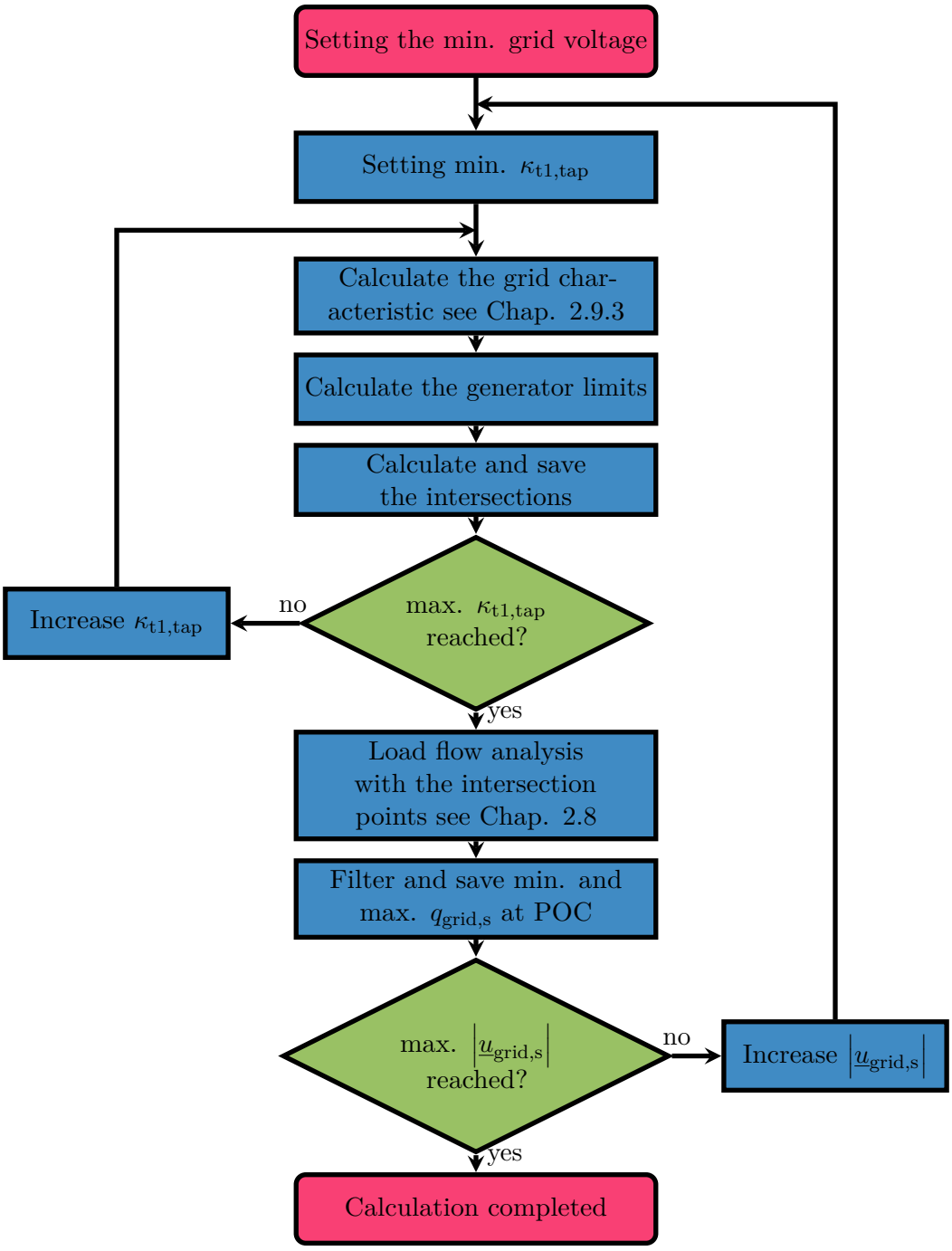


Figure 42: Flow chart of the reactive power supply with optimally controlled tap changer and constant active power at POC

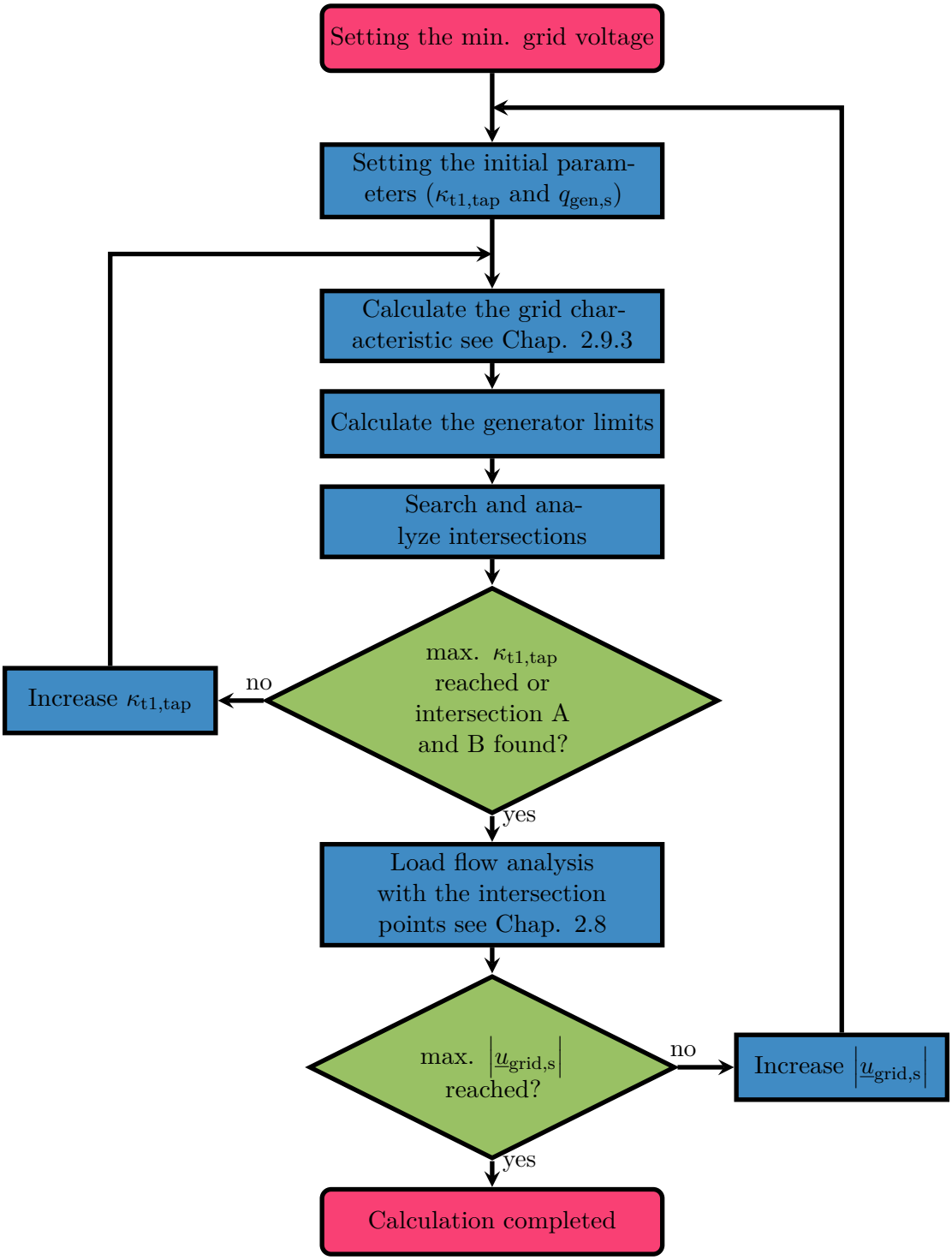


Figure 43: Flow chart of the reactive power supply with classically controlled tap changer and constant active power at POC

## 2.19 Calculation of the required reactive power supply at the generator terminals of a classic power-generating facility

In the previous calculation methods, the reactive power supply at the point of connection was calculated based on the reactive power supply at the generator terminals. The calculation method presented in this section represents a completely different approach. Here, the reactive power supply at the generator terminals is calculated based on the reactive power supply at the POC.

In the TOR, the reactive power supply at the point of connection is calculated at maximum capacity. At the beginning of the calculation, it is necessary to select one of the areas required at the point of connection (see Figure 34). From this diagram, the required overexcited and underexcited reactive and active power can be determined at a defined grid voltage. This means that both the voltage and the reactive and active power (for the overexcited and underexcited cases respectively) are known at the point of connection.

By applying the analytical load flow analysis described in chapter 2.9.4, each point can be converted from the requirements of TOR to the generator terminals. This conversion is carried out for all adjustable tap changer positions $\kappa_{\mathrm{t1,tap}}$. The minimum required reactive power supply can then be determined, taking into account the maximum and minimum generator terminal voltage, so that the requirements of the TOR are met. This calculation method has the great advantage that the operating behavior of the generator does not need to be known with regard to the capability diagram. It is only necessary to know the maximum and minimum terminal voltage of the generator. For this reason, this calculation method is significantly faster than the others presented. Figure 44 shows the flow chart for the calculation method described.

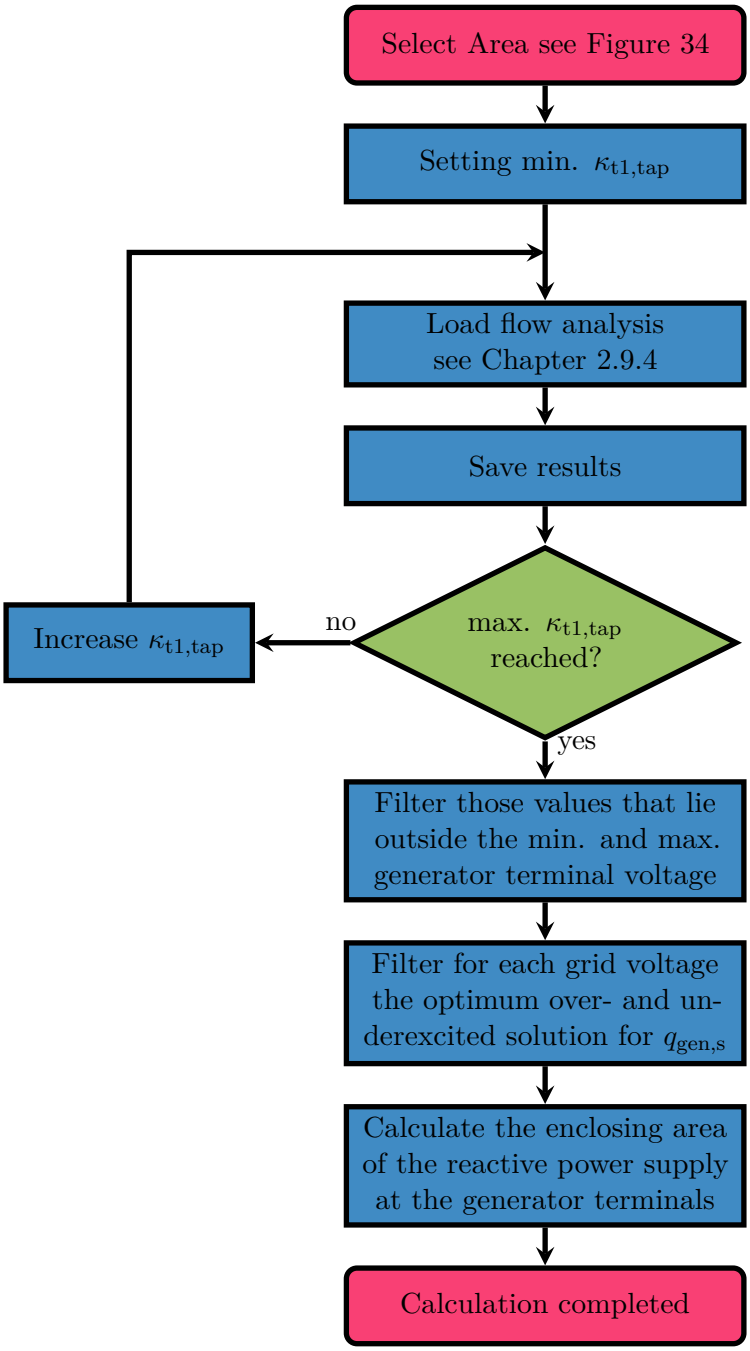


Figure 44: Flow chart of the calculation of the required reactive power supply at the generator terminals of a classic power-generating facility

## 2.20 Calculation approaches for the calculation of the reactive power supply at POC (hybrid power-generating facility)

In addition to the classic power-generating facilities, hybrid power-generating facilities are also considered in this master's thesis. The approach for calculating the reactive power supply at the point of connection for a hybrid power-generating facility, as shown in Figure 17, is again based in the first step on the calculation of the reactive power supply at the generator terminals. For this purpose, it is necessary to calculate the grid characteristics at the generator terminals for the overexcited and underexcited operation (the constrains regarding terminal current and terminal voltage are fulfiled) of the converter for each grid voltage (see Figure 45).

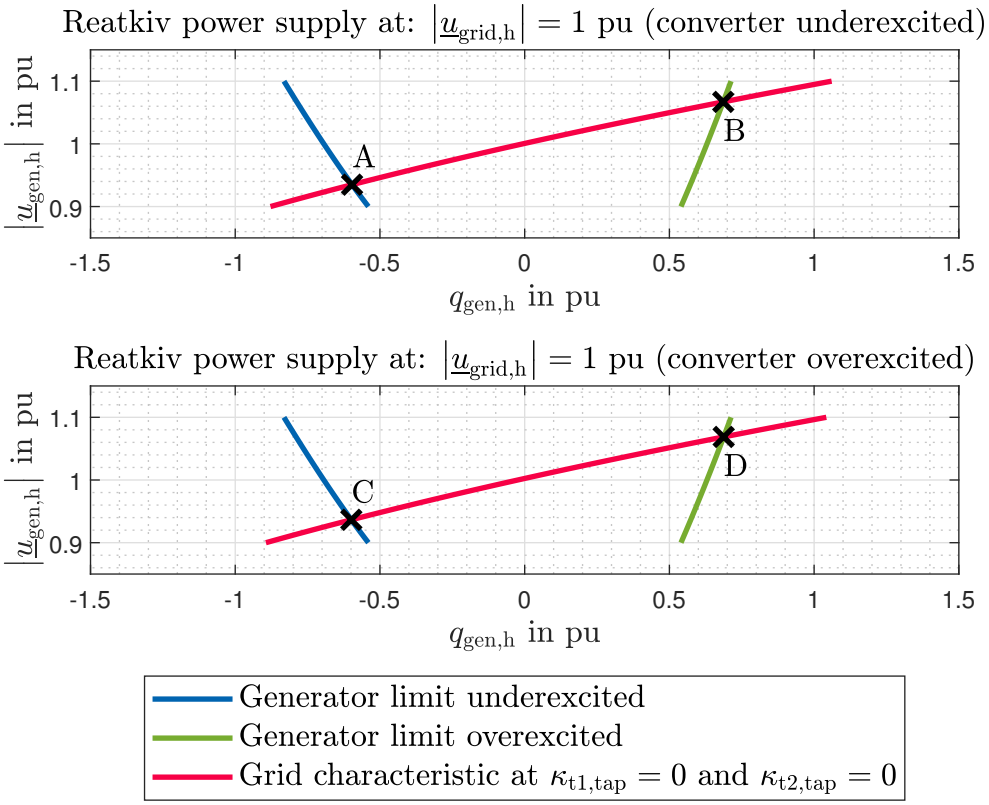


Figure 45: Reactive power provision at the generator terminals with optimum tap changer control (hybrid power-generating facility)

In Figure 45, the two grid characteristics are shown in red. With the grid characteristic in the upper diagram, the converter supplies the lowest possible underexcited reactive power (generator convention), taking into account the operating limits of the converter (see chapter 2.16). In the lower diagram, the grid characteristic shows the reactive power at the generator terminals at the maximum overexcited reactive power that can be supplied by the converter (see chapter 2.16).

In this calculation method, the active power output at the generator terminals and the converter terminals is known and constant. The active power output of the generator or converter is distributed as a percentage of the maximum capacity to the two power-generating modules. Due to the constant active power output at the generator terminals, the generator characteristics (blue and green characteristics) are independent of the actual grid voltage. It is then possible to determine the intersection points (A, B, C, D) between the grid characteristics and the generator characteristics. The intersection points describe the reactive power that can be supplied at the generator terminals.

Since the reactive and active power output is known at both the converter terminals and the generator terminals, this can be converted to the point of connection by applying the calculation from chapter 2.13.3. This process is repeated for the various combinations of tap changer positions ($\kappa_{\mathrm{t1,tap}}$ and $\kappa_{\mathrm{t2,tap}}$) of the two transformers. As a result, the overexcited and underexcited reactive power values at the point of connection are known for a certain grid voltage and for the different tap changer positions. The maximum and minimum reactive power values with the corresponding tap changer positions are filtered out from these values. The grid voltage is then increased and the process is repeated. This continues until the maximum grid voltage is reached.

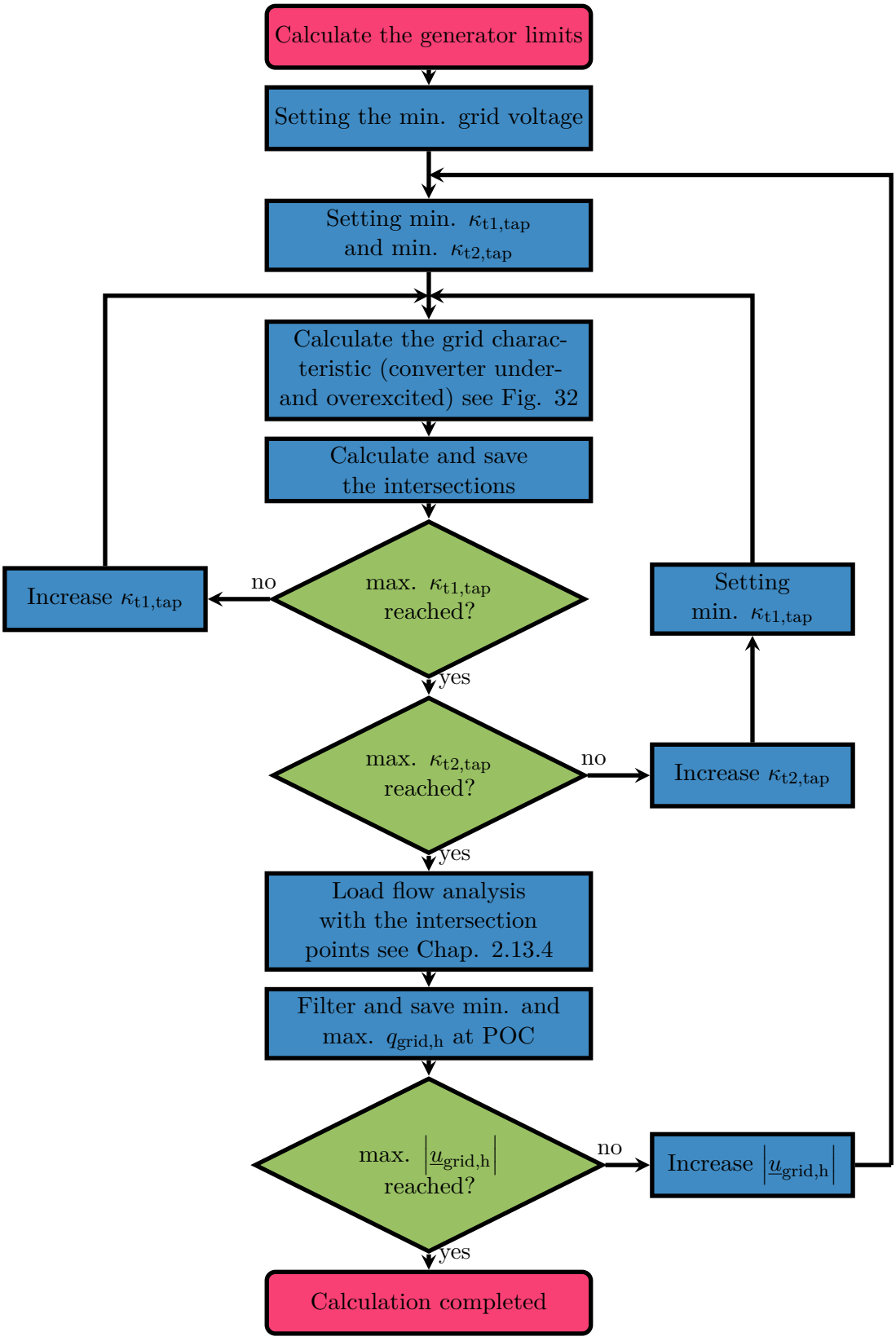


Figure 46: Flow chart of the calculation of the reactive power supply at POC (hybrid power-generating facility)

# 3 Results of the calculations

This chapter analyzes the results of the calculations that were carried out. In order to keep the calculation as understandable as possible, the tables 3 to 8 in the appendix show the parameters used to model the power-generating facilities. Unless otherwise stated, the power in the following figures are based on the maximum capacity. The voltages were based to the respective rated voltages.

The generator capability diagram was modeled with a linear stability limit and constant apparent power limit. For the calculations described below, a simple overhead line was considered in the calculation instead of a double-circuit line (see Figure 58). Unless otherwise noted, all illustrations are in generator convention.

## 3.1 Reactive power supply of the classic power-generating facility at POC

Figure 47 shows the reactive power supply of a classic power-generating facility at the point of connection.

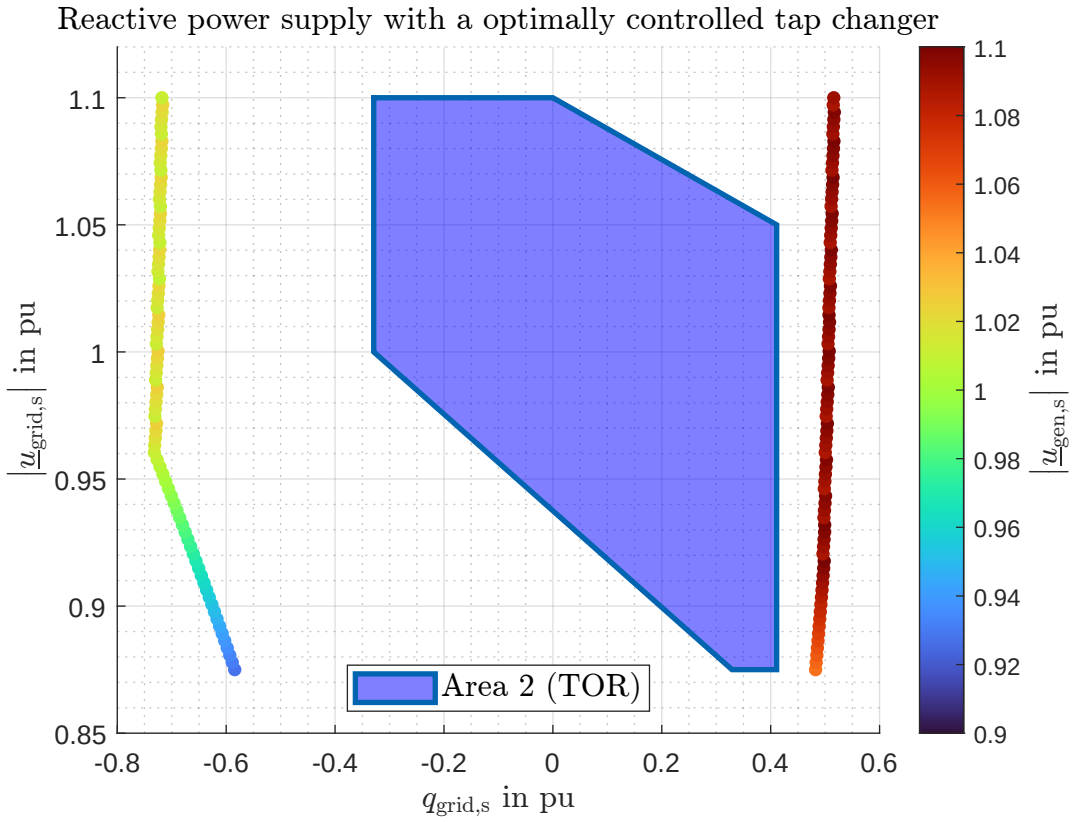


Figure 47: Reactive power supply with optimal controlled tap changer (const. $p_{\mathrm{grid,s}}$)

An optimally controlled tap changer and a constant active power at the point of connection were used for the modeling in Figure 47. The generator terminal voltage is represented by the colorbar. It can be seen that in the overexcited range, the generator terminal voltage is kept as high as possible by the optimally controlled tap changer. In the underexcited area, the generator terminal voltage is in the range of the rated voltage (slightly below the rated voltage).

Figure 48 also shows the reactive power supply at the point of connection.

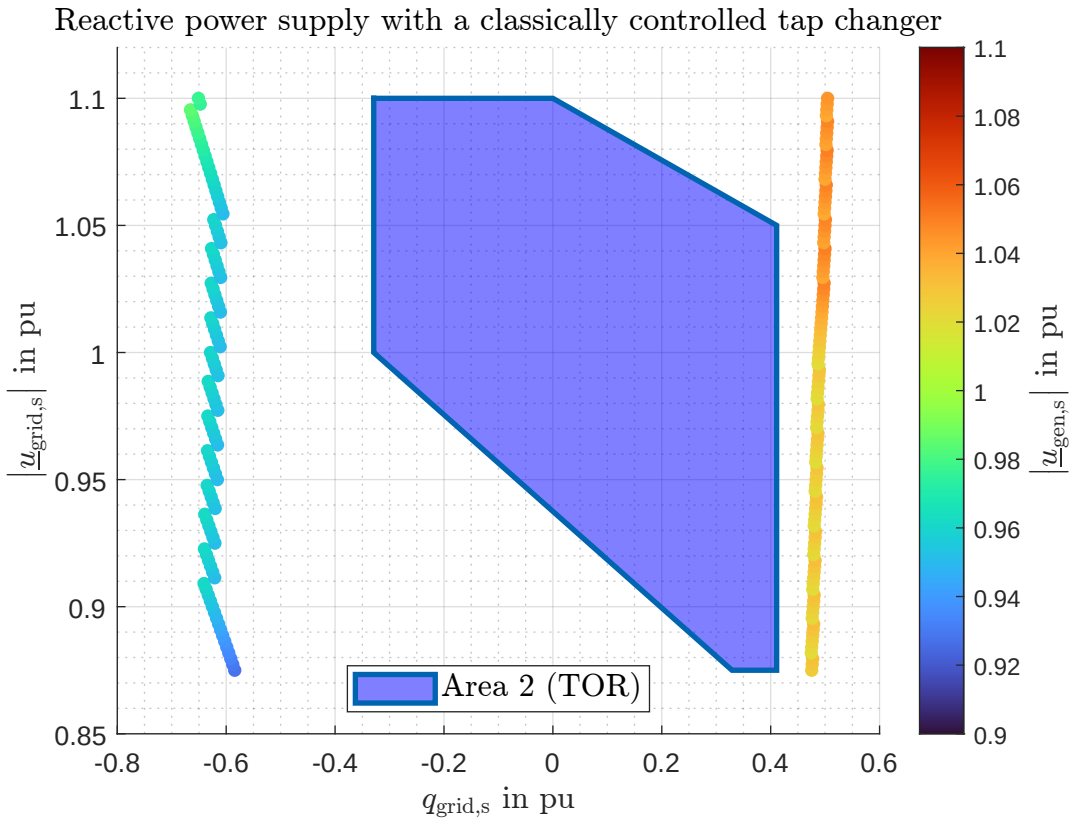


Figure 48: Reactive power supply with classically controlled tap changer (const. $p_{\mathrm{grid,s}}$)

For the modeling in Figure 48, a classically controlled tap changer was used. In this Figure, the active power at the point of connection is also constant. If you compare Figure 48 with Figure 47, it can be seen that the reactive power supply is slightly reduced, especially in the underexcited range. This can be attributed to several reasons.

At the beginning, a linearly decreasing section in the range of the nominal grid voltage can be seen in the underexcited area. This range results from the selected or calculated starting tap changer position and starting reactive power supply of the generator (see chapter 2.18.4). Depending on the selection of these initial conditions, this linearly decreasing section can be shifted vertically.

Another significant difference between Figure 48 and 47 is the generator terminal voltage. Due to the regulation of the transformer, it can keep the generator terminal voltage within the specified limits. This is only the case if the tap changer has a sufficient operating range (number of stages with the corresponding additional voltage). In the example selected, this is the case, so the generator terminal voltage remains within a range of ±5 % of the rated voltage. This leads to a slightly lower reactive power output of the generator, especially for the underexcited range, depending on the choice of modeling of the capability diagram (see chapter 2.15).

### 3.1.1 Differences in modeling between constant active power at the generator terminals and constant active power at the POC

Chapters 2.18.2 and 2.18.4 describe the method for calculating the reactive power supply at the point of connection for a classically controlled tap changer. In this calculation, a distinction can again be made as from whether the active power output of the generator or the active power at the point of connection is kept constant.

If the active power at POC is kept constant, the genertor must cover the active power losses of the transformer and the line. As the generator is operated close to the nominal point, it must be ensured that the turbine is also able to provide the additional active power to cover the active power losses. Figure 49 shows the reactive power supply at the point of connection for the two cases described, using a classically controlled tap changer.

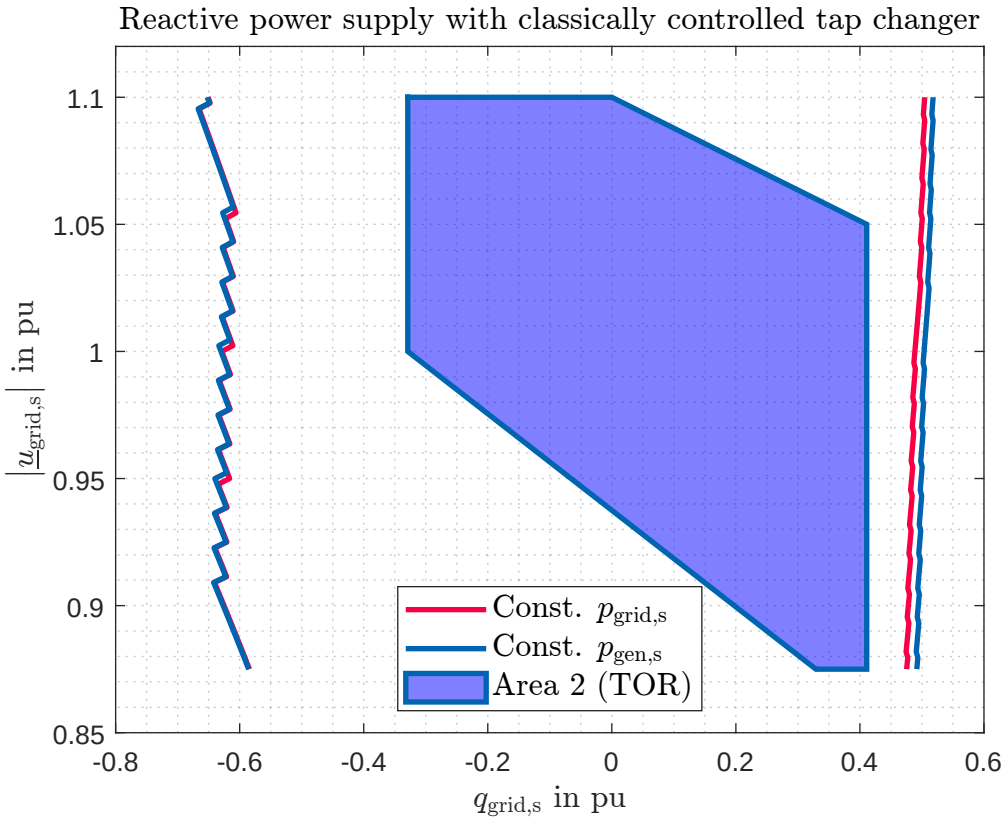


Figure 49: Reactive power supply with classically controlled tap changer (const. $p_{\mathrm{gen,s}}$ and const. $p_{\mathrm{grid,s}}$)

The diagram in Figure 49 is in the generator convention. In the negative range, the deviations between the two models are very small. In the overexcited range, there is a slight shift towards lower reactive power values. The described behavior can be attributed to two effects. On the one hand, the slightly increased active power flow via the transformer and the overhead line also results in an increased inductive reactive power requirement. In addition to this effect, the reactive power output of the generator is also reduced by the increased active power supply (see capability diagram).

Chapters 2.18.1 and 2.18.3 describe the calculation of the reactive power supply at the point of connection when using an optimally controlled tap changer. A distinction is made between a variant with constant active power at the generator terminals and at the point of connection. Figure 50 also shows that the reactive power supply at the point of connection is slightly reduced in the case of the calculation with constant active power at POC due to already above described two reasons.

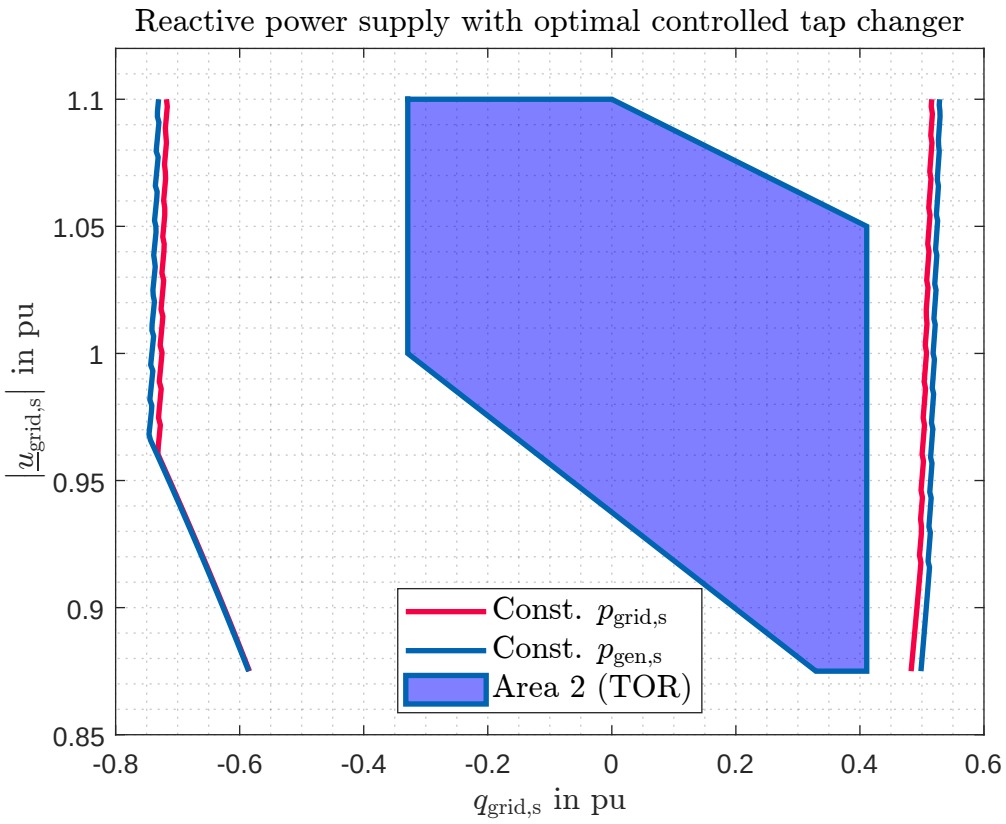


Figure 50: Reactive power supply with optimally controlled tap changer (const. $p_{\mathrm{gen,s}}$ and const. $p_{\mathrm{grid,s}}$)

When analyzing these two Figures, it must be noted that due to the frequent calculation of the capability diagram, the calculation with the constant active power at the point of connection is significantly more time-consuming than the calculation with constant power at the generator terminals.

### 3.1.2 Influence of the tap changer on the reactive power supply

The reactive power supply at the point of connection is restricted by the limits in the generator's capability diagram. Figure 51 shows the mentioned limits that restrict the reactive power supply at the point of connection.

For this purpose, the tap changer was fixed in the middle position. It can be seen that in the overexcited range, the maximum generator terminal voltage and the maximum apparent power is limiting.

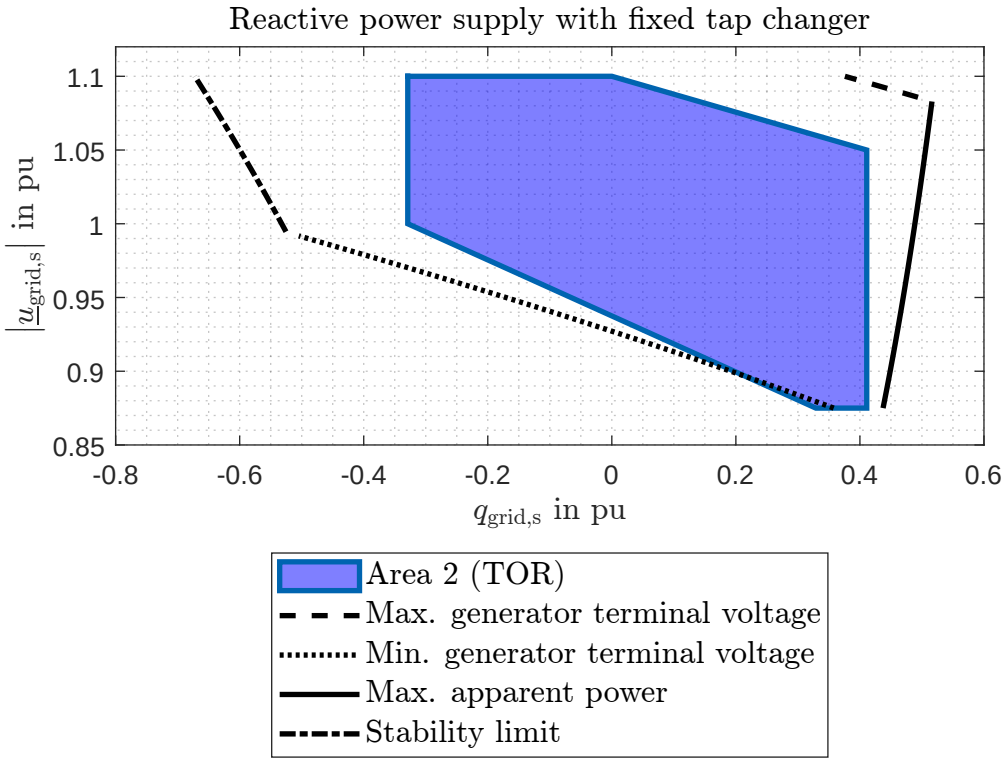


Figure 51: Limits of the capability diagram in reactive power supply (const. $p_{\mathrm{grid,s}}$)

In the underexcited range, the minimum generator terminal voltage and the stability limit have a limiting effect. For higher voltages in the underexcited range, there is also a limit on the maximum apparent power. The generator active power is above the rated active power for every operating point, which is why the maximum excitation current limit does not have a limiting effect in the overexcited range. The same applies to the minimum excitation current limit in the underexcited range.

Figure 52 shows the reactive power supply at the point of connection when the tap changer is fixed. The active power at the point of connection was modeled as constant. This results in the three areas shown.

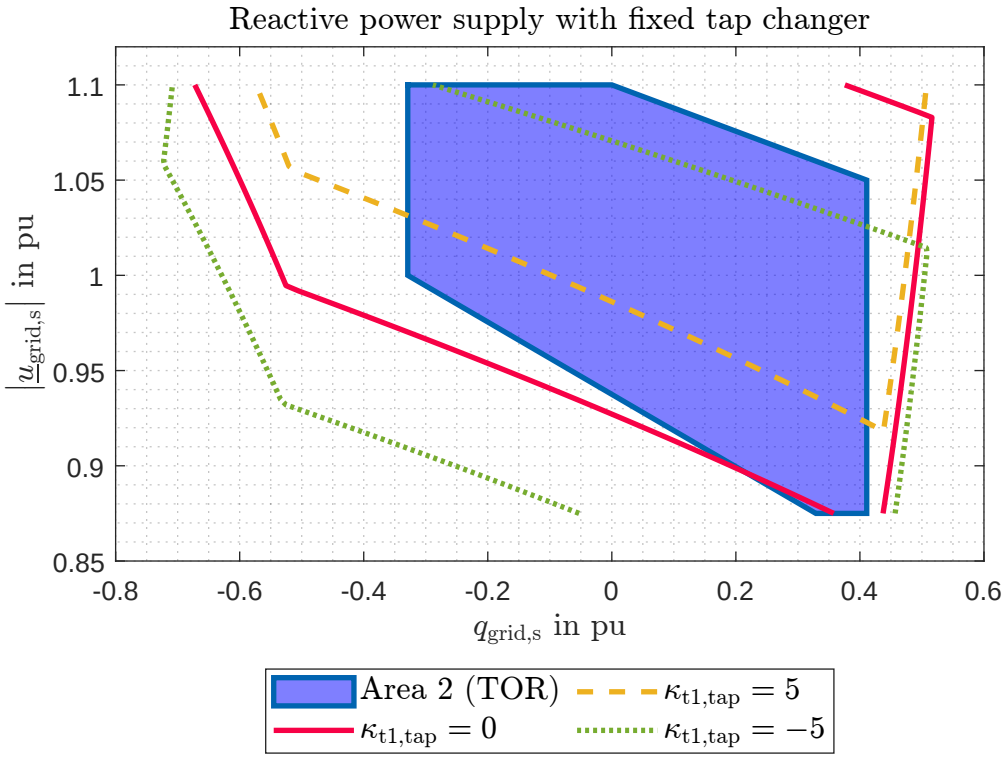


Figure 52: Reactive power supply with different tap changer positions (const. $p_{\mathrm{grid,s}}$)

It can be seen that an increase in the tap changer position results in a shift of the areas towards higher voltages. If the tap changer position is reduced, there is a shift towards lower voltages. By looking at the red area (tap changer position is in the middle position), it can be seen that it intersects area 2 of TOR due to the maximum generator terminal voltage limit. The reactive power supply at the point of connection can be significantly increased by using the classically controlled or optimally controlled transformer tap-changer, as shown in Figure 49.

### 3.1.3 Influence of the transformer short-circuit voltage on the reactive power supply

The short-circuit voltage is a characterizing variable for transformers. The short-circuit voltage also has an influence on the reactive power supply. As already described, the short-circuit impedance of the transformer is described by the short-circuit voltage. For this reason, it also represents a parameter for the reactive power requirement of the transformer. A higher short-circuit voltage also results in a higher reactive power demand during operation. Therefore the reactive power supply at the point of connection also changes with the selected short-circuit voltage.

Figure 53 shows the reactive power supply at the point of connection (constant active power at POC and optimally controlled tap changer). It can be seen that with increasing short-circuit voltage, there is a shift towards lower reactive power values at the point of connection. This is due to the increased inductive reactive power demand of the transformer.

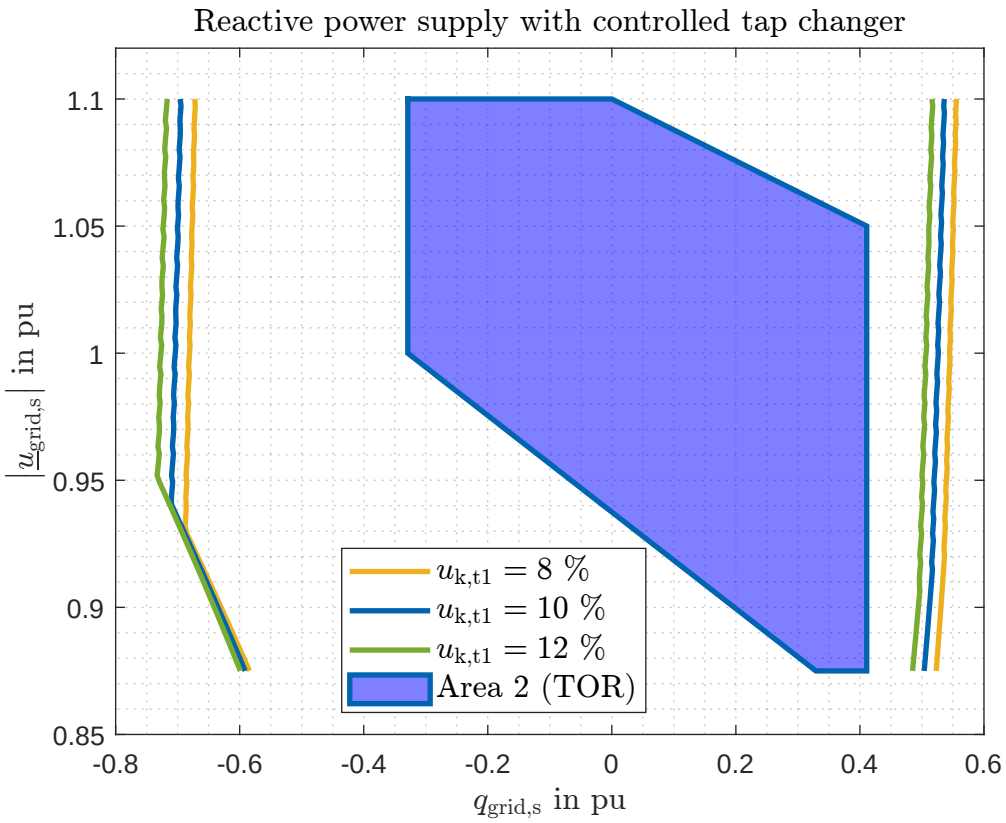


Figure 53: Influence of the transformer short-circuit voltage on the reactive power supply (optimally controlled tap changer and const. $p_{\mathrm{grid,s}}$)

## 3.2 Calculation of the reactive power supply at the generator terminals

The chapter 2.19 already describes that it is also possible to calculate the reactive power supply at the generator terminals based on the analytical load flow analysis. The calculation is designed in such a way that if the reactive power supply at the generator terminals is met, the reactive power supply at the point of connection (see TOR ) is fulfilled.

Figure 54 shows the required reactive power supply at the generator terminals to fulfill the reactive power supply at the point of connection of area 2. For this calculation, the tap changer position was fixed. It can be seen that there is a drift of the ranges towards smaller reactive

power ranges. This is due to the inductive reactive power demand of the transformer and the overhead line. Furthermore, a vertical shift of the ranges can be seen depending on the selected tap changer position.

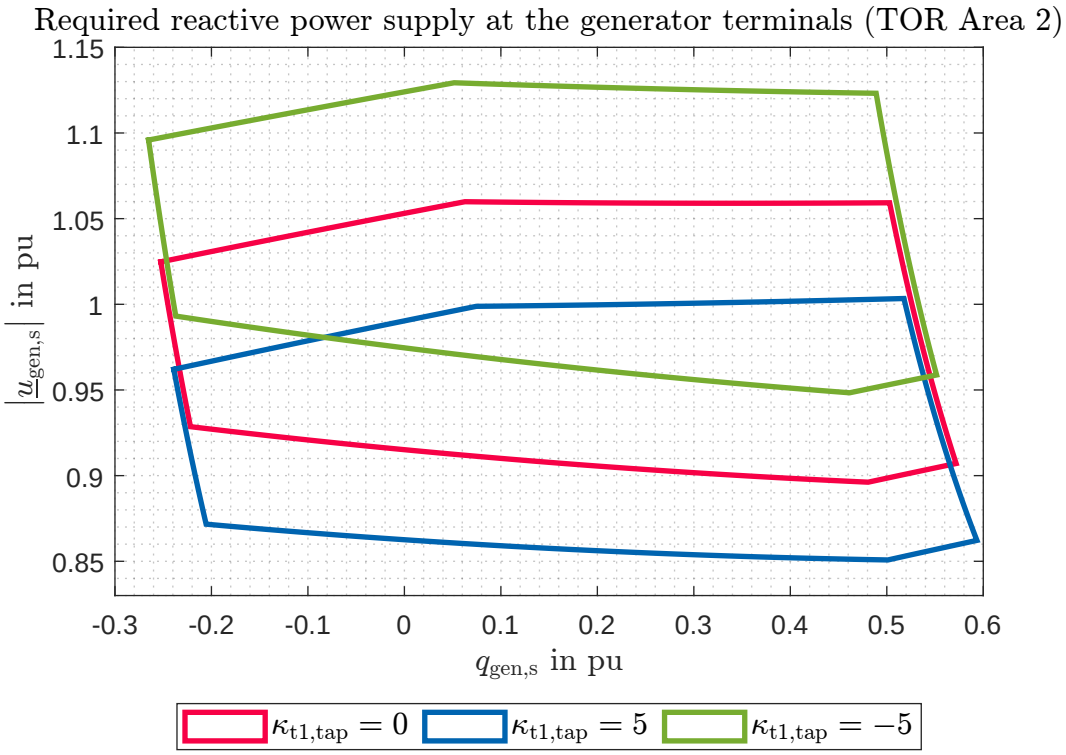


Figure 54: Reactive power supply at the generator terminals when the tap changer is fixed

Figure 55 also shows the reactive power supply at the generator terminals. The tap changer is optimally controlled. This can be interpreted as that the control of the transformer tap changer is set so that the generator has to deliver as little reactive power as possible at the generator terminals in order to fulfill the reactive power supply at the point of connection.

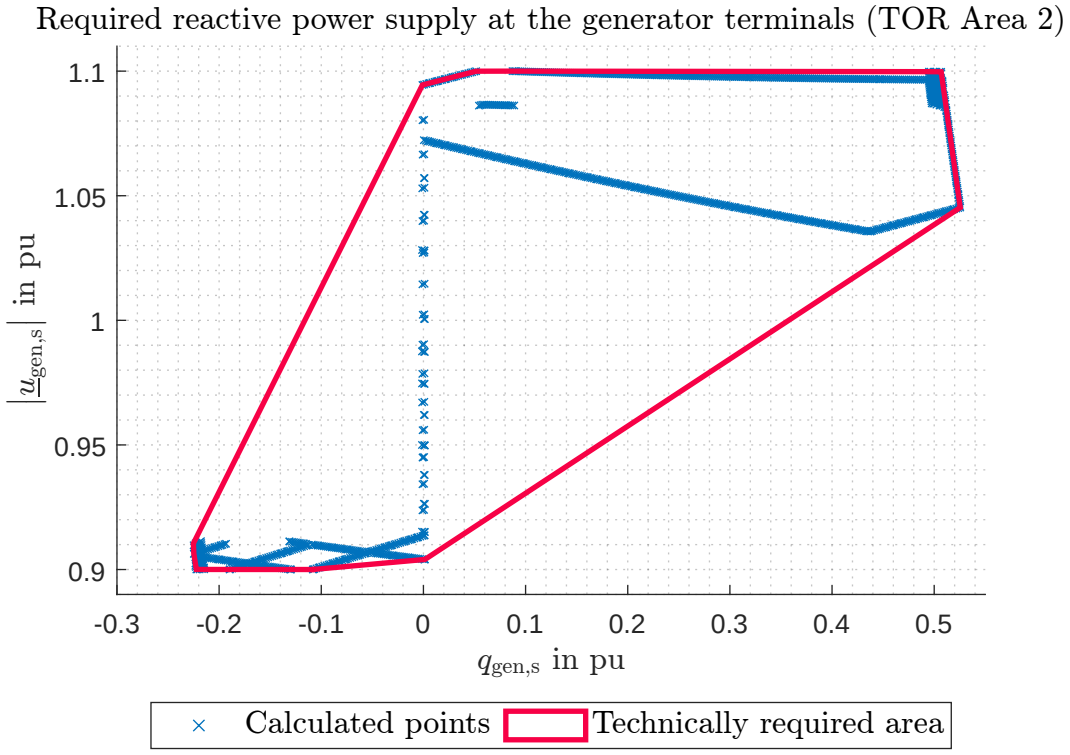


Figure 55: Reactive power supply at the generator terminals with optimally controlled tap changer

As described in chapter 2.19, the operating points indicated with blue crosses are obtained as the calculation result in the first step. When calculating these operating points, attention was paid to compliance with the maximum and minimum generator terminal voltage. If the generator is able to reach these operating points, then the reactive power supply corresponding to area 2 according to TOR.

As these points do not represent a technically meaningful operating range, a technically meaningful operating range (red range) is calculated. This area covers all operating points. The great advantage of this calculation variant is that the capability diagram of the generator does not need to be known. This type of representation can be helpful, especially for power-generating facilities that are in the planning stage.

## 3.3 Reactive power supply of a hybrid power-generating facility at POC

The reactive power supply of a hybrid power-generating facility at the point of connection is analyzed in more detail below. In order to increase the comparability of the results, the same maximum capacity was assumed for the hybrid power-generating facility as for the classic power-generating facilities. Figure 56 shows the reactive power supply of the hybrid power-generating facility.

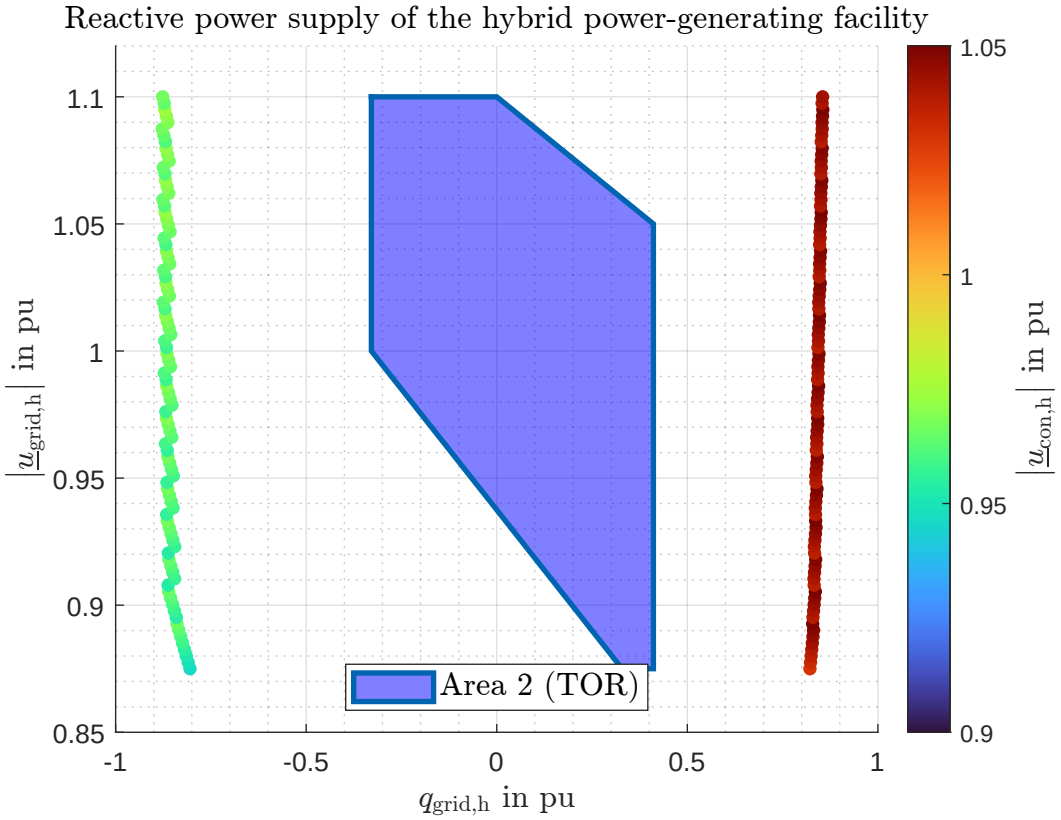


Figure 56: Reactive power supply of a hybrid power-generating facility

Compared to the classic power-generating facilities, a significantly increased reactive power supply at the point of connection can be seen. If the converter terminal voltage is considered, it can be seen that it is as high as possible for the overexcited reactive power, similar to the generator terminal voltage. In the area of underexcited reactive power output, the converter terminal voltage is close to the rated operating voltage. Figure 57 shows the reactive power supply of a hybrid power-generating facility with a reduced number of tap changer positions (-2 to 2) for transformer 2.

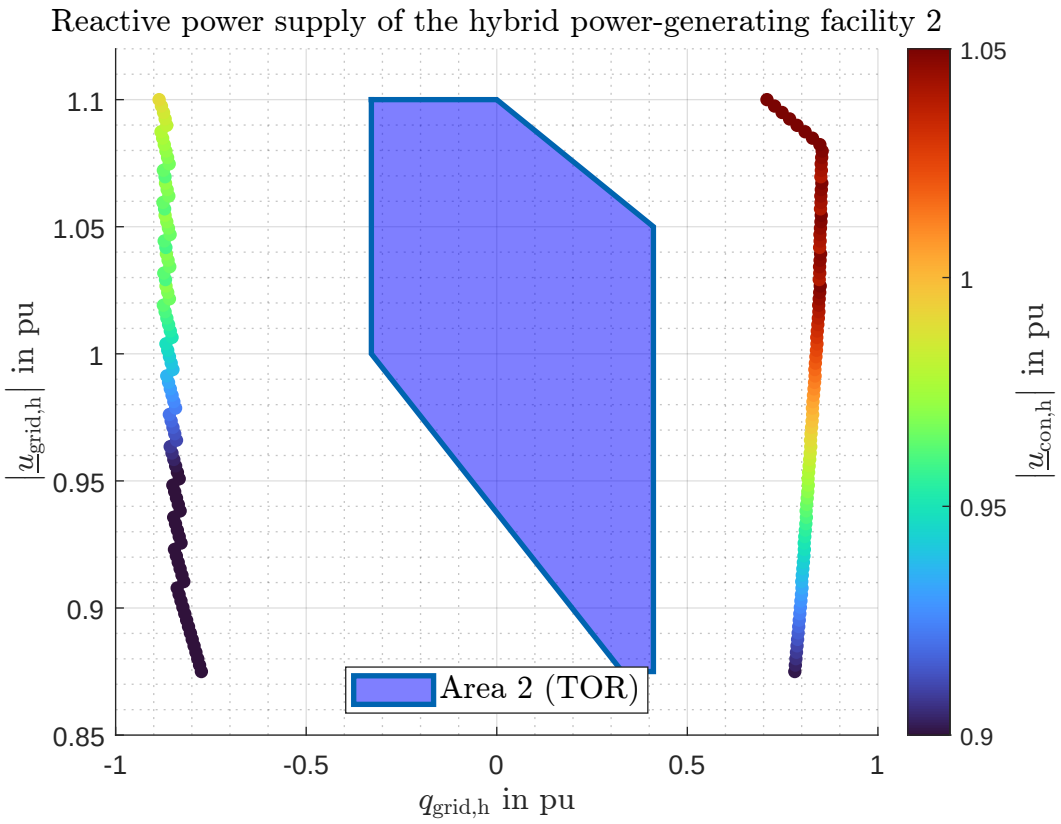


Figure 57: Reactive power supply of a hybrid power-generating facility with a reduced number of tap changer positions

The differences are particularly evident in the overexcited range at higher grid voltages. To ensure that the maximum generator terminal voltage is not exceeded in this range, the converter must reduce its reactive power supply. For this reason, there is also a reduced reactive power supply in the overexcited range compared to Figure 56.

Both diagrams were created in such a way that the tap changer position is optimized. It can also be seen that the converter terminal voltage drops relative sharply in the underexcited range for low voltages. In summary, it can be seen that the operating range (number of taps with the corresponding voltage adjustments) of the transformer influences the reactive power supply at POC.

# 4 Experiments

In order to verify the results of the calculations, the experiments presented here are done in active grid operation. The experiments are performed in cooperation with an Austrian energy supply company and the local grid operator. Prior to the experiments, a detailed test concept was also developed as part of the master's thesis presented here. The following is an excerpt of the results of these experiments.

## 4.1 Power-generating facility to be analyzed

In the course of the experiments, it is possible to disconnect an overhead line in the 110 kV-grid. This overhead line is connected to the 220 kV-grid via a regulating transformer. In this setup, the point of connection is assumed to be at the low voltage terminals of the regulating transformer.

For the experiments, both a classic power-generating facility and a hybrid power-generating facility with an optimized tap changer are considered. The structure for the experiments to verify a classic power-generating facility is shown in Figure 58. The active power, reactive and the voltage are measured at the generator terminals, the high-voltage side transformer terminals and the POC.

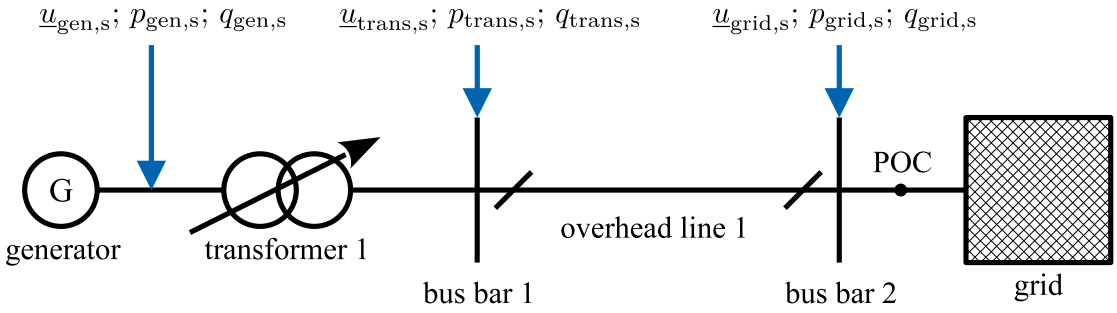


Figure 58: Structure of a classic power-generating facility for the experiments

Figure 59 shows the test setup for verifying the reactive power supply of a hybrid power-generating facility. As there is no converter on site, the stationary operating behavior of the converter is simulated by a generator. Both transformers have tap changers, which are controlled using the method for the optimized tap changer developed in this master's thesis.

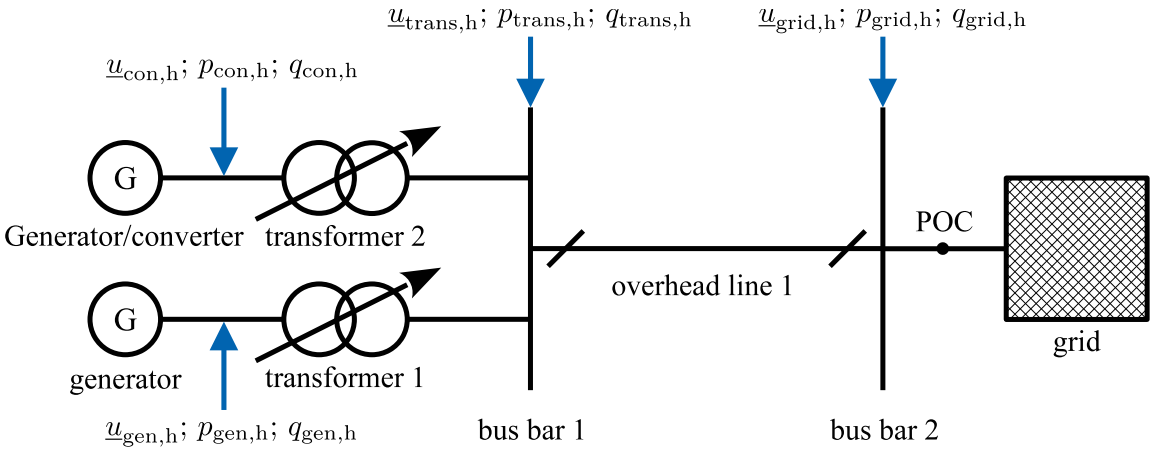


Figure 59: Structure of a hybrid power-generating facility for the experiments

## 4.2 Test sequence of the classic power-generating facility

The electrical parameters used for the experiments are shown in Table 3 to 8. A generator model with a linear stability limit and a constant apparent power limit was selected. The stability limit was dimensioned conservatively in order to be able to reliably rule out possible unstable operation. The tap changer positions are set manually. For this purpose, the optimum tap changer positions for the different grid voltages were determined from the calculations in preparation for the test.

Figure 60 shows an example of the optimum transformer taps for underexcited reactive power at POC. Further plots regarding the optimum tap changer position can be found in the test planning documentation.

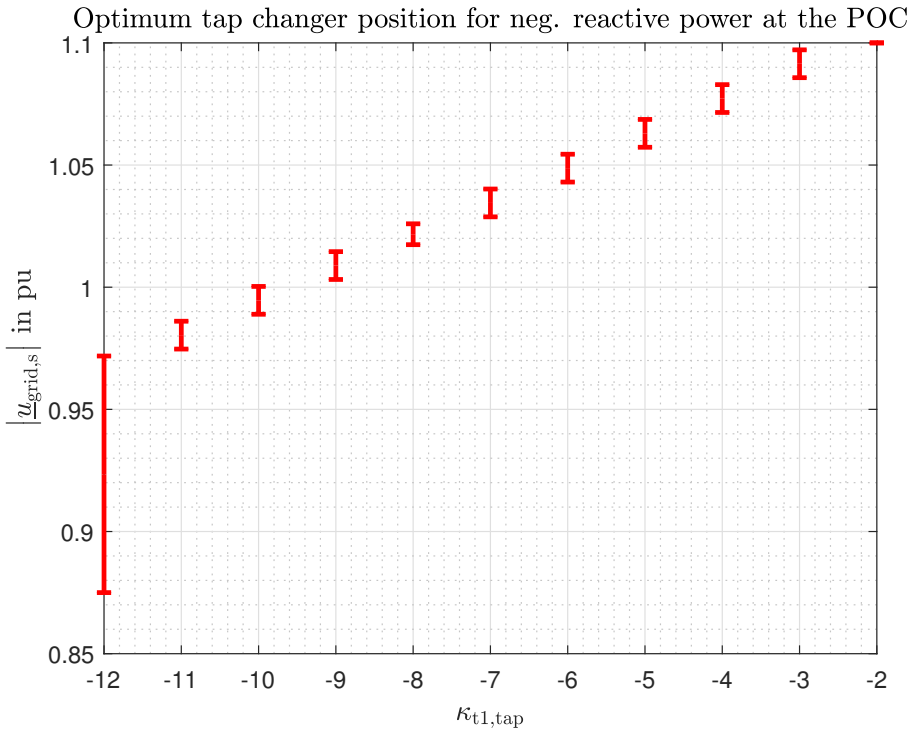


Figure 60: Optimal tap changer position for underexcited reactive power at POC

The first test sequence is shown schematically below (see Figure 61). At the beginning of the test, it is necessary to establish the desired switching state in the grid. To do this, it is necessary that only the generator is switched on bus bar 1 of the power plant. The same applies to bus bar 2. The grid voltage is set to the maximum permitted value using the regulating transformer on bus bar 2.

The reactive power supply of the generator is then increased by increasing the excitation current. At the same time, the tap changer is set according to the calculated optimum tap position. Care must be taken to ensure that the operating limits of the generator are not exceeded when switching the tap changer position. It may therefore be necessary to set the optimum tap changer position in stages as the reactive power output increases.

The excitation current is increased successively and in relatively small steps so that the operating limits (maximum or minimum generator terminal voltage and reactive power output from the MATLAB model) are not exceeded. To ensure this, the generator terminal voltage and the current active power output of the generator are successively entered into the MATLAB model during the excitation current adjustment and the maximum or minimum reactive power output is calculated. Exceeding the maximum or minimum generator terminal voltage can be continuously checked directly on the display instruments.

When the operating limits are reached in the overexcited (voltage-increasing) range, the excitation current is successively reduced and the tap changer position is adjusted to the optimum value. Here too, compliance with the operating limits is continuously checked using the MATLAB model or the display instruments. When the operating limits are reached in the underexcited (voltage-reducing) range, the grid voltage is reduced and the process starts again by increasing the excitation current.

When the minimum grid voltage is reached, the first test is completed. The active power output of the generator is set during the entire test so that the maximum capacity is measured at the point of connection (bus bar 2).

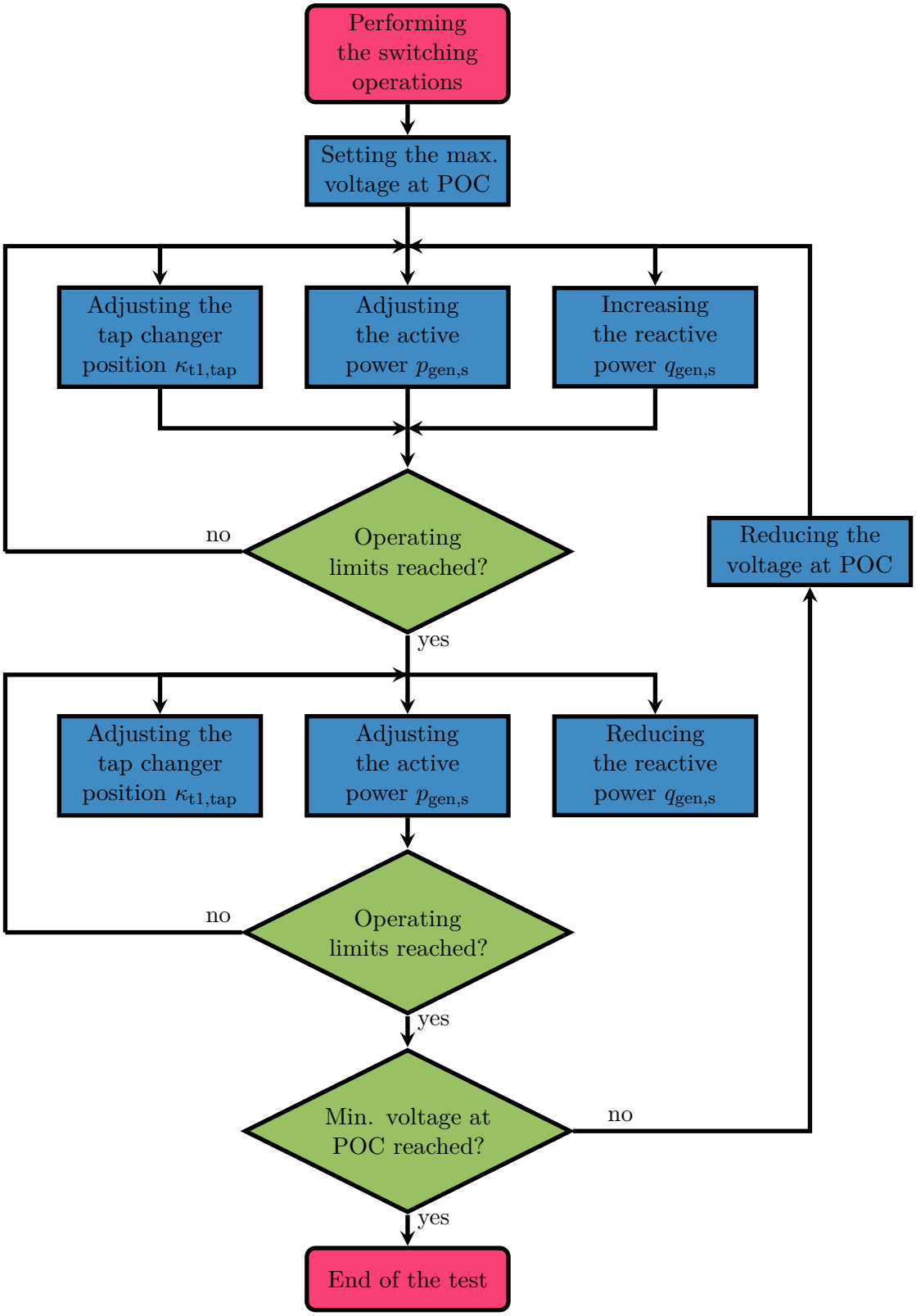


Figure 61: Flow chart of the test sequence of the classic power-generating facility

## 4.3 Test sequence of the hybrid power-generating facility

Figure 62 shows the sequence of the second test in the form of a flow chart. The basic sequence does not differ from that of the first experiment. At the beginning, the switching state is again set and the maximum grid voltage is adjusted with the regulating transformer.

In the second experiment, two synchronous generators are responsible for the reactive power supply, one of them simulates the stationary behavior of a converter (see chapter 2.16 ). After setting the maximum grid voltage, the reactive power output is increased for both machines (increasing the excitation current), and the tap changer position is also optimally set using the previously calculated data.

In contrast to the first test, the active power output of both generators is kept constant. Minor adjustments may be necessary during the test. When the operating limits of both machines are reached, the process can be continued for underexcited (voltage-reducing) operation by reducing the excitation current. If the operating limits in the underexcited (voltage-reducing) range are reached, the grid voltage is reduced. The process is repeated until the minimum grid voltage is reached. When the minimum grid voltage is reached, the second test is completed. In this test, the operating points are also continuously checked with the MATLAB model and corrected if necessary.

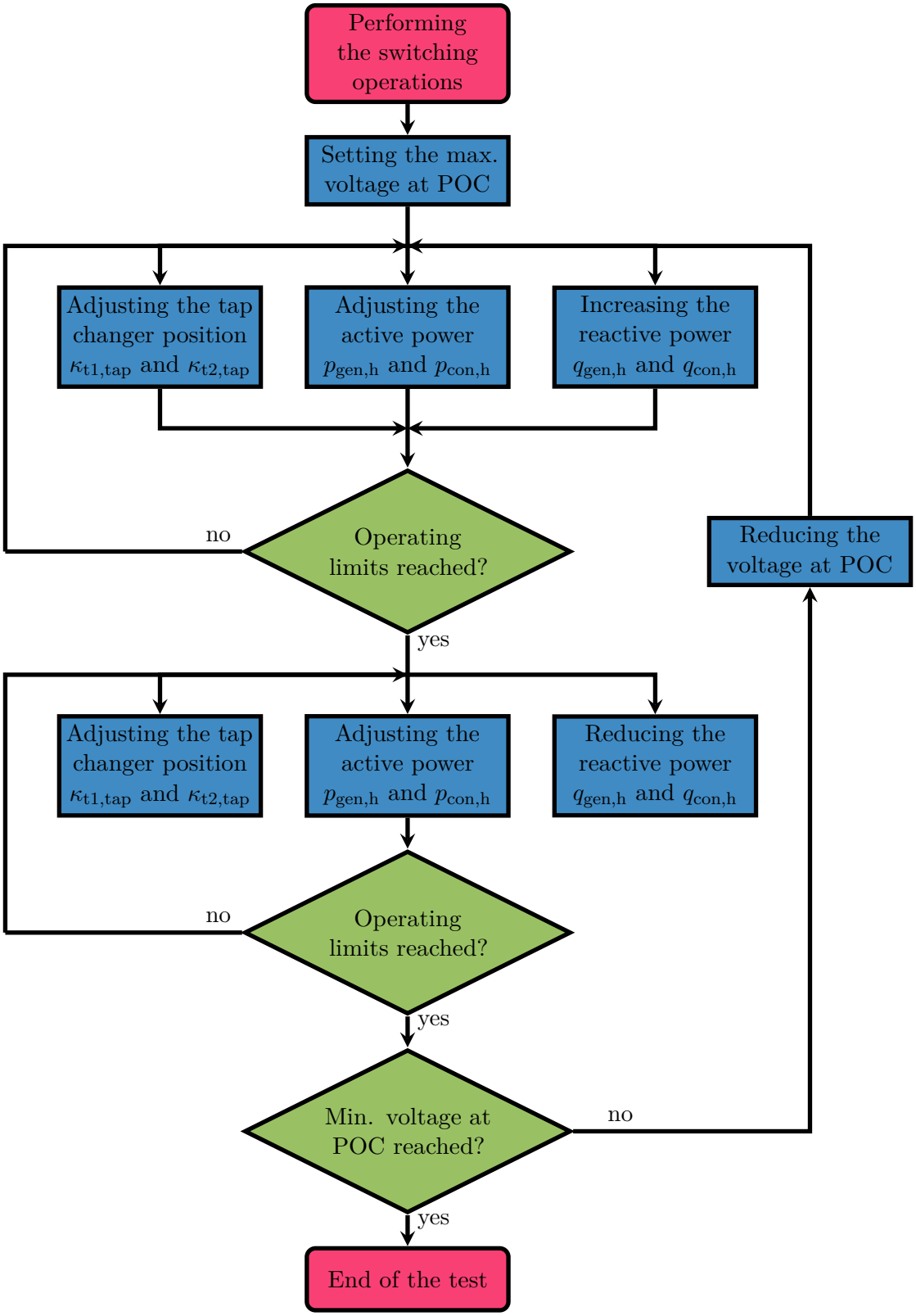


Figure 62: Flow chart of the test sequence of the hybrid power-generating facility

## 4.4 Results for the verification of classic power-generating facility

Figure 63 shows the measurement results of the experiment to verify the reactive power supply at the POC of a classic power-generating facility.

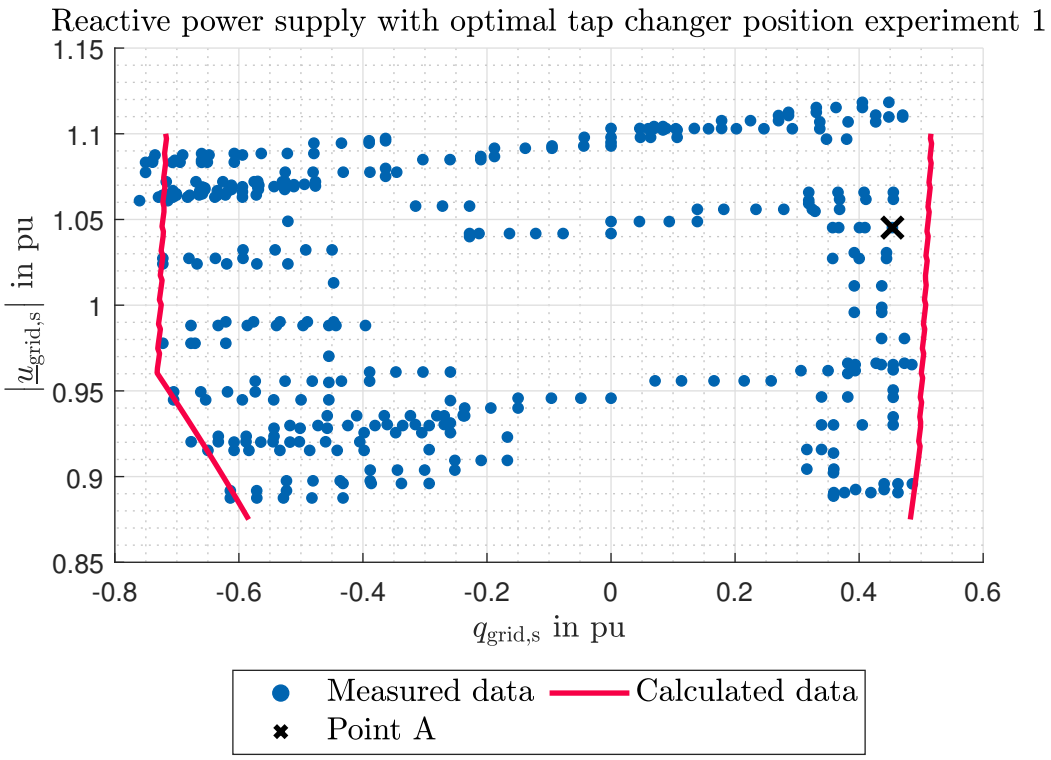


Figure 63: Measurement results for the reactive power supply at the POC of a synchronous power-generating facility

As described in the previous explanations, the optimum tap changer positions at the corresponding grid voltages $\underline{u}_{\mathrm{grid,s}}$ were set manually during the experiment (see Figure 60). The operating limits of the generator were continuously checked using the MATLAB model created in this master's thesis. The parameters for this can be found in table 3. The active power at the generator was set so that the maximum capacity at the point of connection could be kept as constant as possible.

During the experiment, the voltages, active power and reactive power were measured at the nodes. The aim of the measurements is to feed in as much overexcited or underexcited reactive power as possible at the POC. If the measured values of the grid voltage are plotted against the reactive power at the POC, the blue points in Figure 63 are obtained. The red curves represent the results of the previous calculations for an optimally controlled tap changer position.

Looking at the negative reactive power range in Figure 63, it can be seen that the calculated

curve encloses the measured values very well. In particular, the limiting underexcited range for grid voltages below 0.95 pu is represented very well. For higher voltages, there are slight deviations. It should be noted that in practical experiments it is quite difficult to precisely match the operating limits of the generator. For this reason, the measured values that violate the generator limits are not shown in Figure 63.

It should also be noted that the active power at the POC could not always be set exactly at maximum capacity. There were fluctuations of around ± 0.15 MW from the target value (27.2 MW). The active power was set as optimally as possible for the experiment by directly adjusting the nozzle opening of the pelton turbine. For the reasons mentioned, the active power output at the generator terminals is not always exactly the optimum value from the calculations. As a result, the possible reactive power output at the generator terminals is also slightly higher or lower than in the optimum case.

In addition to these aspects, the tolerances of the electrical parameters must also be taken into account. The short-circuit voltage of the transformer should be mentioned here in particular. Varying the tap position also changes the short-circuit voltage. In principle, this tap-changer-dependent short-circuit voltage could be implemented easily in the calculation. Due to time reasons, this has not yet been implemented in the current version. An average value of the short-circuit votage was used for the calculation. This also leads to slight deviations from the optimally calculated result. The aspects listed here explain the slight deviations in the underexcited range.

Also in the overexcited range, the calculated curves enclose the measured points very well. In the overexcited range, it can be seen that there are clusters of points that do not reach the calculated optimum overexcited limit. This is due to the experiment method. The grid voltage at POC is set by adjusting the tap changer position of the regulating transformer (at POC). Before the tap changer position of the regulating transformer can be changed, it is necessary to reduce the reactive power supply at the generator terminals. This ensures that the operating limits of the generator are not violated by the change in grid voltage. During this process, the measurement recording is still active. As a result, clusters of measured values are recorded that do not reach the maximum calculated limits. This behavior must be taken into account when interpreting the measured values.

When looking at the overexcited reactive power range for higher grid voltages, it can be seen that there is a small gap between the calculated values and the measured values. As already mentioned, adjusting the optimum operating point is very difficult and time-consuming. In

the described range, the excitation current is relatively high. The exact adjustment of the excitation current so that the operating limits of the generator are not violated is therfore especially time-consuming in this range. As these points were already measured at the end of the available time limit for the experiments, the reactive power supply of the generator could no longer be set as precisely as for the underexcited limit. For this reason, there is a slight deviation from the precisely calculated limits.

This can be described very well using point A (see Figure 63) as an example. At point A, a maximum reactive power of 15.8 Mvar can be supplied at the generator terminals (taking into account the generator limits). Due to the time-consuming process of precisely setting the reactive power output of the generator, the adjustments of the excitation current were already stopped at a reactive power supply of 15.0 Mvar. This results in a slightly lower reactive power at the point of connection. That can also explain the slight gap in the overexcited range for higher voltages (see Figure 63).

In addition to this aspect, the already mentioned fluctuating active power output and the deviation of the short-circuit voltage must also be taken into account.
In summary, it can be said that the measurement results match those of the calculation very well. The minor deviations can be attributed to the measurement method and the operating conditions.

## 4.5 Results for the verification of classic power-generating facility

Figure 64 shows the measurement results of the experiments to verify the reactive power supply of the hybrid power-generating facility.

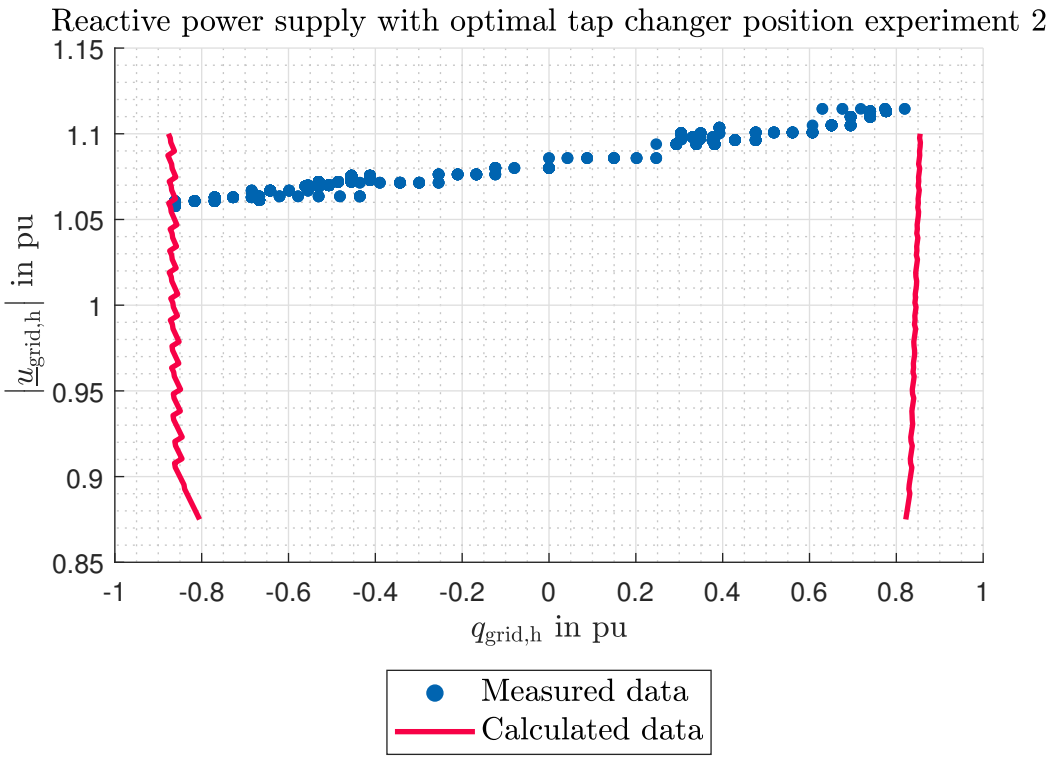


Figure 64: Measurement results for the reactive power supply at the POC of a hybrid power-generating facility

The stationary operating behavior of the converter was simulated using a generator. The operating limits of the generator and the converter were also continuously checked in this process using the MATLAB model.

In this experiment, it is again very difficult to comply with the exact operating limits of the converter or generator. For this reason, the values that violate the operating limits of the two machines were again removed from the diagram in Figure 64. In particular, complying with the maximum converter terminal current is relatively complex. Therefore a deviation from the maximum converter terminals current of 1% was assumed to be acceptable in the experiment.

For time reasons, in this experiment it was only possible to perform the measurement for one grid voltage or tap changer position of the regulating transformer at the point of connection. If the voltage at the point of connection is plotted against the measured reactive power at the point of connection, the blue points shown in Figure 64 are obtained.

The red curves describe the calculation results for the hybrid power-generating facility using optimally controlled tap changer positions (transformer 1 and transformer 2). It can be seen that the measured points match those from the calculation very well. It should be mentioned here that the reactive power output in the overexcited range was determined at a grid voltage of slightly above 1.1 pu. This is due to the fact that the voltage at POC also increases as a result of the overexcited reactive power supplied. This is not a limiting factor for the interpretation of the results.

Due to time constraints and the prevailing water conditions at the hydro power plant, it was not possible to perform the measurements for lower grid voltages. In summary, it can be assumed that the reactive power supply also corresponds to the calculation results for lower grid voltages.

## 4.6 Conclusion of the experiments

Carrying out the experiments required a relatively long preparation time and involved a great deal of organizational effort. In order to carry out the experiments, it was necessary to restrict the operation of the 110 kV grid for a defined period of time with regard to the available power transmission. These experiments were made possible thanks to the cooperation between the local energy supply company, the local grid operator and the Austrian transmission grid operator.

Looking at the findings of the experiments, the results are very positive for both the synchronous power-generating facility and the hybrid power-generating facility. It can be assumed that the calculation results represent the real reactive power supply of the power plants very well. The minor deviations are due to the aforementioned operational challenges during the experiment. In the overall assessment, the test concept developed in this master's thesis represents a suitable way of verifying the reactive power supply.

# 5 Outlook and conclusion

The aim of this master's thesis is to develop a method for verifying the reactive power supply at the point of connection. The previous chapters described a wide range of calculation variants for this purpose. In particular, the analytical load flow analysis method should be mentioned. For the structure described here, this calculation method enables a significantly faster calculation time compared to classic load flow analyses. In addition to the load flow analysis, the modeling of the generator, converter, transformers and cables or overhead lines is a crucial factor in determining the reactive power supply. Particular attention was paid to the modeling of the generator and converter. Experience from this master's thesis has shown that the voltage-dependent modeling of the capability diagrams in particular has a major influence on the reactive power supply. For this reason, modeling these capability diagrams as accurately as possible is essential for calculating the reactive power supply.

The calculation of the reactive power supply at the point of connection was divided into different methods in this master's thesis (see Figure 36). In general, it can be noted that the active power losses at the transformers or the lines should be taken into account in the calculations. If these are not taken into account, a slightly higher reactive power supply is obtained at the point of connection. The reason for this is that a slightly higher reactive power output is also possible at the generator or converter if these active power losses are not taken into account.

In addition to the considerations described above, both a classically controlled tap changer and an optimally controlled tap changer were considered in this master's thesis. The optimally controlled tap changer aims to maximize the reactive power supply at the point of connection. If the reactive power supply with the optimally controlled tap changer and the classically controlled tap changer is compared, a deviation can be observed in the underexcited range. The classical controlled tap changer attempts to keep the generator terminal voltage constant within a lower or upper threshold. Due to this control behavior, the described difference to the optimum tap changer position can be observed in the underexcited range (voltage-dependent stability limit). The initial conditions required for calculating the reactive power supply with the classic controlled tap changer, also have an influence on the reactive power supply at the POC.

In addition to calculating the reactive power supply at the point of connection, a calculation method for calculating the reactive power supply at the generator terminals was also developed as part of this master's thesis. Compared to the calculation of the reactive power supply at the point of connection, this calculation method had the advantage that the capability diagram of the generator does not need to be known. For this reason, the calculation method

for the reactive power supply at the generator terminals is also significantly faster than that for reactive power supply at the point of connection. This method is particularly helpful for the planning phase. It makes it very easy to estimate the effect on the reactive power supply by varying important electrical parameters such as the short-circuit voltage of the transformer.

In addition to synchronous power-generating facilities, hybrid power-generating facilities were also considered in this master's thesis. For this purpose, it is necessary to be able to model the capability diagram of the converter. In contrast to the generator capability diagram, it also depends on the topology of the grid. Due to the additional reactive power supply provided by the converter, the reactive power supply at the POC increases for hybrid power-generating facilities. It must be noted that the operating range of the transformer can also have an influence on the reactive power supply at the POC. If the operating range of the converter's step up transformer is too low, the converter must reduce its reactive power supply to ensure the maximum converter terminal voltage. Therfore the reactive power supply at the POC is also reduced (see Figure 57). In summary, it can therefore be said that not only the capability diagram of the generator or converter has an effect on the reactive power supply at the POC, but also the operating range of the transformer.

As already described in the previous chapter, the calculations carried out in this master's thesis were verified by means of practical experiments. The results of the experiments confirmed the calculations that had been done. The calculation methods described here were implemented in MATLAB. The results are available in the form of various MATLAB functions. Subsequently, these MATLAB functions should be implemented in a graphical user interface. In the course of this process, further optimizations of the functions can be made. This applies to both programming and electrotechnical optimizations. For example, the magnetization losses of the transformer could be taken into account. From a programming point of view, termination conditions could be introduced for the calculation of the optimum tap changer position in order to reduce the calculation time.

# 6 Appendix

The following tables show the electrical parameters for the calculations and experiments carried out in the chapters 3 and 4.

Table 3: Technical parameters of the generator

| Description | Variable | Value | Unit |
|---|---|---|---|
| Modeling | - | const. power (linear stab.) | - |
| Rated apparent power | - | 32.0 | MVA |
| Rated voltage | - | 10.5 | kV |
| Rated power factor | - | 0.85 | 1 |
| Direct-axis synchronous reactance | $x_{\mathrm{d}}$ | 1.19 | pu |
| Quadrature-axis synchronous reactance | $x_{\mathrm{q}}$ | 0.72 | pu |
| Max. terminal voltage | - | 1.10 | pu |
| Min. terminal voltage | - | 0.90 | pu |
| Power safety margin | $e_{\mathrm{q,min}}$ | 0.15 | pu |
| Gradient angle | $\alpha_{\mathrm{gen,c}}$ | 68.0 | ° |
| Active power share (hybrid...) | - | 90.0 | % |
| Active power (hybrid...) | - | 24.48 | MW |

Table 4: Technical parameters of the converter

| Description | Variable | Value | Unit |
|---|---|---|---|
| Rated apparent power | - | 8.0 | MVA |
| Rated voltage | - | 10.5 | kV |
| Max. terminal voltage | $u_{\mathrm{con,h,max}}$ | 1.05 | pu |
| Max. terminal current | $i_{\mathrm{con,h,max}}$ | 440 | A |
| Active power share (hybrid...) | - | 10.0 | % |
| Active power (hybrid...) | - | 2.72 | MW |

Table 5: Technical parameters of the transformer 1

| Description | Variable | Value | Unit |
|---|---|---|---|
| Rated apparent power | $S_{\mathrm{r,t1}}$ | 32.0 | MVA |
| Rated voltage hv | $U_{\mathrm{r,t1,hv}}$ | 115.0 | kV |
| Rated voltage lv | $U_{\mathrm{r,t1,lv}}$ | 10.5 | kV |
| Short-circuit voltage | $u_{\mathrm{k,t1}}$ | 12.0 | % |
| Ohmic short-circuit voltage | $u_{\mathrm{kr,t1}}$ | 0.5 | % |
| Tap changer position | - | hv | - |
| Additional voltage per tap | $\Delta u_{\mathrm{r,t1,hv,tap}}$ | 1.3 | % |
| Number of taps | - | 25 | 1 |
| Lower threshold | - | -5.0 | % |
| Upper threshold | - | 5.0 | % |

Table 6: Technical parameters of the transformer 2

| Description | Variable | Value | Unit |
|---|---|---|---|
| Rated apparent power | $S_{\mathrm{r,t2}}$ | 32.0 | MVA |
| Rated voltage hv | $U_{\mathrm{r,t2,hv}}$ | 115.0 | kV |
| Rated voltage lv | $U_{\mathrm{r,t2,lv}}$ | 10.5 | kV |
| Short-circuit voltage | $u_{\mathrm{k,AF2}}$ | 12.3 | % |
| Ohmic short-circuit voltage | $u_{\mathrm{kr,t2}}$ | 0.5 | % |
| Tap changer position | - | hv | - |
| Additional voltage per tap | $\Delta u_{\mathrm{r,t2,hv,tap}}$ | 1.3 | % |
| Number of taps | - | 25 | 1 |

Table 7: Technical parameters of the overhead line 1

| Description | Variable | Value | Unit |
|---|---|---|---|
| Length | $l_{\mathrm{line,1}}$ | 19.1 | km |
| Resistance | $R'_{\mathrm{line,1}}$ | 0.06 | Ω/km |
| Inductance | $L'_{\mathrm{line,1}}$ | 0.30 | Ω/km |
| Capacity | $C'_{\mathrm{line,1}}$ | 12.36 | nF/km |

Table 8: Technical parameters of the grid

| Description | Variable | Value | Unit |
|---|---|---|---|
| Nominal voltage | $U_{\mathrm{c}}$ | 110.0 | kV |
| Min. voltage | - | 0.875 | pu |
| Max. voltage | - | 1.100 | pu |
| Maximum capacity | $P_{\mathrm{max}}$ | 27.2 | MW |

# References

[1] IPCC, "Summary for Policymakers," in *Climate Change 2023: Synthesis Report.Contribution of Working Groups I, II and III to the Sixth Assessment Report of the Intergovernmental Panel on Climate Change*, H. Lee and J. R. (eds.), Eds., Geneva, Switzerland, 2023. [Online]. Available: `https://www.ipcc.ch/report/ar6/syr/downloads/report/IPCC_AR6_SYR_SPM.pdf`.

[2] M. Strugl and B. Schmidt, *Bruttostromerzeugung in Österreich ab 1950*. [Online]. Available: `https://oesterreichsenergie.at/fakten/energiegrafiken/detailseite/bruttostromerzeugung-in-oesterreich-1`.

[3] Council of European Union, *Commission regulation (EU) 2016/631*, establishing a network code on requirements for grid connection of generators, 2016.

[4] econtrol, *Technische und organisatorische Regeln für Betreiber und Benutzer von Netzen*, Anschluss und Parallelbetrieb von Stromerzeugungsanlagen des Typs A, 2022.

[5] econtrol, *Technische und organisatorische Regeln für Betreiber und Benutzer von Netzen*, Anschluss und Parallelbetrieb von Stromerzeugungsanlagen des Typs B, 2022.

[6] econtrol, *Technische und organisatorische Regeln für Betreiber und Benutzer von Netzen*, Anschluss und Parallelbetrieb von Stromerzeugungsanlagen des Typs C, 2022.

[7] econtrol, *Technische und organisatorische Regeln für Betreiber und Benutzer von Netzen*, Anschluss und Parallelbetrieb von Stromerzeugungsanlagen des Typs D, 2022.

[8] R. Schmaranz, *Betriebsführung elektrischer Netze*, 2022.

[9] N. Hatziargyriou, J. Milanovic, C. Rahmann, V. Ajjarapu, C. Canizares, I. Erlich, D. Hill, I. Hiskens, I. Kamwa, B. Pal, P. Pourbeik, J. Sanchez-Gasca, A. Stankovic, T. Van Cutsem, V. Vittal, and C. Vournas, "Definition and Classification of Power System Stability Revisited and Extended," eng, *IEEE transactions on power systems*, 2021.

[10] R. Schürhuber, *Planung und Betrieb elektrischer Energiesysteme*, 2023.

[11] S. Mishra and Y. S. Brar, "Load Flow Analysis Using MATLAB," in *2022 IEEE International Students' Conference on Electrical, Electronics and Computer Science (SCEECS)*, 2022, pp. 1–4.

[12] A. Nur and A. Kaygusuz, "Load Flow Analysis With Newton–Raphson and Gauss–Seidel Methods in a Hybrid AC/DC System," *IEEE Canadian Journal of Electrical and Computer Engineering*, vol. 44, no. 4, pp. 529–536, 2021.

[13] D. Oeding, *Elektrische Kraftwerke und Netze*, ger ; eng, 8th ed. Netherlands: Springer Nature, 2016.

[14] S. Chatterjee and S. Mandal, "A novel comparison of gauss-seidel and newton- raphson methods for load flow analysis," in *2017 International Conference on Power and Embedded Drive Control (ICPEDC)*, 2017, pp. 1–7.

[15] R. Schürhuber, *Elektrische Energiesysteme 1*, 2023.

[16] P. Schavemaker, *Electrical power system essentials*, eng, Chichester, England ; Hoboken, NJ, 2008.

[17] M. Tesarova and M. Krasl, "Transformer Load-Tap Changers: State-of-Art and Trends," *Advances in Electrical and Electronic Engineering*, vol. 3, no. 2, 2011. [Online]. Available: `http://advances.utc.sk/index.php/AEEE/article/view/376`.

[18] H. Renner, *Regelung und Stabilität Elektrischer Energiesysteme*, 2016.

[19] O. Energie, *Erläuterungsdokument NC RfG / TOR Erzeuger*. 2021.

[20] K. Bonfert, *Betriebsverhalten der Synchronmaschine : Bedeutung der Kenngrößen für Planung und Betrieb elektrischer Anlagen und Antriebe*, ger. 1962.

[21] J. Ranil de Silva, "Capability charts for power systems," Ph.D. dissertation, 1987.

[22] W. Angermann, *Blindleistungsbereitstellung von Erzeugungsanlagen*, 2021.

[23] H. Wrede, "Verhalten von Umrichtern am Netz," 2017.

[24] S. Johansson, G. Asplund, E. V. Jansson, and R. Rudervall, "Power system stabiltiy benefits with VSC DC-Transmission systems," *Cigre*, 2004.

# List of aids

| **Notation** | **Description** |
|---|---|
| DIgSILENT PowerFactory | Simulation software |
| Latex | Word processing |
| LibreOffice Draw | Graphical drawing |
| Deepl | Translation tool |
| Langenscheidt | Translation tool |
| Matlab | Programming language |